MESOSCALE THEORY OF GRAINS AND CELLS: POLYCRYSTALS & PLASTICITY

A Dissertation

Presented to the Faculty of the Graduate School

of Cornell University

in Partial Fulfillment of the Requirements for the Degree of

Doctor of Philosophy

by

Surachate Limkumnerd

January 2007

MESOSCALE THEORY OF GRAINS AND CELLS: POLYCRYSTALS & PLASTICITY

Surachate Limkumnerd, Ph.D.

Cornell University 2007

Solids with spatial variations in the crystalline axes naturally evolve into cells or grains separated by sharp walls. Such variations are mathematically described using the Nye dislocation density tensor. At high temperatures, polycrystalline grains form from the melt and coarsen with time; the dislocations can both climb and glide. At low temperatures under shear the dislocations (which allow only glide) form into cell structures. While both the microscopic laws of dislocation motion and the macroscopic laws of coarsening and plastic deformation are well studied, we hitherto have had no simple, continuum explanation for the evolution of dislocations into sharp walls. We present here a mesoscale theory of dislocation motion. It provides a quantitative description of deformation and rotation, grounded in a microscopic order parameter field exhibiting the topologically conserved quantities. The current of the Nye dislocation density tensor is derived from downhill motion driven by the microscopic Peach–Koehler forces between dislocations, making use of a simple closure approximation. The resulting theory is shown to form sharp dislocation walls in finite time mathematically described by Burgers equation—similar to those seen in the theory of sonic booms and traffic jams. Our finite-difference methods use special upwind and Fourier techniques for dealing with the shock formation. The outcomes of our simulations in one and two

dimensions are in good agreement with experiment and other discrete dislocation simulations. These results provide fundamental insights into the basic phenomena of plastic deformation in crystals, and offers predictions for residual stress, cell-structure refinement, and the distinguish features of different hardening stages in plastic deformation.

BIOGRAPHICAL SKETCH

Surachate Limkumnerd was born during the 1978 Songkran (water throwing) festival in Chiangmai, Thailand. Due to Thai unusually long names, he received his nickname Yor by putting together the first initials of his parents' names. Yor spent his infancy moving from one province to the next following his parents. He began his kindergarten education at the age of three in a local school in suburban Chiangmai, at which point his parents welcomed their second boy. The fear that their first child would make no friends should they continue to move had prompted them to settle down in Lampang where Yor spent substantial parts of the next decade between a swimming pool and piano lessons. All these times his interest in science grew. He was once caned for trying to draw (to scale!) the solar system on the living room wall.[1] His passion in math and science, especially physics, won him a scholarship from the Thai government to pursue his career as a scientist. The scholarship granted him an otherwise–impossible college education anywhere in the U.S. and he chose Cornell University.

Choosing his major in college was not hard. Yor completed his bachelor degree with *summa cum laude* in physics in 2001. As if never detered by Ithaca's winter, Yor decided to stay on at Cornell. He joined Prof. James Sethna's group at the end of his first year as a graduate student. He spent the summer learning Landau approach which he later applied it to formulate his dislocation theory. After each long week of writing *Mathematica*® scripts and teaching wave mechanics, Yor often occupied his Friday evening with a guitar and a Cabernet among the Thais. After nine years in beautiful Ithaca, another chapter of Yor's life is approaching its ending.

[1] To his dismay, the stretch of the living room only allowed for five planets.

To the greatest parents, Yongyoot & Arunrat, and my brother Yee+.

ACKNOWLEDGEMENTS

First and foremost, I am exceedingly grateful to my advisor Professor James Sethna. He always exudes irrepressible enthusiasm which has kept me excited about my work. His incredible intuition has continued to amaze me. He often answered questions that I had pondered for weeks with a series of simple, testable examples. I truly appreciate his trust in me, and my calculations; never once has he checked my work. When I asked if he really believed it, he simply dismissed and said the truth shall come out in the simulations. I would like to thank everybody in our group: Valerie Coffman for her constant inputs on my work and her exceptional Python skill; Joshua Waterfall for always looking out for me and keeping me on track with schedules; Fergal Casey, Ryan Gutenkunst, and the former member of our group, Connie Chang, for numerous fruitful conversations. Finally I would like to thank everyone on the fifth floor, especially Douglas Milton, Connie Wright, and Judy Wilson for helping me from the simplest things like buying stamps to filling out the most complicated travel grant form.

I am grateful to many people over in Rhodes Hall. I greatly appreciate the times I spent with Steven Xu and Paul (Wash) Wawrzynek trying to launch our preliminary numerical work. They also gave me lessons on finite element model, numerical methods and coding in general. Gerd Heber showed me the artistic side of OpenDX® that I have since adapted in our visualization. I would like to thank Paul Dawson, Matthew Miller for letting me sit through their group meetings for a whole semester. These sessions taught me not only the language used in the engineering community, and more importantly the engineers' viewpoints into the same problem. Finally, without the grant from the joint effort of the ASP project led by Professor Tony Ingraffea, I would not have known the luxury of spending

two semesters without teaching.

Life would be monotonous without my Thai crew. I owe the Cornell Thai Association members for 80% of my fond Ithaca memories. What better way to spend your Friday evening than to sing Thai karaoke with a bunch of Thais. I'll always take with me all the mental pictures of every party happening at 43 Fairview Square.

Finally I would like to thank my mom and dad for having so much faith in me, and for always giving me hope while I doubt myself. Their phone calls always come at the times when I need them most. Last but not least, I would like to thank Noque Korbkeeratipong not only for helping with illustrations, but also for encouraging me with her constant smile every time when I'm down.

TABLE OF CONTENTS

LIST OF TABLES

LIST OF FIGURES

CHAPTER 1

INTRODUCTION

1.1 Motivation

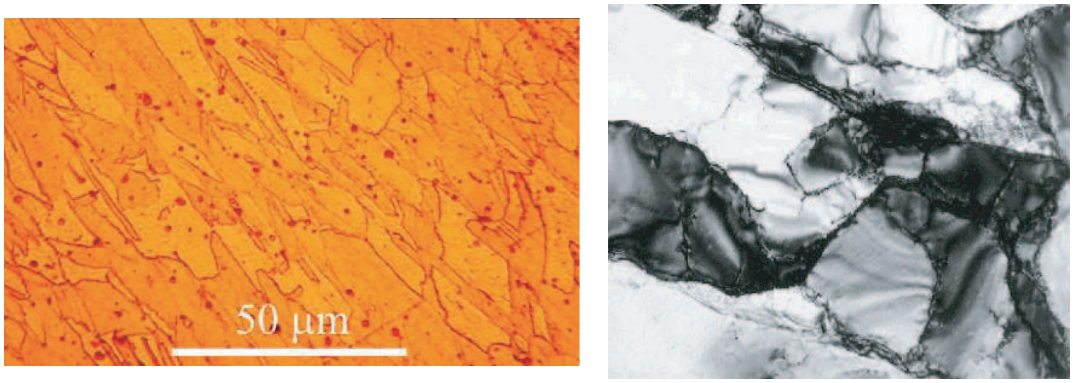

(a) (b)

Figure 1.1: (a) **Grain boundaries** in copper, from the news article in Science [1] covering our theory of plasticity [2] (b) **Cell walls**, from Hughes *et al.* [3].

In condensed-matter physics, crystals are anomalous. Most phases (liquid crystals, superfluids, superconductors, magnets) respond smoothly in space when strained. Crystals, when formed or deformed, relax by developing walls. Common metals (coins, silverware) are polycrystalline; the atoms locally arrange into grains each with a specific crystalline lattice orientation, separated by sharp, flat walls called *grain boundaries* (figure 1.1(a)). When metals are deformed (pounded or permanently bent) new *cell walls* (figure 1.1(b)) form inside each grain [6, 7, 8]. Until now, our only convincing understanding of why crystals form walls has been detailed and microscopic. Our new theory provides an elegant, continuum description of cell wall formation as the development of a *shock front*—a phenomenon hitherto associated with traffic jams and sonic booms.

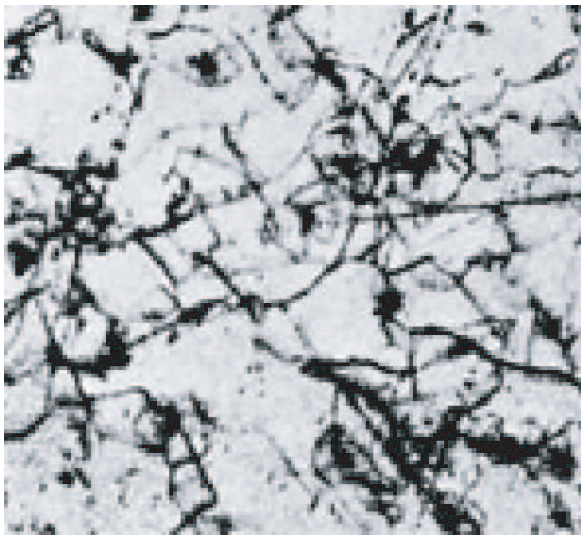

Figure 1.2: **Dislocation tangle** at early stages before wall formation.

Crystals *work harden* when plastically deformed. Figure 1.2 shows a traditional view of work hardening as due to the entanglement of dislocation lines. It is certainly true that as structural metals are plastically deformed the dislocations multiply, and that they form immobile *sessile* junctions when they intersect. In this picture, the yield stress for a crystal with dislocation density ρ is seen to be proportional to $\rho^{1/2}$, the rough distance between pinned sites on a given dislocation. As dislocations multiply and ρ increases, the yield-stress increases and the material work hardens.

However, the spaghetti tangles of figure 1.2 are typical of only the initial stages of hardening (stage I) where only one slip system is involved; in later stages large-scale patterns form. Figure 1.1(b) shows the *cell structures* formed in FCC metals in multiple-slip stage III hardening [6, 7, 8, 9, 10], the dislocations have organized themselves into relatively sharp and flat cell walls, mediating small rotations between relatively dislocation-free crystalline cells.

These cell walls are reminiscent of grain boundaries in polycrystalline met-

als, which also mediate rotations between nearly perfect crystalline grains (figure 1.1(a)). Grain boundaries can form in several different ways. They can form during crystallization from the melt (not described by our theory), where the grains often form a dendritic morphology. They can form under external shear at high temperatures, where the dislocations migrate into grain boundaries in a process known as *polygonization* and then the grains *coarsen*. Grain boundaries can also arise at low temperatures in highly dislocated materials in a process called *recrystallization*; here a small, clean crystalline region can grow by eating the dislocations surrounding it, giving a net outward force on its grain boundary. These dislocation patterns and structures have important consequences for the materials properties.[1]

Our formulation of a plasticity theory rests upon differential geometry approaches to dislocation dynamics, developed in the middle of the last century [17, 18, 19, 20, 21, 22]. These elegant mathematical descriptions stopped at describing the state of the material; our work is aimed at developing a similarly elegant approach to the evolution law, and extracting predictions about experimental systems. By focusing on the Nye dislocation density tensor [23], we do not incorporate the extra framework of slip systems, immobile dislocations, and geometrically unnecessary dislocations which are central features of a community of models used to study texture evolution and sub-grain structure [24, 25, 26, 27, 28, 29, 30, 31]. Apart from intriguing hints in Dawson's simulations [29], wall formation is not

[1]For example, the yield strength σ_Y of clean polycrystalline materials is not determined by the average dislocation density, but rather by the grain size d, according to the Hall–Petch relation $\sigma_Y = \sigma_0 + k\sqrt{d}$. (Here dislocation pile-up, rather than pinning, dominates the yield stress. For nano-crystalline materials, slippage at the grain boundaries dominates the plastic deformation, leading to a reverse Hall–Petch effect [11, 12, 13].) The yield strength dependence on dislocation density in stage III hardening is no longer determined by the simple $\sqrt{\rho}$ dependence of dislocation tangles, but now depends on the scaling of cell size with continuing work hardening deformation [14, 15, 16].

typically observed or studied in these texture evolution models. There have been several recent efforts to develop coarse-grained dynamics for dislocations, both for parallel dislocations [32, 33, 34] and in fully three-dimensional theories [35, 36, 37, 38, 39]. None of these investigators found wall formation in their models.[2]

Our approach to the formulation of a dislocation dynamics theory is minimalist: it ignores many features (geometrically unnecessary dislocations [34], slip systems [29], dislocation tangling, yield surfaces, nucleation of new dislocations) that are known to be macroscopically important in real materials. It does incorporate cleanly and microscopically the topological constraints, long-range forces and energetics driving the dislocation dynamics. As hypothesized by the LEDS (low-energy dislocation structures) approach [40, 41], we find that a dynamics driven by minimizing energy (omitting tangling and nucleation) still produces cell boundary structures. The δ-function wall singularities in our dislocation theory form, however, not from the energy minimization, but from the nonlinear nature of the evolution law. Finally our theory, to our surprise, initially forms sharp walls that are not the usual zero-stress grain boundaries.

1.2 Outline of the dissertation

We begin in chapter 2 by introducing a Nye dislocation tensor as an order parameter to describe dislocations. The evolution equation in the form of a continuity equation relating the dislocation density with a dislocation current is put forward. The relationship between the dislocation density field and other state variables such as the stress and the plastic distortion field are given in chapter 3. Motivated

[2]We discuss the context of our plasticity theory in connection with other approaches in great details in chapter 5.

by the criterion for a decrease in elastic energy and the microscopic Peach–Koehler force, the form of the dislocation current is written down in chapter 4. This completes the description of the evolution law. The last part of this chapter describes wall-like structures and their superpositions as one possible family of stationary state solutions to our law. In chapter 5, connections are made between our plasticity theory and the conventional plasticity theories. The implementation of the evolution equation specialized to one dimension, the mechanism of sharp walls formation for volume conserving systems and systems allowing for climb, and the asymptotics of the one-dimensional solutions at large times near sharp walls are described in chapter 6. Finally, our finite difference simulations for various types of slip systems in two dimensions and the predictions for different slip subsystems against other discrete dislocation simulations are discussed in chapter 7.

Throughout the dissertation, the reader is asked to consult the appendices for prerequisite knowledge on tensors and symmetry group, definitions and conventions for the Fourier transforms, elementary exposure to conventional elasticity theory, the proof of stress-free dislocation states too involved to be incorporated in the main text, a modified one-dimensional theory, different finite difference numerical schemes, and an efficient method to visualize results from two-dimensional simulations.

CHAPTER 2

DISTRIBUTIONS OF DISLOCATIONS AND MODEL EQUATIONS

2.1 Burgers vector and Nye dislocation density tensor

To appropriately describe a dislocation, one needs to introduce the idea of *Burgers vector*. The Burgers vector is the topological charge characteristic of a defect found by counting the net number of extra rows and columns of atoms in a distant path encircling the dislocation. We define the Burgers vector $\mathbf{b}$, according to the procedure outlined by F. C. Frank [42] which can be best illustrated with a hypothetical cubic lattice. For a perfect crystal, if one traverse the crystal in a closed loop in a clockwise direction, one has to have the same number of "up" lattice vectors as "down" lattice vectors, and as many "right" lattice vectors as "left" ones. For a crystal with a dislocation line, this won't be true. If one performs the vector sum of all the lattice vectors going around the loop, the resulting vector is called the *Burgers vector*. In other words, the negative of the Burgers vector is needed in order to close the circuit completely.[1] Figure 2.1 shows images of an edge and a screw dislocation.

The same concept can be generalized to an isotropic material in the continuum theory. From the definition, after a passage around any closed contour L that encircles a dislocation line, the displacement vector $\mathbf{u}$ receives an increment $\mathbf{b}$

[1]This convention has been used by, *e.g.*, J. M. Burgers, T. Mura, F. R. N. Nabarro, W. T. Read, Jr., A. Seeger, and J. Weertman. However, there are many authors who use the opposite convention such as, B. A. Bilby, R. Bullough, E. Smith, F. C. Frank, J. D. Eshelby, J. Friedel, J. P. Hirth, E. Kröner, J. Lothe, N. Thompson, and R. deWit.

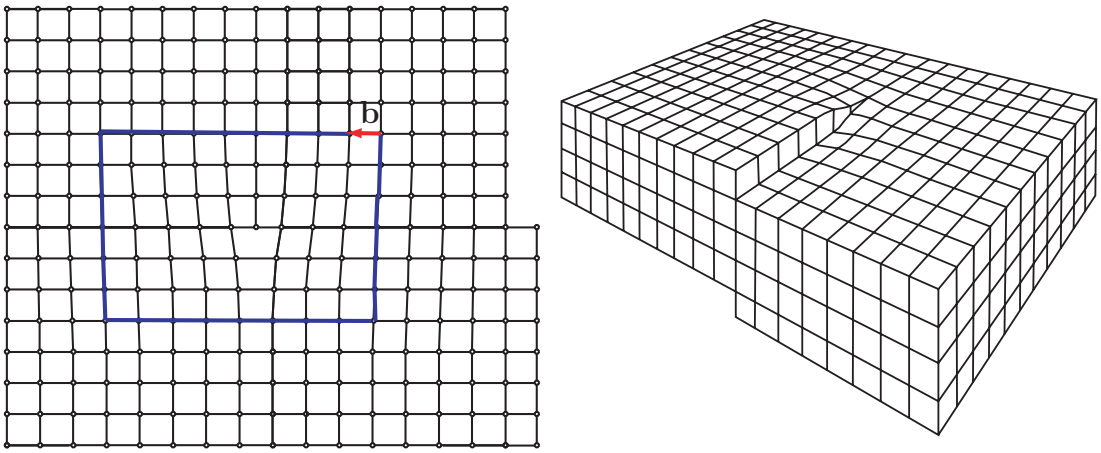

(a) (b)

Figure 2.1: (a) A Burgers vector is described by a traversal around a contour surrounding an edge dislocation. (b) A screw dislocation.

which is equal to one of the lattice vectors. This can be expressed as [2]

$$\oint_L du_i^{\mathrm{P}} = \oint_L \beta_{ij}^{\mathrm{P}}\, dx_j = -b_i\,, \tag{2.1}$$

where $\boldsymbol{\beta}^{\mathrm{P}}$ is the plastic distortion tensor and can be thought of as a primary field by itself.

A *dislocation* is a crystallographic defect associated with crystalline translational order. It represents extra rows or columns of atoms and is characterized by two quantities; the direction of the dislocation line, $\mathbf{t}$, and the Burgers vector direction, $\mathbf{b}$ as defined above. Therefore the dislocation density $\boldsymbol{\rho}$, must be defined as a second-rank tensor in order to carry such information:

$$\boldsymbol{\rho} = (\mathbf{t} \otimes \mathbf{b})\delta(\boldsymbol{\xi})\,, \tag{2.2}$$

where $\delta(\cdot)$ is the Dirac δ-function, and $\boldsymbol{\xi}$ is the two-dimensional radius vector

[2]Here and throughout the manuscript a subscript notation is used to represent a component of a vector or tensor quantity. We also employ Einstein's summation convention where repeated indices are understood to be summed over unless otherwise noted.

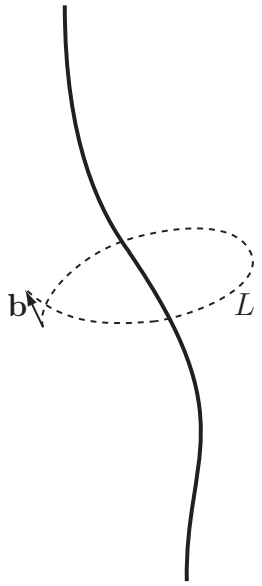

Figure 2.2: The shift in the displacement vector upon a circulation around a dislocation line defines the Burgers vector.

taken from the axis of the dislocation in the plane perpendicular to the vector $\mathbf{t}$ at the given point. This type of tensor is called Nye dislocation density tensor (J. F. Nye, 1953 [23]). One categorizes types of dislocations into edge, screw, and mixed according to the relationship between Burgers vector $\mathbf{b}$ and the direction of dislocation line $\mathbf{t}$. An edge dislocation is one where the Burgers vector lies perpendicular to the direction of the dislocation line. A screw dislocation is one where the Burgers vector is parallel to the line. A mixed dislocation is one with general Burgers vector, *e.g.*, by a superposition of both types of dislocations.

In the presence of many dislocations labeled by an index α,

$$\rho_{ij}(\mathbf{x}) = \sum_{\alpha} t_i^{\alpha} b_j^{\alpha} \delta^{(2)}(\mathbf{x} - \boldsymbol{\xi}^{\alpha}) \,. \tag{2.3}$$

Here $\delta^{(2)}(\cdot)$ is a two-dimensional δ-function, infinite if the position $\mathbf{x}$ lies along the dislocation path $\boldsymbol{\xi}^{\alpha}$. When many dislocations are present, a continuum or *coarse-graining* description of a conglomerate of dislocations is preferred. In this picture,

we can write $\boldsymbol{\rho}$ as

$$\rho_{ij}(\mathbf{x}) = \sum_{\alpha} \int t_i^{\alpha} b_j^{\alpha} \delta^{(2)}(\mathbf{x}' - \boldsymbol{\xi}^{\alpha}) G(\mathbf{x} - \mathbf{x}')\, d^3\mathbf{x}' \,, \tag{2.4}$$

with Gaussian weighting $G(\mathbf{x} - \mathbf{x}') \simeq (1/\sqrt{2\pi}L)^3 \exp[-(\mathbf{x} - \mathbf{r})^2/(2L^2)]$ over some distance scale L large compared to the distance between dislocations and small compared to the dislocation structures being modeled.

In his revolutionary paper [23], Nye provides the relationships between the dislocation density tensor $\boldsymbol{\rho}$ and the lattice curvature tensor $\boldsymbol{\kappa}$. Let $d\phi_i$ be small lattice rotations about three coordinate axes, associated with the displacement vector dx_j, then $\kappa_{ij} \equiv \partial\phi_i/\partial x_j$. He shows that given a curvature tensor $\boldsymbol{\kappa}$, the Nye dislocation tensor $\boldsymbol{\rho}$ can be determined:

$$\rho_{ij} = \kappa_{ij} - \delta_{ij}\kappa_{kk} \tag{2.5}$$

and vice versa:

$$\kappa_{ij} = \rho_{ij} - \frac{1}{2}\,\delta_{ij}\rho_{kk} \tag{2.6}$$

Equation 2.5 offers a means to obtain $\boldsymbol{\rho}$ experimentally by measuring disorientation angles through techniques such as electron back scattering diffraction (EBSD) [43, 44].

Macroscopically, most of the dislocations are geometrically unnecessary with canceling contributions to $\boldsymbol{\rho}$ and to the overall deformation of the material body. Thus most theories of plasticity either ignore them and only keep a scalar for the gross line length dislocation, or incorporate separate dislocation densities for positive and negative Burgers vectors (whose difference and sum give the necessary and unnecessary dislocation densities). Dislocations which are unnecessary on the *macroscale* may be important on the *mesoscale*, perhaps giving rise to interesting

substructural pattern such as an alternating pattern of cell orientations giving an alternating Burgers vector density in neighboring walls (which nearly cancels on longer length scales [45, 46]). In our theory, the net dislocation density tensor $\boldsymbol{\rho}$ that we keep is the sole origin of the long-range stress fields whose screening leads to pattern formation; it determines the net plastic deformation field and the grain and cell mis-orientations that experimentally characterize the mesoscale structure.

2.2 Fundamental equations

A complete macroscopic description of the deformation $\mathbf{u}$ of a material is given by

$$\partial_i u_j = \beta_{ij}^{\mathrm{E}} + \beta_{ij}^{\mathrm{P}} \tag{2.7}$$

where $\boldsymbol{\beta}^{\mathrm{E}}$ represents an elastic, reversible distortion, while the plastic distortion tensor $\boldsymbol{\beta}^{\mathrm{P}}$ describes the irreversible plastic deformation.[3] In this context, the plastic distortion is the result of the creation and motion of dislocations, and cannot be written as the gradient of a single-valued displacement field. Integrating around a loop L enclosing a surface S, the change in such a hypothetical plastic distortion field $\Delta\mathbf{u}^{\mathrm{P}}$ can be written using Stokes' theorem as

$$\Delta u_j^{\mathrm{P}} = -b_j = \oint_L \beta_{ij}^{\mathrm{P}}\, dx_i = \int_S \varepsilon_{ilm}\partial_l \beta_{mj}^{\mathrm{P}}\, dS_i, \tag{2.8}$$

where ε_{ilm} is the totally anti-symmetric tensor.[4] Here and throughout this dissertation, we shall make use of the shorthand notation ∂_i to represent $\partial/\partial x_i$. For a single dislocation, equation 2.3 gives

$$b_j = \int_S t_i b_j \delta(\boldsymbol{\xi})\, dS_i = \int_S \rho_{ij}\, dS_i\,, \tag{2.9}$$

[3] Please consult appendix D for a review on the basic ideas of the theory of elasticity.

[4] See appendix A.1 for more details.

where we have used the property of the Dirac δ-function. Since the contour L can be arbitrarily chosen, equation 2.8 and equation 2.9 provide the relationship between the Nye dislocation density tensor and the plastic distortion field:

$$\rho_{ij} = -\varepsilon_{ilm}\partial_l \beta^{\mathrm{P}}_{mj} \tag{2.10}$$

Thus the natural physicist's order parameter (the topologically conserved dislocation density $\boldsymbol{\rho}$) is a curl of the common engineering state variable (the plastic distortion field $\boldsymbol{\beta}^{\mathrm{P}}$). Analogous to the continuity of magnetic field lines, the microscopic statement that dislocations cannot end (except at grain or cell boundaries) implies that

$$\partial_i \rho_{ij} = 0, \tag{2.11}$$

which follows from (2.10).[5] Due to the compatibility of the displacement, $\varepsilon_{ilm}\partial_l\partial_m u_j = 0$, an equivalent description to (2.10) involving the elastic counterpart is

$$\rho_{ij} = \varepsilon_{ilm}\partial_l \beta^{\mathrm{E}}_{mj}\,. \tag{2.12}$$

In the absence of dislocations or plastic strains, an elastic body subject to an applied stress has a compatible elastic strain. Kröner's *incompatibility tensor* defined by

$$R_{ij} \equiv \varepsilon_{ilm}\varepsilon_{jpk}\,\partial_l\partial_p\,\epsilon^{\mathrm{E}}_{km} = -\varepsilon_{ilm}\varepsilon_{jpk}\,\partial_l\partial_p\,\epsilon^{\mathrm{P}}_{km} = \frac{1}{2}(\varepsilon_{ilm}\partial_l\rho_{jm} + \varepsilon_{jlm}\partial_l\rho_{im})\,, \tag{2.13}$$

where $\epsilon^{\mathrm{E}}_{km}$ and $\epsilon^{\mathrm{P}}_{km}$ are the symmetric parts of β^{E}_{km} and β^{P}_{km} respectively, directly measures the incompatibility of the strain tensor due to the presence of dislocations

[5]Equation (2.11) will not be true if our theory includes disclinations. The idea of disclinations was first used by Frank in the study of cholesteric liquid crystals to describe twisting discontinuities of the crystals allowing discrete jumps of one half-pitch of the helicoidal texture [47]. deWit modified the form of (2.11) to replace 0 by adding a source or a sink term [48, 49]. In the more general form, dislocations can then start or end on disclinations.

or disclinations. $R_{ij} = 0$ coincides with de Saint–Venant's compatibility equation for the components of the strain tensor. In the language of differential geometry, the incompatibility tensor is recognized simply as the Ricci tensor.[6]

2.3 Dislocation current and the continuity equation

The law of conservation of the Burgers vector in a medium implies that the time evolution of the Nye dislocation density tensor must be given in terms of a current. Consider the flow rate of Burgers vector through surface S enclosed by contour C. We can define the *dislocation current* $\boldsymbol{J}$ as a quantity which when summed across the surface S gives the flow of the Burgers vector through the contour:

$$\frac{db_j}{dt} = -\oint_C J_{ij}\, dx_i \tag{2.17}$$

To obtain the continuity equation, we simply substitute the relation between $\mathbf{b}$ and $\boldsymbol{\rho}$ in (2.9) into (2.17),

$$\int_S \frac{\partial \rho_{ij}}{\partial t}\, dS_i = -\int_S \varepsilon_{ilm} \frac{\partial J_{mj}}{\partial x_l}\, dS_i\,, \tag{2.18}$$

[6]There exists a three-dimensional Riemannian space where $\boldsymbol{\epsilon}^{\mathrm{P}}$ can be considered a natural compatible strain field. In such a space, the metric g_{ij} is defined by

$$g_{ij} \equiv \delta_{ij} + 2\epsilon^{\mathrm{P}}_{ij}\,. \tag{2.14}$$

The Ricci tensor can be computed from

$$R_{ijkm} = \varepsilon_{ijp}\varepsilon_{kmq} R_{pq} \tag{2.15}$$

where R_{ijkm} is the Riemann-Christoffel curvature tensor defined by

$$R_{ijkm} \equiv \frac{1}{2}\left(\partial_j\partial_k\, g_{im} + \partial_i\partial_m\, g_{jk} - \partial_j\partial_m\, g_{ik} - \partial_i\partial_k\, g_{jm}\right). \tag{2.16}$$

For a more complete treatment of the elasticity theory on curvilinear coordinates, the reader should consult, *e.g.*, [50, 22].

with one application of Stokes theorem. Since the contour S is arbitrary,

$$\boxed{\frac{\partial \rho_{ij}}{\partial t} + \varepsilon_{ilm} \frac{\partial J_{mj}}{\partial x_l} = 0} \tag{2.19}$$

This continuity equation describes the evolution of dislocations according to the choice of the dislocation current $\boldsymbol{J}$.

Equation 2.19 was derived independently by Kosevich and Mura in 1962–1963 [20, 21]. By taking a time derivative of (2.10) and compares it to (2.19), one can identify the dislocation current with the rate of change of the plastic distortion field,

$$J_{ij} = \frac{\partial \beta^{\mathrm{P}}_{ij}}{\partial t} \,. \tag{2.20}$$

One of the main objectives of this dissertation is to derive the evolution law for these fields (2.20) appropriate for scales large compared to the atoms but small compared to the cell structures and grain boundaries.

We only consider, in our theory, the net density of dislocations. The statistically stored dislocations (those with opposing Burgers vectors which cancel out in the net dislocation density) have been ignored because they do not affect the long range strain fields or the misorientations at grain boundaries and cell walls. Macroscopically they are known to dominate dislocation entanglement and work hardening, and are important in previous continuum theories of plasticity [34, 51, 52, 33, 32, 53]. Much of the macroscopic cancellation in net dislocation density comes from the near alternation of the net rotations in the series of cell walls [54]. Our focus on the sub-cellular, subgrain length scales and our current omission of dislocation tangling make keeping only the net dislocation density natural for our purposes. We also do not explicitly incorporate a yield surface, because we hope eventually to explain work hardening and yield surfaces as properties which emerge from the intermediate length-scale theory.

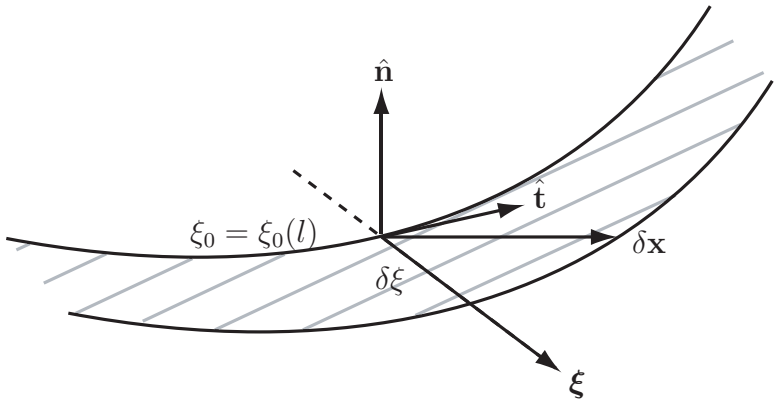

Figure 2.3: The current $\boldsymbol{J}$ due to the motion of a segment of a dislocation loop.

The form of our mesoscopic continuum theory will be motivated by the microscopic motion of a single dislocation. To calculate a dislocation current $\boldsymbol{J}$ for a dislocation loop moving in the direction of the plane of the loop, consider a surface S, whose normal vector is $\hat{\mathbf{n}}$, spanning a dislocation loop l with $\hat{\mathbf{t}}$ denoted the tangential vector along the loop. The plastic distortion tensor $\boldsymbol{\beta}^{\mathrm{P}}$ caused by the slip $\mathbf{b}$ of the plane is given by

$$\beta_{ij}^{\mathrm{P}} = -n_i b_j \, \delta(\zeta)\Theta(\xi - \xi_0)\,, \tag{2.21}$$

where ζ is the length measured in the direction of $\hat{\mathbf{n}}$ while ξ is measured from the position of a point on the line $\xi_0 = \xi_0(l)$ along $\hat{\mathbf{t}} \times \hat{\mathbf{n}}$, and

$$\Theta(x) = \begin{cases} 1, & x > 0; \\ \\ 0, & x < 0\,. \end{cases}$$

If the line is displaced by a small amount $\delta\mathbf{x}$, the distortion field will change by

$$\delta\beta_{ij}^{\mathrm{P}} = -n_i b_j \, \delta(\zeta) \, \frac{d\Theta}{d\xi}\Big|_{\xi=\xi_0} \delta\xi = -n_i b_j \, \delta(\zeta) \, \delta(\xi - \xi_0) \, \delta\xi\,. \tag{2.22}$$

Only the component of $\delta\mathbf{x}$ in the direction of ξ-axis matters; the component along $\hat{\mathbf{t}}$ is meaningless. In terms of $\delta\mathbf{x}$, $\delta\xi = |\delta\mathbf{x}|\sin(\phi)$, where ϕ is the angle between $\hat{\mathbf{t}}$

and $\delta\mathbf{x}$. One can rewrite $\mathbf{n}$ in terms of these quantities as

$$n_i = \frac{\varepsilon_{ikm}\delta x_k t_m}{\delta\xi}\,. \tag{2.23}$$

Substituting (2.23) into (2.22) gives

$$\delta\beta_{ij}^{\mathrm{P}} = \varepsilon_{ilm}t_l b_j \delta x_m \delta^{(2)}(\boldsymbol{\xi})\,, \tag{2.24}$$

where $\delta^{(2)}(\boldsymbol{\xi})$ is the two-dimensional δ-function earlier expressed as $\delta(\zeta)\,\delta(\xi-\xi_0)$. And therefore,

$$J_{ij} = \varepsilon_{ilm}t_l b_j v_m \delta^{(2)}(\boldsymbol{\xi})\,, \tag{2.25}$$

where $\mathbf{v}$ denotes the velocity at the point $(\zeta, \xi-\xi_0)$. We are going to motivate the form of the mesoscopic dislocation current due to the local Peach–Koehler force density using (2.25) in section 4.1.3.

We can distinguish types of dislocation motions according to whether or not the motions cause changes in material's volume. A dislocation is said to be gliding when it is moving in the plane formed by its Burgers vector $\mathbf{b}$ and its line direction $\mathbf{t}$. A dislocation is climbing when it's moving perpendicularly to this plane. The climb motion is *non-conservative*; the crystal volume changes with the motion of the dislocation. Consider, again, the configuration as shown in figure 2.3. The climb motion leads to an increase of the area of the surface S by dS in the direction perpendicular to the plane formed by $\delta\mathbf{x}$ and $d\mathbf{l}$,

$$\delta\mathbf{S} = \delta\mathbf{x}\times d\mathbf{l}\,, \tag{2.26}$$

where $d\mathbf{l}$ denotes the element of the dislocation loop and thus points along $\mathbf{t}$. The change in area therefore introduces the change in volume by

$$dV = \mathbf{b}\cdot\delta\mathbf{S} = -(\mathbf{b}\times d\mathbf{l})\cdot\delta\mathbf{x}\,. \tag{2.27}$$

Since all the changes happen at the core of the dislocation line in the coarse-graining description of the dislocation motion, the relative volume change is associated with $\delta\epsilon^{\mathrm{P}}_{kk}$ according to

$$\delta\epsilon^{\mathrm{P}}_{kk} = \varepsilon_{ijk}(\delta x_i b_j t_k)\delta^{(2)}(\boldsymbol{\xi})\,. \tag{2.28}$$

If the change occurs during the period δt, then

$$\Delta J_{kk} = \frac{\delta\epsilon^{\mathrm{P}}_{kk}}{\delta t} = \varepsilon_{ijk}(v_i b_j t_k)\delta^{(2)}(\boldsymbol{\xi})\,, \tag{2.29}$$

where, again, $\mathbf{v}$ is the speed of the dislocation line. We can therefore identify the type of dislocation motions by calculating the trace of $\boldsymbol{J}$; if $J_{kk} = 0$, the motion is conservative, volume conserving (glide) otherwise the motion contains a non-conservative, vacancy/interstitial diffusion (climb) piece.

CHAPTER 3

RELATIONSHIPS BETWEEN STATE VARIABLES

3.1 Stress fields due to dislocations

In the presence of a dislocation, crystal strains and a stress field is created around it. Peach and Koehler first derived the equation for stress fields due to dislocations in 1950 [55]. A complete theory of dislocation dynamics should include the motions of dislocations due to the effect of their own stresses. In this section, we write down the expression for stress fields in terms of the coarse-grained Nye dislocation density tensor. Our derivation is based on the formulation given by Hirth & Lothe [56].

For an isotropic material, the stress field due to a closed dislocation loop is given by

$$\sigma_{\alpha\beta} = -\frac{\mu}{8\pi}\oint_C b_m \varepsilon_{im\alpha}\frac{\partial}{\partial x'_i}\nabla'^2 R\, dx'_\beta - \frac{\mu}{8\pi}\oint_C b_m \varepsilon_{im\beta}\frac{\partial}{\partial x'_i}\nabla'^2 R\, dx'_\alpha \\ - \frac{\mu}{4\pi(1-\nu)}\oint_C b_m \varepsilon_{imk}\left(\frac{\partial^3 R}{\partial x'_i \partial x'_\alpha \partial x'_\beta} - \delta_{\alpha\beta}\frac{\partial}{\partial x'_i}\nabla'^2 R\right) dx'_k\,, \quad (3.1)$$

where $\sigma_{\alpha\beta}$ signifies the stress field, with the shear modulus μ, and Poisson's ratio ν.[1] $R = |\mathbf{r} - \mathbf{r}'|$, where $\mathbf{r}$ is measured from the origin to the observer, while $\mathbf{r}'$ is measured from the origin to the point on the dislocation line. The Kronecker delta δ_{ij} gives the value of 1 when $i = j$, and 0 when $i \neq j$. We can explicitly write out the integration along dx'_β as $\oint_C \ldots dx'_\beta \Rightarrow \oint_C \ldots t_\beta\, dl'$, parametrized by l' with tangent direction $\mathbf{t}$. It is now possible to represent a line integral as a volume integral over a two-dimensional δ-function, $\oint_C \ldots t_\beta\, dl' \Rightarrow \int_V \ldots \delta(\boldsymbol{\xi})\, d^3\mathbf{r}'$, where the contour of integration is defined by $\boldsymbol{\xi}$. The collection of Burgers vector

[1] See appendix D on how to relate these two quantities with others.

$\mathbf{b}$, the direction along the dislocation $\mathbf{t}$, and $\delta(\boldsymbol{\xi})$ signifying a diminishing density away from the core of the dislocation make up a Nye dislocation density tensor $\boldsymbol{\rho}$. Equation 3.1 becomes

$$\sigma_{\alpha\beta}(\mathbf{r}) = -\frac{\mu}{8\pi}\int_V (\varepsilon_{im\alpha}\rho_{\beta m}(\mathbf{r}') + \varepsilon_{im\beta}\rho_{\alpha m}(\mathbf{r}'))\frac{\partial^3 R}{\partial x_i' \partial x_j' \partial x_j'}\, d^3\mathbf{r}' \\ - \frac{\mu}{4\pi(1-\nu)}\int_V \varepsilon_{imk}\rho_{km}(\mathbf{r}')\left(\frac{\partial^3 R}{\partial x_i' \partial x_\alpha' \partial x_\beta'} - \delta_{\alpha\beta}\frac{\partial^3 R}{\partial x_i' \partial x_j' \partial x_j'}\right) d^3\mathbf{r}' \,. \quad (3.2)$$

It is clear that each term in (3.2) can be written as a convolution between two functions. This suggests that such formula is more naturally expressed in Fourier space[2] as a product between two functions. By performing the transformation on all terms, $\boldsymbol{\sigma}$ becomes

$$\widetilde{\sigma}_{\alpha\beta}(\mathbf{k}) = K_{\alpha\beta\mu\nu}(\mathbf{k})\widetilde{\rho}_{\mu\nu}(\mathbf{k})\,, \quad (3.3)$$

where

$$K_{\alpha\beta\mu\nu}(\mathbf{k}) = -\frac{i\mu k_\gamma}{k^2}\left[\varepsilon_{\gamma\nu\alpha}\delta_{\beta\mu} + \varepsilon_{\gamma\nu\beta}\delta_{\alpha\mu} + \frac{2\varepsilon_{\gamma\nu\mu}}{1-\nu}\left(\frac{k_\alpha k_\beta}{k^2} - \delta_{\alpha\beta}\right)\right].$$

The detailed calculation of the above expression is provided in appendix C. By formulating everything in Fourier space,[3] we can avoid complicated integrations, but at the expense of an extra assumption that the material has periodic boundary conditions or has an infinite extent.

[2]Throughout the manuscript, we shall denote a Fourier quantity by putting $\widetilde{\ }$ on top of its real-space counterpart.

[3]A happy coincidence happens in one dimension where stress fields are local and the transformation into Fourier space can be avoided. See chapter 6 for the complete analysis of our theory in one dimension.

3.2 Plastic distortion fields due to dislocation density fields

From equation 2.10 in section 2.2, we are able to write down a dislocation density field given a plastic distortion configuration,

$$\rho_{ij} = -\varepsilon_{ilm}\partial_l \beta^{\mathrm{P}}_{mj}\,. \tag{2.10'}$$

To invert this relation, we note that this equation has a close analog in electromagnetic theory, namely

$$\boldsymbol{\nabla} \times \mathbf{B} = \mu_0 \mathbf{J}\,, \tag{3.4}$$

which relates the charge density $\mathbf{J}$ to the magnetic field $\mathbf{B}$ in free space with magnetic permeability μ_0. Many standard textbooks in electromagnetic theory (see, *e.g.* [57]) provide the inverse expression of (3.4), and we shall only quote the result:

$$\mathbf{B} = \frac{\mu_0}{4\pi}\,\nabla \times \int \frac{\mathbf{J}(\mathbf{x}')}{|\mathbf{x}-\mathbf{x}'|}\,d^3\mathbf{x}' \tag{3.5}$$

By appealing to the analogy to the above expression, the form of the plastic distortion field on the Nye tensor is immediate:

$$\begin{aligned}\beta^{\mathrm{P}}_{ij} &= \frac{1}{4\pi}\int \varepsilon_{ilm}\rho_{mj}(\mathbf{x}')\frac{x_l - x'_l}{|\mathbf{x}-\mathbf{x}'|^3}\,d^3\mathbf{x}' + \partial_i\psi_j \\ &= -\frac{1}{4\pi}\,\varepsilon_{ilm}\,\partial_l\left(\int \frac{\rho_{mj}(\mathbf{x}')}{|\mathbf{x}-\mathbf{x}'|}\,d^3\mathbf{x}'\right) + \partial_i\psi_j\end{aligned} \tag{3.6}$$

Here we have used the identity $\dfrac{\mathbf{x}-\mathbf{x}'}{|\mathbf{x}-\mathbf{x}'|^3} = -\boldsymbol{\nabla}\left(\dfrac{1}{|\mathbf{x}-\mathbf{x}'|}\right)$. The above relationship is defined up to a gradient of an arbitrary vector field $\boldsymbol{\psi}$. When one writes down a dislocation density tensor from a plastic distortion field, $\boldsymbol{\nabla}\boldsymbol{\psi}$ is automatically cast away in the process of taking a curl. This term should be thought of as an elastic distortion arising from the displacement field $\boldsymbol{\psi}$. Since the *elastic* distortion tensor is written as a gradient of a displacement field and since the dislocation

density tensor cares only about the *plastic* portion of the total distortion field, this term is neglected by the dislocation density description. This field, however, is very crucial to uniquely describe the displacement field $\mathbf{u}$ of a material subject to various constraints such as boundary conditions. This point is to be illustrated in the following section.

The relationship is simpler in Fourier space:

$$\widetilde{\beta}^{\mathrm{P}}_{ij} = -\frac{i}{k^2}\,\varepsilon_{ilm}k_l\widetilde{\rho}_{mj} + ik_i\widetilde{\psi}_j \tag{3.7}$$

3.3 Displacement field u due to $\boldsymbol{\beta}^{\mathbf{P}}$ and $\boldsymbol{\rho}$

In order to express total displacement vector according to dislocation arrangements in an isotropic medium in equilibrium, we first express the equilibrium condition,

$$\partial_i\sigma_{ij} = \partial_j\sigma_{ij} = 0\,. \tag{3.8}$$

From (D.5) and (D.1) in appendix D, we are able to replace the stress with the total and plastic distortion fields,

$$\begin{aligned} \partial_j\left(C_{ijkm}(\beta^{\mathrm{T}}_{km} - \beta^{\mathrm{P}}_{km})\right) &= 0 \\ C_{ijkm}\partial_m\partial_j u_k &= C_{ijkm}\partial_j\beta^{\mathrm{P}}_{km}. \end{aligned} \tag{3.9}$$

In the first line we use the symmetry under interchanging the last two indices of C_{ijkm} to replace $\epsilon^{\mathrm{T}}_{km}$ and $\epsilon^{\mathrm{P}}_{km}$ by $\partial_m u_k$ and β^{P}_{km} respectively.

One way to solve (3.9) is to first transform the equation, then write out C_{ijkm} as given by (D.6), and finally algebraically solve for $\widetilde{u}_i$. A straightforward but tedious calculation for an isotropic system shows,

$$\widetilde{u}_i = -\frac{i}{k^2}\left[\left(\frac{\nu}{1-\nu}\right)k_i\widetilde{\beta}^{\mathrm{P}}_{jj} + k_j\left(\widetilde{\beta}^{\mathrm{P}}_{ij} + \widetilde{\beta}^{\mathrm{P}}_{ji}\right)\right] + \frac{i}{k^4}\left(\frac{1}{1-\nu}\right)k_ik_jk_l\widetilde{\beta}^{\mathrm{P}}_{jl}\,. \tag{3.10}$$

Let us now return to the question of determining an extra displacement field $\boldsymbol{\psi}$ mentioned in the previous section. If one expresses $\boldsymbol{\beta}^{\mathrm{P}}$'s in (3.10) using (3.7), one gets

$$\widetilde{u}_i = -\frac{1}{k^2}\left\{\left(\frac{\nu}{1-\nu}\right)\varepsilon_{jlm}\frac{k_i k_l}{k^2} + \varepsilon_{ilm}\frac{k_j k_l}{k^2}\right\}\widetilde{\rho}_{mj} + \left(\frac{1}{1-\nu}\right)\frac{k_i k_j}{k^2}\widetilde{\psi}_j + \widetilde{\psi}_i. \quad (3.11)$$

For the sake of comparing, let's re-express $\widetilde{\boldsymbol{\rho}}$'s back to $\boldsymbol{\beta}^{\mathrm{P}}$'s. This becomes

$$\widetilde{u}_i = -\frac{i}{k^2}\left[\left(\frac{\nu}{1-\nu}\right)k_i\widetilde{\beta}^{\mathrm{P}}_{jj} + k_j\widetilde{\beta}^{\mathrm{P}}_{ij}\right] + \frac{i}{k^4}\left(\frac{1}{1-\nu}\right)k_i k_j k_l\widetilde{\beta}^{\mathrm{P}}_{jl} + \left(\frac{1}{1-\nu}\right)\frac{k_i k_j}{k^2}\widetilde{\psi}_j + \widetilde{\psi}_i\,. \quad (3.12)$$

Equating $\widetilde{u}_i$ in (3.10) and (3.12) gives

$$-\frac{i}{k^2}k_j\widetilde{\beta}^{\mathrm{P}}_{ji} = \left(\frac{1}{1-\nu}\right)\frac{k_i k_j}{k^2}\widetilde{\psi}_j + \widetilde{\psi}_i\,. \quad (3.13)$$

However from (3.7) and a few contractions, we know that $-\frac{i}{k^2}k_j\widetilde{\beta}^{\mathrm{P}}_{ji} = \widetilde{\psi}_i$. The condition that $\widetilde{\boldsymbol{\psi}}$ needs to satisfy in order to give a correct $\widetilde{u}$ is

$$\frac{k_i k_j}{k^2}\widetilde{\psi}_j = 0\,, \qquad \text{or} \qquad k_j\widetilde{\psi}_j = 0\,. \quad (3.14)$$

Looking back at (3.11), we see that the second to last term is zero, and ψ_j in the last term has to be divergent-free in real space. This reflects the fact that a total displacement field is defined only up to an overall translation of zero divergence.

We can now rewrite (3.11) safely as

$$\widetilde{u}_i = -\frac{1}{k^2}\left\{\left(\frac{\nu}{1-\nu}\right)\varepsilon_{jlm}\frac{k_i k_l}{k^2} + \varepsilon_{ilm}\frac{k_j k_l}{k^2}\right\}\widetilde{\rho}_{mj} + \widetilde{\psi}_i\,. \quad (3.15)$$

Once we have the total displacement field, and hence, the total distortion field, and the plastic distortion field, the elastic distortion tensor can easily be obtained by a simple subtraction.

CHAPTER 4

EVOLUTION LAW AND STRESS-FREE STATE SOLUTIONS

4.1 Energy decreasing condition and the evolution equation

A sensible evolution law for dislocation motion should make the elastic energy decrease with time. In this section, we provide the most general form of a dislocation current that allows for a decrease in energy satisfying symmetry requirements. Out of an infinite possibilities, we pick the form of $\boldsymbol{J}$ motivated by the microscopic Peach–Koehler force acting on a single dislocation.

We begin by expressing the energy decreasing condition in terms of the state variables.

4.1.1 Elastic energy and power due to dislocations inside a material

The elastic energy can be expressed in terms of the integral over a volume V of the stress contracted with the strain inside the material body:

$$\mathcal{E}_{\text{total}} = \frac{1}{2} \int_V \sigma_{ij}\, \epsilon^{\text{E}}_{ij}\, d^3\mathbf{r} \tag{4.1}$$

This equation can be expressed in terms of the total displacement field and the plastic distortion tensor in the following manner,[1]

$$\begin{aligned}
\mathcal{E}_{\text{total}} &= \frac{1}{2}\int_V \sigma_{ij}(\epsilon^{\text{T}}_{ij} - \epsilon^{\text{P}}_{ij})\, d^3\mathbf{r} \\
&= \frac{1}{2}\int_V \sigma_{ij}\frac{1}{2}\left(\frac{\partial u_j}{\partial x_i} + \frac{\partial u_i}{\partial x_j}\right) d^3\mathbf{r} - \frac{1}{2}\int_V \sigma_{ij}\,\epsilon^{\text{P}}_{ij}\, d^3\mathbf{r} \\
&= \frac{1}{2}\int_V \sigma_{ij}\,\frac{\partial u_j}{\partial x_i} d^3\mathbf{r} - \frac{1}{2}\int_V \sigma_{ij}\,\epsilon^{\text{P}}_{ij}\, d^3\mathbf{r} \\
&= \frac{1}{2}\int_{\partial V} (\hat{n}_j\sigma_{ij}) u_i dS - \frac{1}{2}\int_V \frac{\partial \sigma_{ij}}{\partial x_j}\, u_i\, d^3\mathbf{r} - \frac{1}{2}\int_V \sigma_{ij}\,\epsilon^{\text{P}}_{ij}\, d^3\mathbf{r}\,.
\end{aligned} \tag{4.2}$$

The first two terms of the last line were obtained by integrating by parts the first term of the previous line. Under the assumptions that there is no surface traction $\hat{n}_j\sigma_{ij} = 0$, and the body force is zero $\partial_j\sigma_{ij} = 0$, the elastic energy expression is reduced to

$$\mathcal{E}_{\text{total}} = -\frac{1}{2}\int_V \sigma_{ij}\,\epsilon^{\text{P}}_{ij}\, d^3\mathbf{r}\,. \tag{4.3}$$

As a remark, it is not hard to consider the elastic energy of a body in equilibrium subject to external surface tractions F_i which causes the displacement field u^0_i in the absence of plastic strains. Under such a circumstance, the elastic energy becomes

$$\mathcal{E}_{\text{ext}} = \frac{1}{2}\int_V \sigma^0_{ij}\,\frac{\partial u^0_i}{\partial x_j}\, d^3\mathbf{r} - \frac{1}{2}\int_V \sigma_{ij}\,\epsilon^{\text{P}}_{ij}\, d^3\mathbf{r}\,, \tag{4.4}$$

where $\sigma^0_{ij} = C_{ijkl}\,\partial_l u^0_k$ is the stress due to the externally imposed displacement field $\mathbf{u}^0$.

The time rate of change of elastic strain energy, or the power, can be computed from (4.1) resulting in the expression,

$$\begin{aligned}
\frac{d\mathcal{E}_{\text{total}}}{dt} &= \int_{\partial V} (\hat{n}_j\sigma_{ij})\dot{u}_i dS - \int_V \frac{\partial \sigma_{ij}}{\partial x_j}\,\dot{u}_i\, d^3\mathbf{r} - \int_V \sigma_{ij}\,\dot{\epsilon}^{\text{P}}_{ij}\, d^3\mathbf{r} \\
&= \int_{\partial V} (\hat{n}_j\sigma_{ij})\dot{u}_i dS - \int_V \frac{\partial \sigma_{ij}}{\partial x_j}\,\dot{u}_i\, d^3\mathbf{r} - \int_V \sigma_{ij}\, J_{ij}\, d^3\mathbf{r}\,,
\end{aligned} \tag{4.5}$$

[1]Consult appendix D for a brief review on the elasticity theory.

where we identify $\dot{\boldsymbol{\epsilon}}^{\mathrm{P}}$ with the dislocation flux density $\boldsymbol{J}$ introduced in the earlier chapter. The factor 1/2 in (4.2) disappears from (4.5) because

$$\frac{1}{2}\frac{d}{dt}(\sigma_{ij}\,\epsilon^{\mathrm{E}}_{ij}) = \frac{1}{2}\left(\dot{\sigma}_{ij}\,\epsilon^{\mathrm{E}}_{ij} + \sigma_{ij}\,\dot{\epsilon}^{\mathrm{E}}_{ij}\right) = \frac{1}{2}\left(\dot{\epsilon}^{\mathrm{E}}_{kl}\,C_{ijkl}\,\epsilon^{\mathrm{E}}_{ij} + \sigma_{ij}\,\dot{\epsilon}^{\mathrm{E}}_{ij}\right) = \sigma_{ij}\,\dot{\epsilon}^{\mathrm{E}}_{ij}\,.$$

Here we have used one intrinsic symmetry of C_{ijkl} namely that $C_{ijkl} = C_{klij}$. With two additional assumptions that both the traction and the body force are zero,

$$\frac{d\mathcal{E}_{\mathrm{total}}}{dt} = -\int_V \sigma_{ij}\,J_{ij}\,d^3\mathbf{r}\,. \tag{4.6}$$

4.1.2 Isotropic tensors and the energy decreasing criterion

It is possible to write down conditions on the current $\boldsymbol{J}$ that guarantees that the elastic energy of the system does not increase with time. Note that the continuity equation (2.19)

$$\frac{\partial \rho_{ij}}{\partial t} + \varepsilon_{ilm}\frac{\partial J_{mj}}{\partial x_l} = 0 \tag{2.19'}$$

relates the evolution of dislocations according to the curl of the dislocation flux. From the previous section, we derived an expression for the rate of change of the strain energy (equation 4.6). If the integrand is positive definite, or at least positive semidefinite, then the elastic energy of the system will not increase as time progresses forward.

The most obvious *ansatz* is $J_{ij} = c\,\sigma_{ij}$ for any positive real constant c. This turns out to be a special case of a more general expression:

$$J_{ij} = B_{ijkm}\sigma_{km} \tag{4.7}$$

where B_{ijkm} is a linear combination of rank-four isotropic tensors. (See appendix A.3 for a detailed discussion on general isotropic tensors.) There are three

isotropic fourth rank tensors. They can be rearranged in the following manner,

$$B_{ijkm} = c_1 \left[\frac{1}{2}(\delta_{ik}\delta_{jm} + \delta_{im}\delta_{jk}) - \frac{1}{3}\,\delta_{ij}\delta_{km}\right] + c_2\,[\delta_{ik}\delta_{jm} - \delta_{im}\delta_{jk}] + c_3\,\delta_{ij}\delta_{km}\,. \quad (4.8)$$

with some unknown constants c_1, c_2, and c_3 to be determined. Upon contracting with σ_{km}, the second term becomes identically zero which means that the c_2-term does not contribute to either the current or the strain energy, and therefore can be omitted. Following the discussion at the end of section 2.3, we can separate B_{ijkm} into two terms according to the nature of their motion:

$$B_{ijkm} = c_{\rm gl} \left[\frac{1}{2}(\delta_{ik}\delta_{jm} + \delta_{im}\delta_{jk}) - \frac{1}{3}\,\delta_{ij}\delta_{km}\right] + c_{\rm cl}\,\delta_{ij}\delta_{km} \quad (4.9)$$

The subscripts in $c_{\rm gl}$ and $c_{\rm cl}$ distinguish between the *glide* (conservative) contribution to the current from the *climb* (non-conservative) contribution. Substituting the form of $\boldsymbol{J}$ into (2.19'), we obtain our (linear) evolution equation,

$$\frac{\partial \rho_{ij}}{\partial t} = -\varepsilon_{ilm} B_{mjpq} \frac{\partial \sigma_{pq}(\boldsymbol{\rho})}{\partial x_l}\,. \quad (4.10)$$

The tensor $\boldsymbol{B}$ contributes to the most general dynamics allowed by symmetry to lowest order in $\boldsymbol{\rho}$. This equation was first derived, with $c_{\rm cl} = 0$ using a different approach by Rickman and Viñal in 1997 [58].[2] It is not enough for B_{ijkm} to be isotropic to guarantee that the elastic energy is a non-increasing function of time; the eigenvalues of B_{ijkm} needs to be at least non-negative. One can calculate the eigenvalues of B_{ijkm} by grouping the first two and the last two indices, $B_{(ij)(km)}$ to form a new 9×9 matrix. The eigenvalues are computed numerically using *Mathematica® 5.0*. Provided that $c_{\rm gl}, c_{\rm cl} \geq 0$, all eigenvalues of the 9×9 matrix

[2] In order to identify (4.10) with that of Rickman and Viñal, one needs to identify their variational derivative of Free energy F with respect to dislocation density ρ_{ij} with negative of the stress field $-\sigma_{ij}$ of the system, namely, $\delta F/\delta \rho_{at} = -\sigma_{at}$.

are non-negative. Let's denote these eigenvalues by λ^α and the corresponding eigentensor $\boldsymbol{\sigma}^\alpha$, where α runs from 1 to 9. The rate of change of the elastic energy

$$\begin{aligned}\frac{d\mathcal{E}_{\text{total}}}{dt} &= -\int_V \sigma_{ij}\, J_{ij}\, d^3\mathbf{r} \\ &= -\int_V \sigma_{ij} B_{ijkm} \sigma_{km}\, d^3\mathbf{r} \\ &= -\sum_{\alpha=1}^{9} \left[\int_V \lambda^\alpha \sigma_{ij}^\alpha\, \sigma_{ij}^\alpha\, d^3\mathbf{r}\right] \quad \leq 0\,,\end{aligned} \tag{4.11}$$

clearly shows the flow of energy down hill for all non-negative values of λ^αs.

4.1.3 Nonlinear current motivated by the Peach–Koehler interaction

The main objective in this study is to see the formation of cell structures under the motion of dislocations according to equation 2.19. Physically speaking, a dislocation current should vanish in the absence of dislocations, and the time rate of change of dislocations should depend on the number of dislocations available. Equation 4.7 seems to contradict this statement; the current depends only on the local stress of the system and not at all on the density of dislocations. Such consideration leads us to set the constraints $B_{ijkl} = 0$ and, instead, to explore the incorporation of a nonlinear term. A dislocation in the presence of a stress field feels the force called a *Peach–Koehler force*. Our nonlinear term was motivated by the form of the dislocation current for a single dislocation moving under the influence of the Peach–Koehler force.

We shall see that the Peach–Koehler dislocation current $\boldsymbol{J}^{\text{PK}}$ is cubic in $\boldsymbol{\rho}$. It is difficult to construct currents quadratic in $\boldsymbol{\rho}$ that are guaranteed to decrease the energy because the rate of change of energy (equation 4.21) is then cubic in $\boldsymbol{\rho}$; if the energy for $\boldsymbol{\rho}$ decreases with time, the (equal) energy for the (physically

rather different density) $-\boldsymbol{\rho}$ would increase. (Groma and collaborators [33, 34] have a current quadratic in $\boldsymbol{\rho}$, but they keep separate densities for positive and negative Burgers vectors and hence negative densities are not allowed in their formulation; see section 5.3.) Our closure approximation yields a theory whose current is cubic in $\boldsymbol{\rho}$ and is guaranteed to decrease the energy. The group–theory calculation shows that the most general equation cubic in $\boldsymbol{\rho}$ allowed by symmetry in an isotropic system has 15 undetermined coefficients (appendix B.2). To derive the conditions on these coefficients that guarantee that energy decreases involves a positivity condition on all the eigenvalues of a 54×54 matrix (section 4.1.5)—a nonlinear constraint problem we bypassed by choosing a microscopically motivated evolution law.

Peach and Koehler were the first to write down the formula for the force on a section of a dislocation loop due to the stress field present at that point [55],

$$f_i^{\mathrm{PK}} = -\varepsilon_{ijk} t_j b_l \sigma_{kl} \,. \tag{4.12}$$

From (2.25), the dislocation flux density of a single dislocation moving with velocity $\mathbf{v}$ reads

$$J_{ij} = \varepsilon_{ilm} t_l b_j v_m \delta^{(2)}(\boldsymbol{\xi}). \tag{2.25'}$$

Suppose the dislocation is moving in the direction of the applied force, therefore $\mathbf{v} \propto \mathbf{f}^{\mathrm{PK}}$, and

$$J_{ij} \propto \varepsilon_{imn} t_m b_j \varepsilon_{nrs} \sigma_{tr} t_s b_t \delta^{(2)}(\boldsymbol{\xi}). \tag{4.13}$$

We can then generalize this statement to

$$J_{ij} = D_{ijkmpqrs} \sigma_{pq} \rho^{(4)}_{kmrs} \,, \tag{4.14}$$

where $D_{ijkmpqrs}$ is the most general eight-index tensor that makes the energy of

the system decrease, and

$$\rho^{(4)}_{ijkm} = \sum_{\alpha} t^{\alpha}_i b^{\alpha}_j t^{\alpha}_k b^{\alpha}_m \delta^{(2)}(\xi^{\alpha}). \tag{4.15}$$

The new J_{ij} term does not close on ρ_{ij} when plugging into the continuity equation (2.19). The evolution of ρ_{ij} now depends on a new quantity $\rho^{(4)}_{ijkl}$. To have an expression which depends only on ρ_{ij}, we therefore perform a *closure approximation* similar in spirit to Hartree–Fock approximation in many-body physics, and in theories of turbulence. We would like to approximate $\rho^{(4)}_{ijkl}$ as a tensor product of two ρ_{ij}, $\boldsymbol{\rho}^{(4)} \to \boldsymbol{\rho} \otimes \boldsymbol{\rho}$. One can see from (4.15) that $\rho^{(4)}_{ijkl}$ is symmetric under interchanging $i \leftrightarrow k$, and $j \leftrightarrow m$. With these symmetries,

$$\begin{aligned} \rho^{(4)}_{ijkm} &\simeq C_1 \Big[\sum_{\alpha} t^{\alpha}_i b^{\alpha}_j \delta^{(2)}(\xi^{\alpha}) \Big] \Big[\sum_{\alpha'} t^{\alpha'}_k b^{\alpha'}_m \delta^{(2)}(\xi^{\alpha'}) \Big] \\ &\qquad + C_2 \Big[\sum_{\alpha} t^{\alpha}_i b^{\alpha}_m \delta^{(2)}(\xi^{\alpha}) \Big] \Big[\sum_{\alpha'} t^{\alpha'}_k b^{\alpha'}_j \delta^{(2)}(\xi^{\alpha'}) \Big] \\ &= C_1 \rho_{ij} \rho_{km} + C_2 \rho_{im} \rho_{kj}. \end{aligned} \tag{4.16}$$

C_1 and C_2 have units of distance. It is to be shown below that only the first term guarantees a decrease of elastic energy with time. We therefore shall omit the second term and set $C_1 \to C$. In principle C can be dislocation-dependent provided that $C(\boldsymbol{\rho})$ remains positive everywhere. For example, we can introduce a density-dependent C,

$$C(\boldsymbol{\rho}) = \frac{1}{|\boldsymbol{\rho}|} = \frac{1}{\sqrt{\rho_{ij}\rho_{ij}}}, \tag{4.17}$$

as being the inverse of an average dislocation length in the volume. (This particular choice will be discussed in sections 4.1.4 and 5.1.)

Several authors [33, 32, 34] coarse-grain their dislocation density and take a closure approximation as we do. Their closure approximation involves the long-range correlation function (which we also assume factorizes); our closure approximation

for them is trivial (because, for a single slip system, the ij piece of $\boldsymbol{\rho}^{(4)}$ in equation 4.15 factors out and $\boldsymbol{\rho}^{(4)} \propto \boldsymbol{\rho}$). In the end, their evolution law for $\boldsymbol{J}$ has one fewer factor of the dislocation density $\boldsymbol{\rho}$. While we cannot generalize their approach to the three-dimensional tensorial theory, we can reproduce their results by choosing our constant $C(\boldsymbol{\rho})$ (in equation 4.24 shown below) to be density dependent as shown above (equation 4.17) and specializing to two dimensions and one slip system.

With the addition of the nonlinear Peach–Koehler term, the new J_{ij} is of the form,

$$J_{ij} = B_{ijkm}\sigma_{km} + CD^{\mathrm{PK}}_{ijkmpqrs}\sigma_{pq}\rho_{km}\rho_{rs}\,, \tag{4.18}$$

where $\boldsymbol{D}^{\mathrm{PK}}$ for Peach–Koehler model is

$$D^{\mathrm{PK}}_{ijkmpqrs} = \frac{D}{2}\big[\delta_{iq}\delta_{jm}\delta_{kr}\delta_{ps} - \delta_{ir}\delta_{jm}\delta_{kq}\delta_{ps} - \frac{\lambda}{3}\left(\delta_{ij}\delta_{mq}\delta_{kr}\delta_{ps} - \delta_{ij}\delta_{mr}\delta_{kq}\delta_{ps}\right)\big]. \tag{4.19}$$

Here D is a materials constant with units of [length]^2[time]/[mass] giving the mobility of dislocation glide. At $\lambda = 0$ climb and glide have equal mobilities, and at $\lambda = 1$ $\boldsymbol{J}$ is traceless and, according to the discussion at the end of section 2.3, only glide is allowed.

In the case of $\boldsymbol{D}^{\mathrm{PK}}$ treating glide and climb on an equal footing, one can directly show that the elastic energy does decrease without calculating the eigenvalues. From the expression regarding the rate of change of the elastic energy (4.6), one can substitute the expression for the Peach–Koehler flux (4.19) with $\lambda = 0$,

$$J^{\mathrm{PK}}_{ij} = -\frac{CD}{2}\varepsilon_{ilm}f^{\mathrm{PK}}_{l}\rho_{mj} = \frac{CD}{2}\left(\sigma_{ic}\rho_{ac} - \sigma_{ac}\rho_{ic}\right)\rho_{aj}\,, \tag{4.20}$$

to get

$$\frac{d\mathcal{E}_{\mathrm{total}}}{dt} = -\frac{CD}{2}\int_V \left(\sigma_{ij}\sigma_{ic}\rho_{ac}\rho_{aj} - \sigma_{ij}\sigma_{ac}\rho_{ic}\rho_{aj}\right)\, d^3\mathbf{r}\,. \tag{4.21}$$

Next, let's call $\Gamma_{ij} \equiv \sigma_{ic}\rho_{jc}$, then the integrand becomes simply $(CD/2)\,\Gamma_{ia}(\Gamma_{ia} - \Gamma_{ai})$. Since the sums are taken over all a and i, consider the sum of the pair (a,i) and (i,a),

$$CD(\Gamma_{ia}\Gamma_{ia} + \Gamma_{ai}\Gamma_{ai} - \Gamma_{ia}\Gamma_{ai} - \Gamma_{ai}\Gamma_{ia}) = CD\,(\Gamma_{ia} - \Gamma_{ai})^2 \geq 0\,. \tag{4.22}$$

This is true for each fixed (a,i) and (i,a). Therefore

$$\frac{d\mathcal{E}_{\text{total}}}{dt} = -CD \sum_{a,i=1}^{3} \int_V (\Gamma_{ia} - \Gamma_{ai})^2\, d^3\mathbf{r} \leq 0\,. \tag{4.23}$$

We note in passing that a general case allowing for an arbitrary value of λ is much more complicated and the energy minimization has not been shown analytically. The continuity equation (2.19) together with the Peach–Koehler motivated current $\boldsymbol{J}^{\text{PK}}$ form the basis of our evolution law:

$$\frac{\partial \rho_{ij}}{\partial t} + \varepsilon_{ilm}\frac{\partial J^{\text{PK}}_{mj}}{\partial x_l} = 0 \tag{2.19'}$$

$$J_{ij} = \frac{C(\boldsymbol{\rho})D}{2}\Big[\,(\sigma_{ic}\rho_{ac} - \sigma_{ac}\rho_{ic})\,\rho_{aj} - \frac{\lambda}{3}\,\delta_{ij}\,(\sigma_{kc}\rho_{ac} - \sigma_{ac}\rho_{kc})\,\rho_{ak}\Big] \tag{4.24}$$

4.1.4 Simple derivation of $\boldsymbol{J}^{\text{PK}}$ by Roy & Acharya

The form of the current (equation 4.20) for $\lambda = 0$ (both glide and climb) has a simple interpretation due to Roy & Acharya [38]. The Peach–Koehler force density on $\boldsymbol{\rho}$ in the local volume (from equation 2.25) is

$$f^{\text{PK}}_l = -\varepsilon_{lmn}\sum_{\alpha} t^{\alpha}_m b^{\alpha}_c \sigma_{nc} = -\varepsilon_{lmn}\rho_{mc}\sigma_{nc}\,. \tag{4.25}$$

The current due to a single dislocation moving with velocity v is $J^{\text{single}}_{ij} = \varepsilon_{ial}t_a b_j v_l \delta^{(2)}(\boldsymbol{\xi})$ (equation 2.25). We introduced a density–dependent function

$$C(\boldsymbol{\rho}) = \frac{1}{|\boldsymbol{\rho}|} = \frac{1}{\sqrt{\rho_{ij}\rho_{ij}}} \tag{4.17'}$$

in our closure approximation to reproduce the closure approximations developed recently for single slip systems; we can think of $C(\boldsymbol{\rho})$ as being the inverse of an average dislocation length in the volume. If we assume that the velocity of each dislocation in the volume is proportional to the average force per unit length on the dislocations in that volume $v_l = (DC_l(\boldsymbol{\rho})/2)f_l^{\mathrm{PK}}$, we find

$$J_{ij}^{\mathrm{RA}} = \frac{D}{2}\varepsilon_{ial}f_l^{\mathrm{PK}}\rho_{aj} = \frac{D}{2}\varepsilon_{ial}(-C(\boldsymbol{\rho})\varepsilon_{lmn}\rho_{mc}\sigma_{nc})\rho_{aj} = \frac{C(\boldsymbol{\rho})D}{2}(\sigma_{ic}\rho_{ac} - \sigma_{ac}\rho_{ic})\rho_{aj} \tag{4.26}$$

reproducing the result of our energy–decreasing closure approximation (equation 4.20).

4.1.5 Other possible choices for $\boldsymbol{D}$'s

Can we explore more general forms for the current $\boldsymbol{J}$, beyond the Peach–Koehler motivated choice in section 4.1.3? We argued in section 5.1 that currents $\boldsymbol{J}$ that are quadratic in $\boldsymbol{\rho}$ would not flow to decrease the energy. But what other theories cubic in $\boldsymbol{\rho}$ are possible? What other choices for the tensor $\boldsymbol{D}$ will lead to energy decreasing? In this section, we formulate the criteria for this more general theory, but do not solve it.

There are 91 linearly independent isotropic tensors $D_{ijkmpqrs}$ of eighth rank out of the possible 105 fundamental isotropic tensors constructed from all possible combinations of products of Kronecker delta's [59]. Only fifteen of these, however, satisfy the imposed symmetries.[3] The antisymmetric terms that do not meet the symmetry requirements are projected out in the power expression (4.6), even though they may be responsible for the evolution of dislocations.[4] To list all the

[3]For the detailed calculation, please refer to appendix B

[4]To illustrate this point, note that the dislocation flux density J_{ij} is in general not a symmetric tensor. However only the symmetric piece contributes to the

symmetries, let's first take a look at the second term of (4.18),

$$J_{ij}^{\mathrm{II}} = C D_{ijkmpqrs} \sigma_{pq} \rho_{km} \rho_{rs} \,. \tag{4.27}$$

The two stress indices p and q are interchangeable. From the two $\boldsymbol{\rho}$'s retaining the decomposition in (4.16), we can pairwise interchange $(k, m) \leftrightarrow (r, s)$ so that

$$D_{ijkmpqrs} = D_{ijkmqprs} = D_{ijrspqkm} \,. \tag{4.28}$$

Additional symmetries are taken from the power integral,

$$\frac{d\mathcal{E}_{\mathrm{total}}^{\mathrm{II}}}{dt} = -C \int_V D_{ijkmpqrs} \sigma_{ij} \rho_{km} \sigma_{pq} \rho_{rs} \, d^3\mathbf{r} \,. \tag{4.29}$$

Interchanging both the other two stress indices $i \leftrightarrow j$ and the two $\boldsymbol{\sigma}$'s immediately yields

$$D_{ijkmpqrs} = D_{jikmpqrs} = D_{pqkmijrs} \,. \tag{4.30}$$

The most general isotropic tensor of rank eight that meets the above requirements is given in table 4.1 as a reference.

As for the fourth rank tensor $\boldsymbol{B}$, there are non-trivial conditions on $\boldsymbol{D}$ needed to ensure that the energy decreases with time. We proceed in the same spirit as we did with the analysis of tensor $\boldsymbol{B}$ at the end of section 4.1.2. The indices of $\boldsymbol{D}$ are arranged in such a way that it is convenient to convert a given eighth rank expression for the elastic power,

$$\frac{d\mathcal{E}_{\mathrm{total}}}{dt} = -\int_V \sigma_{ij} J_{ij} \, d^3\mathbf{r} \,, \tag{4.6'}$$

because σ_{ij} is symmetric and therefore if one decomposes J_{ij} into symmetric and antisymmetric pieces, $J_{ij} = J_{ij}^{\mathrm{S}} + J_{ij}^{\mathrm{A}}$, then

$$\sigma_{ij} J_{ij}^{\mathrm{A}} = -\sigma_{ji} J_{ji}^{\mathrm{A}} = -\sigma_{ij} J_{ij}^{\mathrm{A}} = 0 \,,$$

and therefore, $\sigma_{ij} J_{ij} = \sigma_{ij} J_{ij}^{\mathrm{S}}$.

Table 4.1: The eighth-rank isotropic tensor with the required symmetries comprises fifteen terms.

$$
\begin{aligned}
D_{ijkmpqrs} = \quad & d_1\,\delta_{ij}\delta_{km}\delta_{pq}\delta_{rs} + d_2\,\delta_{ij}\delta_{pq}\delta_{kr}\delta_{ms} + d_3\,\delta_{ij}\delta_{pq}\delta_{mr}\delta_{ks} \\
& + \frac{d_4}{2}\left(\delta_{km}\delta_{jp}\delta_{iq}\delta_{rs} + \delta_{km}\delta_{ip}\delta_{jq}\delta_{rs}\right) \\
& + \frac{d_5}{2}\left(\delta_{jp}\delta_{iq}\delta_{kr}\delta_{ms} + \delta_{ip}\delta_{jq}\delta_{kr}\delta_{ms}\right) \\
& + \frac{d_6}{2}\left(\delta_{jp}\delta_{iq}\delta_{mr}\delta_{ks} + \delta_{ip}\delta_{jq}\delta_{mr}\delta_{ks}\right) \\
& + \frac{d_7}{4}\left(\delta_{jm}\delta_{pq}\delta_{kr}\delta_{is} + \delta_{im}\delta_{pq}\delta_{kr}\delta_{js} + \delta_{ij}\delta_{mq}\delta_{kr}\delta_{ps} + \delta_{ij}\delta_{mp}\delta_{kr}\delta_{qs}\right) \\
& + \frac{d_8}{4}\left(\delta_{jk}\delta_{pq}\delta_{ir}\delta_{ms} + \delta_{ik}\delta_{pq}\delta_{jr}\delta_{ms} + \delta_{ij}\delta_{kq}\delta_{pr}\delta_{ms} + \delta_{ij}\delta_{kp}\delta_{qr}\delta_{ms}\right) \\
& + \frac{d_9}{8}\left(\delta_{km}\delta_{pq}\delta_{jr}\delta_{is} + \delta_{km}\delta_{pq}\delta_{ir}\delta_{js} + \delta_{ij}\delta_{km}\delta_{qr}\delta_{ps} + \delta_{ij}\delta_{km}\delta_{pr}\delta_{qs}\right. \\
& \qquad \left. + \delta_{ij}\delta_{mp}\delta_{kq}\delta_{rs} + \delta_{ij}\delta_{kp}\delta_{mq}\delta_{rs} + \delta_{jk}\delta_{im}\delta_{pq}\delta_{rs} + \delta_{ik}\delta_{jm}\delta_{pq}\delta_{rs}\right) \\
& + \frac{d_{10}}{8}\left(\delta_{mp}\delta_{kq}\delta_{jr}\delta_{is} + \delta_{kp}\delta_{mq}\delta_{jr}\delta_{is} + \delta_{mp}\delta_{kq}\delta_{ir}\delta_{js} + \delta_{kp}\delta_{mq}\delta_{ir}\delta_{js}\right. \\
& \qquad \left. + \delta_{jk}\delta_{im}\delta_{qr}\delta_{ps} + \delta_{ik}\delta_{jm}\delta_{qr}\delta_{ps} + \delta_{jk}\delta_{im}\delta_{pr}\delta_{qs} + \delta_{ik}\delta_{jm}\delta_{pr}\delta_{qs}\right) \\
& + \frac{d_{11}}{8}\left(\delta_{jk}\delta_{pq}\delta_{mr}\delta_{is} + \delta_{ik}\delta_{pq}\delta_{mr}\delta_{js} + \delta_{jm}\delta_{pq}\delta_{ir}\delta_{ks} + \delta_{im}\delta_{pq}\delta_{jr}\delta_{ks}\right. \\
& \qquad \left. + \delta_{ij}\delta_{mq}\delta_{pr}\delta_{ks} + \delta_{ij}\delta_{mp}\delta_{qr}\delta_{ks} + \delta_{ij}\delta_{kq}\delta_{mr}\delta_{ps} + \delta_{ij}\delta_{kp}\delta_{mr}\delta_{qs}\right) \\
& + \frac{d_{12}}{8}\left(\delta_{jm}\delta_{kq}\delta_{pr}\delta_{is} + \delta_{jm}\delta_{kp}\delta_{qr}\delta_{is} + \delta_{im}\delta_{kq}\delta_{pr}\delta_{js} + \delta_{im}\delta_{kp}\delta_{qr}\delta_{js}\right. \\
& \qquad \left. + \delta_{jk}\delta_{mq}\delta_{ir}\delta_{ps} + \delta_{ik}\delta_{mq}\delta_{jr}\delta_{ps} + \delta_{jk}\delta_{mq}\delta_{ir}\delta_{qs} + \delta_{ik}\delta_{mp}\delta_{jr}\delta_{qs}\right) \\
& + \frac{d_{13}}{8}\left(\delta_{mp}\delta_{jq}\delta_{kr}\delta_{is} + \delta_{jp}\delta_{mq}\delta_{kr}\delta_{is} + \delta_{mp}\delta_{iq}\delta_{kr}\delta_{js} + \delta_{ip}\delta_{mq}\delta_{kr}\delta_{js}\right. \\
& \qquad \left. + \delta_{jm}\delta_{iq}\delta_{kr}\delta_{ps} + \delta_{im}\delta_{jq}\delta_{kr}\delta_{ps} + \delta_{jm}\delta_{ip}\delta_{kr}\delta_{qs} + \delta_{im}\delta_{jp}\delta_{kr}\delta_{qs}\right) \\
& + \frac{d_{14}}{8}\left(\delta_{jk}\delta_{mq}\delta_{pr}\delta_{is} + \delta_{jk}\delta_{mp}\delta_{qr}\delta_{is} + \delta_{ik}\delta_{mq}\delta_{pr}\delta_{js} + \delta_{ik}\delta_{mp}\delta_{qr}\delta_{js}\right. \\
& \qquad \left. + \delta_{jm}\delta_{kq}\delta_{ir}\delta_{ps} + \delta_{im}\delta_{kq}\delta_{jr}\delta_{ps} + \delta_{jm}\delta_{kp}\delta_{ir}\delta_{qs} + \delta_{im}\delta_{kp}\delta_{jr}\delta_{qs}\right) \\
& + \frac{d_{15}}{8}\left(\delta_{kp}\delta_{jq}\delta_{ir}\delta_{ms} + \delta_{jp}\delta_{kq}\delta_{ir}\delta_{ms} + \delta_{kp}\delta_{iq}\delta_{jr}\delta_{ms} + \delta_{ip}\delta_{kq}\delta_{jr}\delta_{ms}\right. \\
& \qquad \left. + \delta_{jk}\delta_{iq}\delta_{pr}\delta_{ms} + \delta_{ik}\delta_{jq}\delta_{pr}\delta_{ms} + \delta_{jk}\delta_{ip}\delta_{qr}\delta_{ms} + \delta_{ik}\delta_{jp}\delta_{qr}\delta_{ms}\right)
\end{aligned}
$$

tensor $\boldsymbol{D}$ to an 81×81 matrix by grouping the first and last four indices together to make $D_{(ijkm)(pqrs)}$. The resulting matrix is to be calculated its eigenvalues. The rate of change of the elastic energy in this case can be written in the following manner

$$\begin{aligned}\frac{d\mathcal{E}_{\text{total}}}{dt} &= -\int_V \sigma_{ij}\, J_{ij}\, d^3\mathbf{r} \\ &= -C\int_V [\sigma\rho]_{(ijkm)} D_{(ijkm)(pqrs)} [\sigma\rho]_{(pqrs)}\, d^3\mathbf{r} \\ &= -C\sum_{\alpha=1}^{81}\left[\int_V \lambda^\alpha [\sigma\rho]^\alpha_{(ijkm)}\, [\sigma\rho]^\alpha_{(ijkm)}\, d^3\mathbf{r}\right] \quad \le 0\,,\end{aligned} \tag{4.31}$$

provided that all the eigenvalues λ^α's of $D_{(ijkm)(pqrs)}$ are either positive or zero. Here we treat $[\sigma\rho]_{(ijkm)}$ as an 81 vector, while the superscript $[\cdot]^\alpha$ indicates that this vector is the eigenvector corresponding to the eigenvalue λ^α. The eigenvalues of the Peach–Koehler $\boldsymbol{D}^{\text{PK}}$ for an arbitrary $\lambda \neq 0$ introduced in the previous section are computed numerically using *Mathematica® 5.0* to give 54 positive reals and 27 zeros.

In general, the task of finding all the eigenvalues of an 81×81 matrix with 15 parameters can be daunting.[5] If one randomly assigns values into each parameter and finds the eigenvalues numerically, one would discovers that there will almost always be at least 27 zero eigenvalues.[6] The reason for this lies in the symmetry

[5]There is perhaps an easier method to ensure whether or not a Hermitian matrix $\boldsymbol{A}$ is positive semidefinite. A set of necessary and sufficient conditions for a quadratic form $(\mathbf{x}, \boldsymbol{A}\mathbf{x})$ to be positive semidefinite is if all the principal minors in the top-left corner of $\boldsymbol{A}$ are non-negative, in other words

$$A_{11} \ge 0, \qquad \begin{vmatrix} A_{11} & A_{12} \\ A_{21} & A_{22} \end{vmatrix} \ge 0, \qquad \begin{vmatrix} A_{11} & A_{12} & A_{13} \\ A_{21} & A_{22} & A_{23} \\ A_{31} & A_{32} & A_{33} \end{vmatrix} \ge 0, \qquad \ldots \quad [60,\, 61]. \tag{4.32}$$

With this method, we still need to solve, at best, a system of 54 inequalities. (See the discussion that follows.)

[6]Additional symmetries can result in more zero eigenvalues, *e.g.*, when one or

of stress field $\boldsymbol{\sigma}$. The 27 zeros represent the unphysical antisymmetric piece of $\boldsymbol{\sigma}$ which naturally gets projected away. Out of the nine elements, only six of these are independent. Therefore one can reduce the representation of the product $\boldsymbol{\sigma} \otimes \boldsymbol{\rho}$ as a 54 vector instead of an 81 vector. This means that the actual independent representation is a 54×54 matrix, which in general gives 54 distinct eigenvalues.

4.2 Stress-free dislocation densities

A crucial aspect of dislocation evolution, and a key prediction of our dynamical theory, is the formation of grain boundaries and cell walls. Microscopically, the anisotropic, long–range interaction between dislocations can be minimized and screened by the arrangement of dislocation lines into walls. A flat grain boundary will be stress-free at long distances if it satisfies the Frank condition. A general stress-free wall in our notation has

$$\rho_{ij}^{\mathrm{SF}} = [\theta_i n_j - \theta_k n_k \delta_{ij}]\, \delta(n_m(x_m - \Delta_m)). \tag{4.33}$$

This is a boundary that is perpendicular to $\mathbf{n}$ (lying along $\mathbf{n} \cdot (\mathbf{x} - \boldsymbol{\Delta}) = 0$) with grain misorientation $\boldsymbol{\theta}$ (rotating around $\hat{\theta}$ by a small angle $|\boldsymbol{\theta}|$). The derivation is given in section 5.4.

Microscopically, these ideal walls have a stress field which decays exponentially with distance away from the wall (reminiscent of the Meissner effect [62]), with a characteristic decay length that is roughly the spacing d between the dislocations composing the wall. To see this, consider the energy of a single edge dislocation per unit length [63]

$$E = \frac{Gb^2}{4\pi(1-\nu)} \ln\!\left(\frac{r}{b}\right) + B_e\,, \tag{4.34}$$

more of the 15 parameters are zero. The chance of this to happen is infinitesimal provided that the parameters are chosen completely at random.

where G is the shear modulus, b is the magnitude of the Burgers vector of the dislocation, ν is Poisson's ratio, r is the distance to which the elastic distortion produced by the dislocation reaches, and B_e is the core energy of the edge dislocation. When a dislocation lies in an array forming a boundary, the elastic strain vanishes exponentially at distances greater than the separation d between similar dislocations in the boundary, so $r \sim d$. The relation between the orientation difference θ of the two crystals and the number of dislocations per unit length can be determined geometrically (see figure 4.1):

$$n = \frac{1}{d} = \frac{1}{b}\sin\theta \approx \frac{\theta}{b} \tag{4.35}$$

(This is the Frank condition in disguise.) Therefore the interface energy per unit area is

$$E_{\text{bdry}} = \frac{1}{d}E = \frac{Gb\theta}{4\pi(1-\nu)}\ln\left(\frac{1}{\theta}\right) + \frac{\theta}{b}B_e = E_0\theta(A - \ln\theta), \tag{4.36}$$

where $E_0 = Gb/(4\pi(1-\nu))$ and $A = 4\pi(1-\nu)B_e/Gb^2$. The same equation holds for a twist boundary but with $E_0 = Gb/2\pi$ and $A = 2\pi B_s/Gb^2$. Therefore

$$E_{\text{bdry}} \sim -b\,\theta\ln(\theta/\theta_0) \tag{4.37}$$

where θ_0 can be used to incorporate the core energy of the dislocations. This strain energy vanishes in our continuum limit where $b \to 0$ and $d \to 0$ in such a way that $b/d \sim \theta$ stays fixed.

Hence, it is *not* energetically favorable for a wall to be sharp within our continuum theory. A continuous superposition of low angle boundaries wall is as good a candidate to be a cell wall or a grain boundary as a sharp wall. Blurry walls, however, are not observed in our simulations. The mechanism which is responsible for the sharp feature of walls therefore cannot be energetics. The reason turns out to lie in the nonlinear nature of our evolution law. The analysis of why sharp

cellular/grain walls form is one of the key results of our theory and is the subject of discussion in chapter 6.

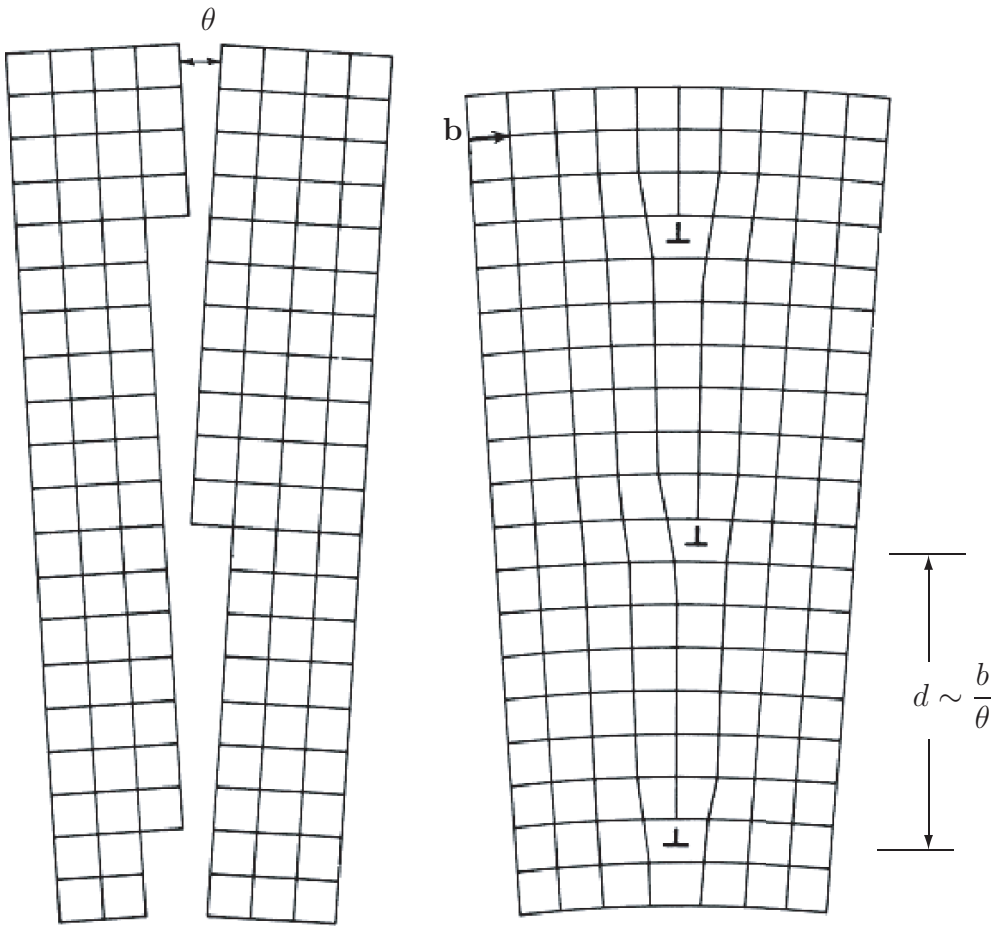

Figure 4.1: Two patches of crystal one tilted with an angle θ with respect to the other are joined together by a parallel set of edge dislocations making a tilt boundary.

In this section, we show that *any stress-free state can be written as a superposition of flat cell walls*. Every cell wall or grain boundary can be decomposed into two types: tilt and twist boundaries [64]. A simple *tilt boundary* is one at which the orientation difference between the two crystals, one on either side of the boundary, is equal to a rotation about an axis which lies in the plane of the

boundary. This can be constructed from a series of regularly spaced parallel edge dislocations because in every row above each dislocation line, there must be one more atom than the row below it.

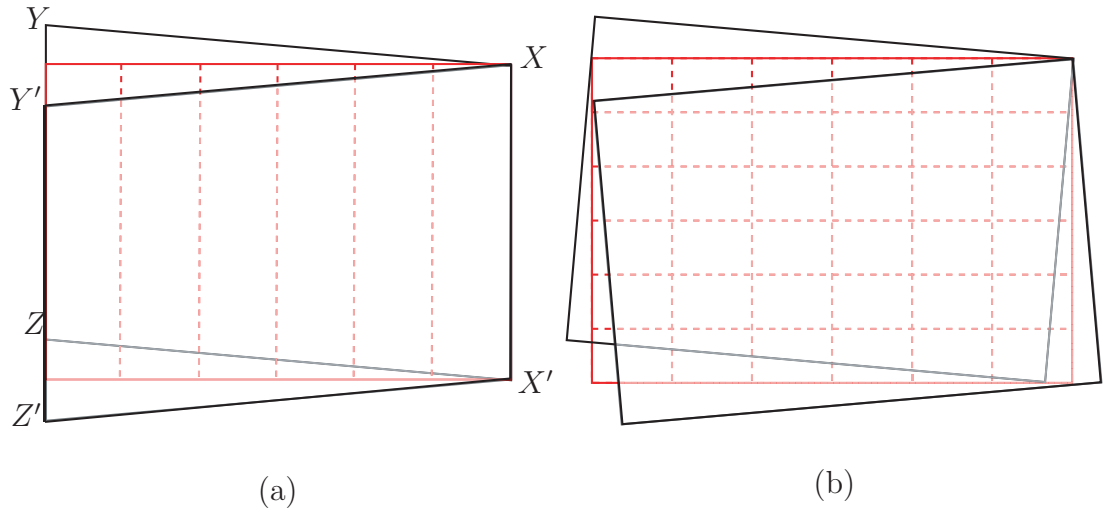

Figure 4.2: (a) A simple shear due to one parallel set of screw dislocations. (b) A twist boundary is formed from two parallel sets of screw dislocations making a 90° angle relative to one another.

A set of parallel screw dislocations (figure 4.2(a)) produces shear in the position $XYZX'$ relative to $XY'Z'X'$. To cancel the effect of this shear, another set of parallel screw dislocations at right angles to the first set is needed (figure 4.2(b)). This results in a net rotation where the axis of rotation is perpendicular to the common plane shared by the two crystals. This type of boundary is called a *twist boundary*.

4.2.1 Basis tensors for the stress-free dislocation state

From the previous section we observe that a stress-free dislocation configuration is a stationary-state solution to the evolution equation. Therefore it is interesting to systematically write out all possible stationary solutions. This problem is

equivalent to finding all the basis matrices that span the null space of operator $\boldsymbol{K}$ in

$$\widetilde{\sigma}_{\alpha\beta}(\mathbf{k}) = K_{\alpha\beta\mu\nu}(\mathbf{k})\widetilde{\rho}_{\mu\nu}(\mathbf{k})\,, \tag{3.3'}$$

where

$$K_{\alpha\beta\mu\nu}(\mathbf{k}) = -\frac{i\mu k_\gamma}{k^2}\left[\varepsilon_{\gamma\nu\alpha}\delta_{\beta\mu} + \varepsilon_{\gamma\nu\beta}\delta_{\alpha\mu} + \frac{2\varepsilon_{\gamma\nu\mu}}{1-\nu}\left(\frac{k_\alpha k_\beta}{k^2} - \delta_{\alpha\beta}\right)\right].$$

The solution also has to satisfy the continuity of the dislocation lines, which in Fourier space looks like

$$ik_i\widetilde{\rho}_{ij} = 0\,. \tag{4.38}$$

The easiest way is to write out the system of equations which incorporate both setting $K_{ijkm}\widetilde{\rho}_{km} = 0$ and $ik_i\widetilde{\rho}_{ij} = 0$.

Component-wise, the solutions are

$$\begin{aligned}
&\widetilde{\rho}_{xx} = -\frac{k_y}{k_z}\widetilde{\rho}_{yz} - \frac{k_z}{k_y}\widetilde{\rho}_{zy}\,, \quad \widetilde{\rho}_{yy} = -\frac{k_x}{k_z}\widetilde{\rho}_{xz} - \frac{k_z}{k_y}\widetilde{\rho}_{zy}\,, \quad \widetilde{\rho}_{zz} = -\frac{k_x}{k_z}\widetilde{\rho}_{xz} - \frac{k_y}{k_z}\widetilde{\rho}_{yz}\,,\\
&\widetilde{\rho}_{xy} = \frac{k_y}{k_z}\widetilde{\rho}_{xz}\,, \qquad\qquad \widetilde{\rho}_{yx} = \frac{k_x}{k_z}\widetilde{\rho}_{yz}\,, \qquad\qquad \widetilde{\rho}_{zx} = \frac{k_x}{k_y}\widetilde{\rho}_{zy}\,.
\end{aligned} \tag{4.39}$$

The matrix $\boldsymbol{K'}$, whose null space gives a complete collection of stress-free dislocation states, is formed by arbitrary substitutions of values into $\widetilde{\rho}_{xz}$, $\widetilde{\rho}_{yz}$, and $\widetilde{\rho}_{zy}$.

$$\boldsymbol{K'} = \begin{pmatrix}
1 & 0 & 0 & 0 & 0 & \frac{k_y}{k_z} & 0 & \frac{k_z}{k_y} & 0\\
0 & 0 & \frac{k_x}{k_z} & 0 & 1 & 0 & 0 & \frac{k_z}{k_y} & 0\\
0 & 0 & \frac{k_x}{k_z} & 0 & 0 & \frac{k_y}{k_z} & 0 & 0 & 1\\
0 & 1 & -\frac{k_y}{k_z} & 0 & 0 & 0 & 0 & 0 & 0\\
0 & 0 & 0 & 1 & 0 & -\frac{k_x}{k_z} & 0 & 0 & 0\\
0 & 0 & 0 & 0 & 0 & 0 & 1 & -\frac{k_x}{k_y} & 0
\end{pmatrix} \tag{4.40}$$

The nine numbers in each line represent the nine components of a 3×3 tensor. With the explicit form of $\boldsymbol{K}'$, getting its null space is an exercise in linear algebra. Since any given $\widetilde{\boldsymbol{\rho}}$ has nine components, and only six constraints, three basis tensors are expected . We label them $\boldsymbol{E}^x, \boldsymbol{E}^y$ and $\boldsymbol{E}^z$.

$$\boldsymbol{E}^x = \begin{pmatrix} 0 & ik_y & ik_z \\ 0 & -ik_x & 0 \\ 0 & 0 & -ik_x \end{pmatrix}, \boldsymbol{E}^y = \begin{pmatrix} -ik_y & 0 & 0 \\ ik_x & 0 & ik_z \\ 0 & 0 & -ik_y \end{pmatrix}, \boldsymbol{E}^z = \begin{pmatrix} -ik_z & 0 & 0 \\ 0 & -ik_z & 0 \\ ik_x & ik_y & 0 \end{pmatrix}. \tag{4.41}$$

Or simply:

$$\boxed{E^\alpha_{ij} = -ik_\alpha \delta_{ij} + ik_j \delta_{i\alpha} = ik_l \varepsilon_{ilm} \varepsilon_{j\alpha m}} \tag{4.42}$$

Direct substitutions of the form of $\boldsymbol{E}^\alpha$ in place of $\widetilde{\boldsymbol{\rho}}$ show that (3.3') and (4.38) are simultaneously satisfied for all values of α. The reason for including the imaginary number i into the expression for $\boldsymbol{E}^\alpha$ is a matter of convention and convenience.

4.2.2 Decompositions of a stress free state

These three basis tensors naturally give rise to the two types of cell wall structures discussed earlier. As an example, consider a tilt boundary in the x-y plane constructed from a set of parallel dislocation lines pointing along the $\hat{\mathbf{x}}$ direction with the Burgers vector $\mathbf{b}$ pointing along the $\hat{\mathbf{z}}$ direction. The number of dislocation lines per unit length is denoted by n. To make a plane in real space, we need two δ-functions in Fourier space. The boundary can be written as

$$\widetilde{\boldsymbol{\rho}}^{\text{tilt}} = \frac{nb}{ik_z}\, \delta(k_x)\delta(k_y) \boldsymbol{E}^x = nb\, \delta(k_x)\delta(k_y) \begin{pmatrix} 0 & 0 & 1 \\ 0 & 0 & 0 \\ 0 & 0 & 0 \end{pmatrix}. \tag{4.43}$$

Another example, a twist boundary in the x-y plane generated by two sets of parallel dislocations oriented perpendicular to one another, one pointing in the $\hat{\mathbf{x}}$ direction while another pointing in the $\hat{\mathbf{y}}$ direction can be written simply as

$$\begin{aligned}\widetilde{\boldsymbol{\rho}}^{\text{twist}} &= -\frac{nb}{ik_z}\,\delta(k_x)\delta(k_y)\boldsymbol{E}^z = nb\,\delta(k_x)\delta(k_y)\begin{pmatrix}1&0&0\\0&1&0\\0&0&0\end{pmatrix},\\ &= nb\,\delta(k_x)\delta(k_y)\left[\begin{pmatrix}1\\0\\0\end{pmatrix}\otimes\begin{pmatrix}1\\0\\0\end{pmatrix}+\begin{pmatrix}0\\1\\0\end{pmatrix}\otimes\begin{pmatrix}0\\1\\0\end{pmatrix}\right].\end{aligned} \tag{4.44}$$

The fact that one needs two perpendicular sets of parallel dislocations comes out naturally in this formulation. Because the number densities of the screw dislocations are the same in both directions, n here denotes the number density in one of the two directions.

Utilizing the three basis matrices derived in the previous section, it is possible to write down any type of grain boundary as a superposition of the two or more types of fundamental boundaries (twist and tilt) rotated and translated by some specific amounts. The most general form of a stress-free boundary can be written as follows,

$$\widetilde{\rho}_{ij}^{\text{GB}}[\mathbf{k},\boldsymbol{\omega},\Omega,\boldsymbol{\Delta}] = (2\pi)^2\,\frac{\delta(R_{xp}^{-1}k_p)\delta(R_{yq}^{-1}k_q)}{iR_{zr}^{-1}k_r}\,\omega_n E_{ij}^n\,\mathrm{e}^{-i\mathbf{k}\cdot\boldsymbol{\Delta}}\,, \tag{4.45}$$

where

$$\begin{aligned}\boldsymbol{R}^{-1}[\Omega=(\theta,\phi)] &= [\boldsymbol{R}_{\hat{\mathbf{z}}}(\phi)\cdot\boldsymbol{R}_{\hat{\mathbf{y}}}(-\theta)]^{-1}\\ &= \begin{pmatrix}\cos(\theta)\cos(\phi) & \cos(\theta)\sin(\phi) & -\sin(\theta)\\ -\sin(\phi) & \cos(\phi) & 0\\ \sin(\theta)\cos(\phi) & \sin(\theta)\sin(\phi) & \cos(\theta)\end{pmatrix}\end{aligned} \tag{4.46}$$

is the inverse of a three-dimensional rotation obtained by first rotating about $\hat{\mathbf{y}}$-axis by $-\theta$, then about $\hat{\mathbf{z}}$ by ϕ. θ and ϕ define a unit vector $\hat{\mathbf{n}}$ normal to the plane of the boundary. The angle θ is measured with respect to $\hat{\mathbf{z}}$, while ϕ is the angle between $\hat{\mathbf{x}}$ and the projection of $\hat{\mathbf{n}}$ onto the x-y plane. The boundary separates two grains where their relative rotation is defined by $\boldsymbol{\omega}$ whose magnitude expresses the amount by which one is rotated with respect to the other. $\boldsymbol{\Delta}$ is the vector pointing from the origin to the plane of the boundary perpendicularly. The connection between our formulation with the well-established Frank condition of a general five-parameter grain boundary shall be discussed in section 5.4.

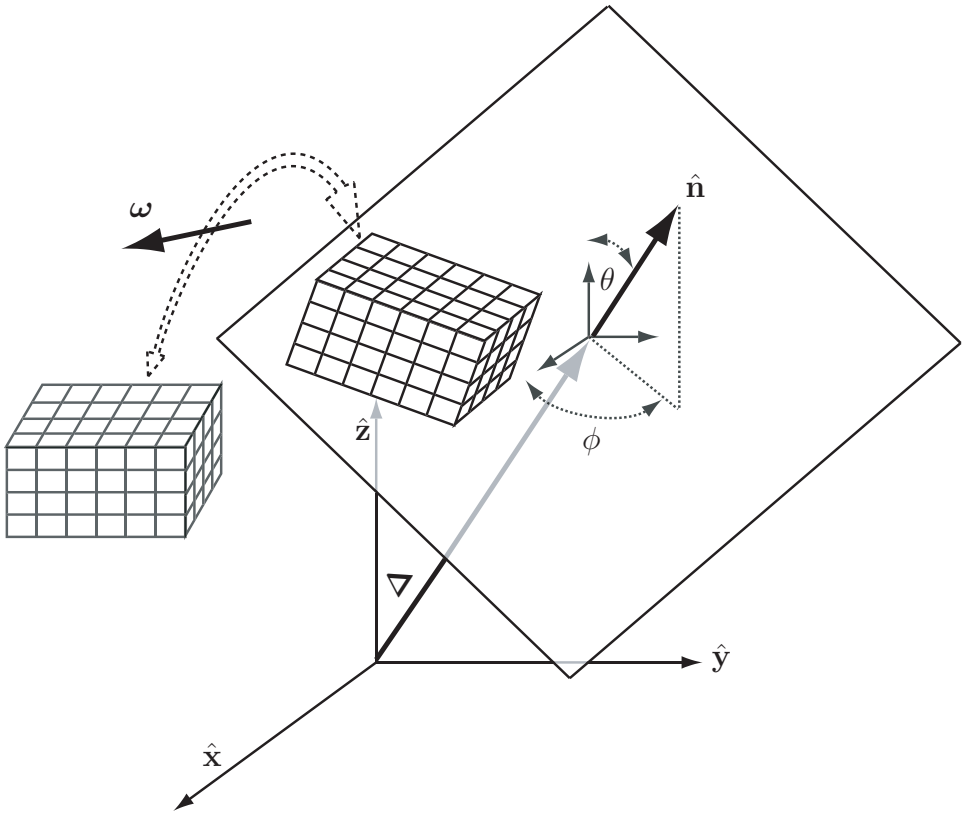

Figure 4.3: A general grain boundary whose normal is $\hat{\mathbf{n}}$ positioned at the distance $\boldsymbol{\Delta}$ away from the origin separates two unstrained regions with a relative orientation defined by $\boldsymbol{\omega}$.

To take this one step further, since it is possible to decompose any stress-free state into a linear combination of the tensor $\boldsymbol{E}^{\alpha}$, it should also be possible to write a stress-free state as a superposition of flat cell walls.

Theorem 1 *Any stress-free state $\widetilde{\boldsymbol{\rho}}^{SF}$ can be written as a superposition of flat cell walls. Or more precisely,*

$$\widetilde{\rho}_{ij}^{SF}(\mathbf{k}) = \widetilde{\Lambda}^{l}(\mathbf{k}) E_{ij}^{l} = \int_{-\infty}^{\infty} d\Delta \int d\Omega \int d^{3}\boldsymbol{\omega} \, \left(a[\mathbf{k}, \boldsymbol{\omega}, \Omega, \Delta] \cdot \widetilde{\rho}_{ij}^{GB}[\mathbf{k}, \boldsymbol{\omega}, \Omega, \boldsymbol{\Delta}] \right), \tag{4.47}$$

where $\widetilde{\rho}_{ij}^{GB}$ is as previously defined, and

$$\begin{aligned} a[\mathbf{k}, \boldsymbol{\omega}, \Omega, \Delta] = & \frac{i\,\omega_{l}}{(2\pi)^{3}\pi^{3/2}} \, \mathrm{e}^{-|\boldsymbol{\omega}|^{2}} \\ & \times \int_{-\infty}^{\infty} dk' \, k'^{3} \widetilde{\Lambda}^{l} \left[\{ k' \sin(\theta)\cos(\phi), k' \sin(\theta)\sin(\phi), k' \cos(\theta) \} \right] \mathrm{e}^{ik'\Delta}. \end{aligned} \tag{4.48}$$

To get a general stress-free dislocation distribution, one needs to integrate over the five degrees of freedom, plus the position of each grain component. An interested reader can see the proof of the theorem and some examples in appendix E. One can group the coefficients in front of each E_{ij}^{l} in the decomposition to form a vector $\widetilde{\Lambda}^{l}(\mathbf{k})$ which turns out to be a valid vector field (*i.e.* $\widetilde{\boldsymbol{\Lambda}}$ transforms like a vector). This vector will play a special role in determining the grain orientation inside each cell.

4.2.3 What is $\boldsymbol{\Lambda}$?

In this section we first show that the vector field $\boldsymbol{\Lambda}(\mathbf{x})$ introduced in the previous section is precisely the Rodrigues vector field giving the rotation matrix that describes the local orientation of the crystalline axes at position $\mathbf{x}$. Then we develop an analytical approach to extract the local orientation $\widetilde{\boldsymbol{\Lambda}}(\mathbf{k})$ from $\widetilde{\boldsymbol{\rho}}(\mathbf{k})$,

which is exact for stress-free dislocation fields $\boldsymbol{\rho}^{\mathrm{SF}}$ and serves to define the local orientation field for general $\boldsymbol{\rho}$. Finally the real-space formulæ for $\boldsymbol{\Lambda}$ in terms of $\boldsymbol{\rho}$ and the plastic distortion tensor $\boldsymbol{\beta}^{\mathrm{P}}$ are derived.

To understand the meaning of $\widetilde{\boldsymbol{\Lambda}}$ in real space, let's first determine the corresponding $\boldsymbol{\Lambda}^{\mathrm{GB}}$ of a general grain boundary $\boldsymbol{\rho}^{\mathrm{GB}}$. To do so, we follow these steps:

$$\rho_{ij}(\mathbf{r}) \underset{\mathbb{F}.\mathbb{T}.}{\Longrightarrow} \widetilde{\rho}_{ij}(\mathbf{k}) = \widetilde{\Lambda}^{l} E^{l}_{ij} \underset{\mathbb{I}.\mathbb{F}.\mathbb{T}.}{\Longrightarrow} \Lambda^{l}(\mathbf{r}) \tag{4.49}$$

The volume integration over all k-space is readily reduced to a one-dimensional integral due to the presence of two δ-functions. The last integral can be evaluated by integrating around a semi-circular contour in the upper complex plane, resulting in the identity,

$$\int_{-\infty}^{\infty} \frac{\mathrm{e}^{iAk_z}}{k_z}\, dk_z = i\pi\, \mathrm{sign}[A]\,, \tag{4.50}$$

where sign$[A]$ is the sign of A. Essentially,

$$\boldsymbol{\Lambda}^{\mathrm{GB}} = \frac{1}{2}\, \mathrm{sign}[\hat{\mathbf{n}} \cdot (\mathbf{r} - \boldsymbol{\Delta})]\boldsymbol{\omega}\,. \tag{4.51}$$

Again $\hat{\mathbf{n}}$ is the vector normal to the plane. Due to the sign$[\cdot]$ function, $\boldsymbol{\Lambda}^{\mathrm{GB}}$ flips its sign across the cell boundary.

In general $\boldsymbol{\Lambda}(\mathbf{x})$ provides the information about the local crystal orientation at point $\mathbf{x}$ relative to the global fixed orientation.

Theorem 2 *The direction of* $\boldsymbol{\Lambda}$ *gives the axis of rotation of the local crystal orientation with respect to a fixed global coordinates by the amount provided by its magnitude.*

In other words, the Rodrigues vector $\boldsymbol{\Lambda}(\mathbf{x})$ describes the local crystal orientations due to the presence of the stress-free dislocation density field $\boldsymbol{\rho}^{\mathrm{SF}}$. To see this, note that

$$\widetilde{\rho}^{\mathrm{SF}}_{ij} = \widetilde{\Lambda}^{(\alpha)} E^{(\alpha)}_{ij} = ik_j \widetilde{\Lambda}_i - \delta_{ij} ik_m \widetilde{\Lambda}_m\,, \tag{4.52}$$

which, in real space, corresponds to

$$\rho_{ij}^{\mathrm{SF}} = \partial_j \Lambda_i - \delta_{ij} \partial_m \Lambda_m \,. \tag{4.53}$$

According to the discussion in section 2.1, together with the definition of the lattice curvature tensor $\kappa_{ij} = \partial \phi_i / \partial x_j$, where $\boldsymbol{\phi}$ gives the local lattice orientation, equation 2.5 becomes

$$\rho_{ij} = \kappa_{ij} - \delta_{ij} \kappa_{mm} = \partial_j \phi_i - \delta_{ij} \partial_m \phi_m \,. \tag{4.54}$$

Thus, we can identify $\boldsymbol{\Lambda}$ with the Rodrigues vector describing the local orientations.

The decomposition of $\widetilde{\rho}_{ij}^{\mathrm{SF}} = \widetilde{\Lambda}^{\alpha} E_{ij}^{\alpha}$ is somewhat different from the problem of breaking up a vector into projections on various basis vectors. The main distinction lies in the fact that the three E_{ij}^{α}'s are not orthogonal to one another. One common method that has been used to perform such decomposition is to find a minimization of the square of the difference between the actual $\widetilde{\rho}_{ij}^{\mathrm{SF}}$ and the decomposition $\widetilde{\Lambda}^{\alpha} E_{ij}^{\alpha}$. Let's define

$$f \equiv \sum_{ij} \left(\widetilde{\rho}_{ij}^{\mathrm{SF}} - \widetilde{\Lambda}^{\alpha} E_{ij}^{\alpha} \right)^2 . \tag{4.55}$$

Then the minimization occurs when the derivative with respect to the component $\widetilde{\Lambda}^{\beta}$ is zero:

$$\begin{aligned} 0 &= \frac{\partial f}{\partial \widetilde{\Lambda}^{\beta}} \\ &= \frac{\partial}{\partial \widetilde{\Lambda}^{\beta}} \sum_{ij} \left(\widetilde{\rho}_{ij}^{\mathrm{SF}} - \widetilde{\Lambda}^{\alpha} E_{ij}^{\alpha} \right)^2 \\ &= -2 E_{ij}^{\beta} \left(\widetilde{\rho}_{ij}^{\mathrm{SF}} - \widetilde{\Lambda}^{\alpha} E_{ij}^{\alpha} \right) \\ E_{ij}^{\beta} \, \widetilde{\rho}_{ij}^{\mathrm{SF}} &= \underbrace{E_{ij}^{\beta} \, E_{ij}^{\alpha}}_{M_{\alpha\beta}} \, \widetilde{\Lambda}^{\alpha} \end{aligned} \tag{4.56}$$

Or,

$$\widetilde{\Lambda}^{\alpha} = M_{\alpha\beta}^{-1} \, E_{ij}^{\beta} \, \widetilde{\rho}_{ij}^{\mathrm{SF}} \,, \tag{4.57}$$

where

$$M^{-1}_{\alpha\beta} = \frac{1}{2k^4}(k_\alpha k_\beta - 2k^2\delta_{\alpha\beta}) = \frac{1}{2k^4}\begin{pmatrix} k_x^2 - 2k^2 & k_xk_y & k_xk_z \\ k_xk_y & k_y^2 - 2k^2 & k_yk_z \\ k_xk_z & k_yk_z & k_z^2 - 2k^2 \end{pmatrix},$$

and $k^2 \equiv |\mathbf{k}|^2$.

It is possible to directly compute $\mathbf{\Lambda}$ in real space. From

$$\begin{aligned} \widetilde{\Lambda}^i &= M^{-1}_{ij} E^j_{mn} \widetilde{\rho}^{\mathrm{SF}}_{mn} \\ &= \frac{1}{2k^4}\left[k_ik_j - 2k^2\delta_{ij}\right]\left[-ik_j\delta_{mn} + ik_n\delta_{jm}\right]\widetilde{\rho}^{\mathrm{SF}}_{mn} \\ &= \frac{1}{2k^4}\left[ik_ik_mk_n + 2ik^2k_i\delta_{mn} - 2ik^2k_n\delta_{im}\right]\widetilde{\rho}^{\mathrm{SF}}_{mn} \\ &= \frac{i}{k^2}\left[\frac{k_ik_mk_n}{2k^2} + k_i\delta_{mn} - k_n\delta_{im}\right]\widetilde{\rho}^{\mathrm{SF}}_{mn} \\ &= \frac{i}{k^2}\left[k_i\widetilde{\rho}^{\mathrm{SF}}_{nn} - k_n\widetilde{\rho}^{\mathrm{SF}}_{in}\right]. \end{aligned} \tag{4.58}$$

The expression of the Rodrigues vector $\mathbf{\Lambda}$ in real space, therefore, is

$$\Lambda^i(\mathbf{x}) = \frac{1}{4\pi}\int \frac{\partial'_n\rho^{\mathrm{SF}}_{in}(\mathbf{x}') - \partial'_i\rho^{\mathrm{SF}}_{nn}(\mathbf{x}')}{|\mathbf{x}-\mathbf{x}'|}\, d^3\mathbf{x}'. \tag{4.59}$$

Since all of our simulations are performed using the plastic distortion field, it is natural to express $\mathbf{\Lambda}$ in terms of this field. According to $\rho_{ij} = -\varepsilon_{ilm}\partial_l\beta^{\mathrm{P}}_{mj}$,

$$\Lambda^i(\mathbf{x}) = \frac{1}{4\pi}\left[\varepsilon_{ipm}\partial_p\partial_n - \varepsilon_{pmn}\partial_i\partial_p\right]\int \frac{\beta^{\mathrm{P}}_{mn}(\mathbf{x}')}{|\mathbf{x}-\mathbf{x}'|}\, d^3\mathbf{x}'. \tag{4.60}$$

In principle, we can use the above expression for $\mathbf{\Lambda}(\mathbf{x})$ corresponding to the rotation matrix $\boldsymbol{R}(\mathbf{x})$ that best describes (in a least-squares sense) the misorientations developed by the dislocation density $\boldsymbol{\rho}(\mathbf{x})$. Therefore equation 4.59 can be used to extract the information about the misorientation angle distribution, the wall positions, and hence the grain and cell size distributions [16].

CHAPTER 5

CONNECTIONS WITH CONVENTIONAL PLASTICITY THEORIES

We begin this chapter by giving a broad overview of previous work on continuum dislocations. We shall draw direct connections between our theory and these earlier approaches in the remaining of the chapter.

5.1 Previous work and related approaches

Under loading and unloading, certain features are similar for all materials. Depending on the loading condition, the response may be classified roughly into five categories: elastic, plastic, viscoelastic, viscoplastic, and fracture [65]. The response is called *linear elastic* if upon loading and unloading, stress associated with the processes moves along a straight-line path. As further load is applied until reaching a sufficiently large value, the stress-strain curve becomes nonlinear.

If the unloading process is nonlinear but reversible, *i.e.*, the loading and unloading paths coincide, the process is called *nonlinear elastic*. Reversible nonlinearities are small for most crystalline materials; plastic deformation usually arises when the strains are on the order of 1%. A material whose unloading path does not follow the loading path is called an *inelastic* material. If the unloading path does not take the state back to the original unstrained state, the response is called *plastic*. Some material response changes with time under the unloading process. Upon load removal, a *viscoelastic* material will travel along a path, different from the one under loading process, that returns the state to its previously unstrained state. The response for a *viscoplastic* material also changes with time under un-

loading. However, after complete unloading, some permanent strain will remain and the material state will not return to the original one.

In this work, we focus only on the plastic responses that are independent of time upon load removal. In a uniaxial tension test, sometimes the transition from linear elastic to plastic response is abrupt; a kink can be observed in the stress-strain curve. The stress at which the kink occurs is called *yield stress* σ_Y. After the yield point if the stress remains constant with increasing strain, the material is said to be *perfectly elasto-plastic*. Most structural metals exhibit *hardening* behavior. After the initial yield point, the stress continues to increase with increasing strain, although usually at a slower rate than in the elastic region. Upon unloading, the material becomes again elastic and follows a new stress-strain curve. The yield point also moves to the unloading point which is now at the highest point of the curve. The point will continue to move to higher strains as the applied stress exceeds the current yield point.

The study of dislocation pattern formation in metals has been subject to considerable theoretical and numerical investigations in the field of mesoscale plasticity. Several models have been proposed to describe their origins. The discrete dislocation approaches [66, 67, 68, 69, 70, 5] have been very useful in providing insights into the formation processes despite the computational limitations due to the enormous number of dislocation segments in a typical physical system and the long-range nature of the dislocation-dislocation interaction. Alternatively, many continuum approaches have been devised to bypass this difficulty.

Traditional engineering plasticity often makes use of the simple von Mises law, which presumes an elastic response when a yield stress σ_Y is reached, after which the distortion tensor evolves according to the local deviatoric stress (stress with

the isotropic pressure removed). There are many variants of this formulation, with different rules of work hardening giving shapes and evolution laws for the yield surface. The yield surface from our point of view is an emergent property, arising on macroscales from the complexities of grain boundaries, cellular structures, and dislocation tangles that we wish to describe on the mesoscale.

There are generalizations of the von Mises approach which incorporate corrections due to gradients in the local distortion tensor. These gradients are precisely our ρ_{ij}, here called the density of *geometrically necessary dislocations*. These generalizations have grown out of early work on size-dependent hardness [71] and dislocation patterns [72, 73, 51, 52]. One key feature needed in these strain-gradient theories is a new length scale, typically much larger than atomic scales. Much progress has been made in this community in finding alternative explanations for the size-dependence of hardening and the origin of these new mesoscopic length scales. Our more microscopic theory should allow us to explore some of the proposed mechanisms, and the intriguing possible relations to the mesoscale cellular dislocation structures.

There are a variety of *reaction–diffusion* models which have been used to describe the widths of persistent slip bands and other dislocation patterns [72, 73, 51, 52], cellular structures [74, 75], double cross-slip [76], dislocation vein structures [77], and many other effects [78]. These models typically use scalar order parameters to describe mobile and immobile dislocation segment densities. By ignoring the tensor structure of the dislocation density, they both lose the ability to predict the rotational and deformation morphology and they lose the connection between the microscopic Peach–Koehler forces and the continuum dynamics. Finally, these theories do not show the sharp wall formation seen in our approach

(figures 7.1, 7.2, and 7.3 in section 7.1). Sethna *et al.* also had investigated a scalar theory of plasticity [79], which produced a three-dimensional Burgers equation that did form sharp walls (and phenomenologically described work hardening as well); we have moved on to the tensor approaches precisely to regain the predictive power and the connection to the microscopics.

There are a number of recent re-examinations of plasticity using rather different approaches. Langer and Falk's shear-transformation-zone theories of plasticity in metallic glasses [80, 81] note that the deformation in these amorphous systems is not mediated by dislocation line motion, but rather by localized rearrangements of atoms (with suggestive links to the two-level systems in the low temperature theory of glasses); recent work [82] suggests that these rearrangements are spatially extended, with avalanche-like fractal properties. Plastic flow in metallic glasses shows shear banding and work softening, and does not exhibit the work hardening (due presumably to dislocation entanglement) seen in crystalline metals. Ortiz's analogies between plasticity pattern formation and patterns formed in non-convex energy minimization for martensitic and magnetic systems [83] incorporate the full three-dimensional structures of the theory, but rest upon a variational ansatz and are not expressible in terms of evolution laws writable as partial differential equations evolving in time.

Several groups have used Landau-like expansions to expand the most general theory allowed by symmetry within a given framework in powers of the order parameter. Fleck and Hutchinson's strain gradient plasticity [71] does so within a yield-surface approach. As mentioned earlier, our group [79] systematically found the most general evolution law for a scalar order parameter consistent with rate-independent plasticity, yielding a 3D Burgers equation. In this earlier theory, the

formation of sharp walls was the onset of irreversibility and defined the yield stress. Rickman and Vinãls [58], within a tensor theory, write the most general climb-free evolution law for $\boldsymbol{J}$ allowed by symmetry to linear order in $\boldsymbol{\rho}$ (similar to our equation 4.8 below). Since the stress field is linear in $\boldsymbol{\rho}$, this roughly corresponds to von Mises' plasticity; in both cases one gets the (microscopically unintuitive) result that the dislocation current $\boldsymbol{J}$ is independent of the local net density of dislocations. On macroscopic scales where most of the dislocations are geometrically unnecessary (canceling out in $\boldsymbol{\rho}$) this assumption is not a serious approximation, but on the mesoscale (where the dislocation density tensor is needed) we ought to attach dislocation flow to existing geometrically necessary dislocations.

Groma and collaborators [33, 34] use a similar approach to study plastic deformation in two dimensions with only one slip system (*i.e.*, allowing only parallel edge dislocations with one direction of Burgers vector, leading to scalar order parameters). They do a closure-like factorization of a two-point dislocation density correlation function which leads to a theory with one fewer factor of $\boldsymbol{\rho}$ in the evolution law than our equation has. While we cannot generalize their approach to the three-dimensional tensor theory, we can reproduce their continuum theory by choosing $C(\boldsymbol{\rho}) = C_0/\sqrt{\mathrm{tr}(\boldsymbol{\rho}^\dagger\boldsymbol{\rho})}$ (section 4.1.3) and specializing to two dimensions and one slip system (section 5.3). On the one hand, we have checked that all of the wall–singularity formation we describe here persists for this alternative choice for $C(\boldsymbol{\rho})$. On the other hand, we find that no wall singularities form when we specialize to Groma's glide-only slip system: their special case happens to miss the cell-wall physics we describe here. Instead of sharp walls corresponding to jump singularities in $\boldsymbol{\beta}^{\mathrm{P}}$, we see formation of cusps (see chapter 7). When we include climb for Groma's system, our simulation develops parallel walls of dislo-

cations reminiscent of those seen in discrete dislocation dynamics simulations [5], with spacing comparable to our lattice cutoff.[1] El-Azab [37] provides a different three-dimensional multiple-slip generalization of Groma's approach, retaining the densities on different slip systems as independent order parameters and incorporating the momentum field corresponding to the moving dislocations (where our theory is overdamped). El-Azab's approach has not been implemented numerically, and the question of wall formation in his approach has not been explored. Mika and Dawson [29, 84, 26] keep dislocation densities on multiple slip systems, where the dependence of one slip system strength depends upon the others: their simulations show misorientation distributions between finite elements which scale as do those of experimental cell walls [29]. The relatively sharp walls in these last simulations was one of the motivations for our analytically more tractable model.

A community of researchers, growing out of pre-computer work by Taylor [31], simulate plastic flow in crystals using separate scalars $\gamma^{(\alpha)}$ representing the net slip on each slip system. These simulations have been used to study texture (grain orientation distribution) evolution in polycrystal plasticity and the evolution of subgrain structures, either for their own sake [29, 26, 84, 24, 25, 28] or as a precursor for other computations (like recrystallization simulations [30]). The constitutive relations (evolution rules) for $\dot{\gamma}^{(\alpha)}$ may involve flow and hardening rules described as power laws [29, 30, 26, 84, 24, 25], or may be more microscopically related to a decomposition into forest and parallel dislocation densities [28]. This decomposition of $\boldsymbol{\rho}$ into the local density of (typically mobile and immobile) dis-

[1] Since the $\theta \ln \theta$-dependence of the low angle grain boundary energy which drives the 'zip' merging of dislocations is missing in continuum dislocation theories, the fact that the wall separation is set by the grid spacing is as expected. See section 4.2 for a more detailed discussion.

location segments on each slip system leads to a formulation which would seem more microscopic than our dislocation density tensor formulation. (We have questioned the naturalness of separating the dislocations into mobile and immobile subpopulations.) Their slip-system formulation is most clearly motivated in plasticity stages I and II, before secondary slip systems and cross slip [85, 86] are important; after this point each dislocation will have segments on different slip systems, and the separation becomes more artificial. The cellular structures we study are characteristic of stage III, whose onset is associated with cross-slip [85]. We propose to study the relation between our model and these slip-system models in more detail, but we note (apart from intriguing hints in Dawson's simulations [29]) that wall formation is not typically observed or studied in these models.

Much interesting work has emerged recently on extracting the long-wavelength, collective dynamics of interacting dislocations by coarse-graining from laws of discrete dislocation dynamics. Much of this work focuses on dislocation avalanches [4, 87, 88] and crackling noise [89] in these systems. Wall formation has not emerged from these theoretical models or simulations.The fact that wall formation has not been observed in these simulations is likely due to their initial focus on a single slip system (allowing only parallel edge dislocations with one Burgers vector direction, leading to scalar order parameters). Single slip is appropriate for HCP ice and zinc, two of the materials in which crackling noise has been seen, where only one slip system is activated. Our results (section 7.2) show that sharp walls do not form in systems with only a single slip system activated. Indeed, it has been suspected for some time based on discrete dislocation simulations that cellular structures only form in systems with at least two slip systems [90, 91, 92, 93, 94, 95, 96, 97].

Roy and Acharya have developed models of plasticity which, although derived

from a different perspective, use the dislocation density tensor ρ as the order parameter [38, 35, 39, 36] and indeed our equation of motion for glide and climb (equation 6.1 with $\lambda = 0$) was written down first by them (section 4.1.4).[2] They did not realize that their evolution law generated walls; with additional terms in the evolution law they developed microstructure at the lattice scale [39, figure 9]; initial walls under stress became numerically unstable [38, figure 12]; and shocks formed with the annihilation of walls of opposite sign [98, figure 3]—but they did not discover the walls formation that emerges naturally from the simplest variant of their equations.

5.2 Prandtl–Reuss relation and the von Mises law

The Mises flow rule is known as *the Prandtl–Reuss equation*. In 1924 Prandtl [99] introduced a scalar model of elasto-plasticity theory which was then extended to tensors by Reuss [100] in 1930. According to their theory, the plastic strain rate $\dot{\epsilon}^{\mathrm{P}}_{ij}$ is proportional to the instantaneous deviatoric stress s_{ij},

$$\dot{\epsilon}^{\mathrm{P}}_{ij} = \lambda s_{ij} \,, \tag{5.1}$$

where $s_{ij} = \sigma_{ij} - {}^1\!/_3(\sigma_{kk}\delta_{ij})$. λ is a positive scalar generally depending on time t and location $\mathbf{x}$. The above constitutive law is well known as the simplest, and rather useful, three-dimensional theory for describing a class of perfectly elasto-plastic materials. The reason for the use of the deviatoric stress s_{ij} is that the material being considered deforms plastically by gliding of crystalline lattices.

The similarity between (5.1) and our linear theory introduced in section 4.1.2

[2] They do not enforce zero climb in their equations, even though they are interested in modeling plastic flow. Instead, in their later papers [35, equation 25] they introduce terms to make their evolution law pressure independent.

is hard to miss. If only glide motion is considered, then $c_{\rm cl} = 0$, and (4.7) and (4.9) give

$$\begin{aligned} J_{ij} = \dot{\beta}^{\rm P}_{ij} &= c_{\rm gl} \left[\frac{1}{2}(\delta_{ik}\delta_{jm} + \delta_{im}\delta_{jk}) - \frac{1}{3}\,\delta_{ij}\delta_{km} \right] \sigma_{km} \\ &= c_{\rm gl} s_{ij} \,. \end{aligned} \tag{5.2}$$

Symmetrizing over $\dot{\beta}^{\rm P}_{ij}$ yields the equation for the plastic strain rate,

$$\dot{\epsilon}^{\rm P}_{ij} = c_{\rm gl} s_{ij} \,. \tag{5.3}$$

The value of $c_{\rm gl}$ can be derived from a simple tension test.

The simple von Mises law used in macroscopic plasticity, written in our notation, would look like

$$J^{\rm vM}_{ij} = \kappa \left(\sigma_{ij} - \frac{\sigma_{kk}}{3}\delta_{ij} \right) \Theta \left[\frac{1}{2}\sigma_{pq}\sigma_{pq} - \frac{1}{3}\sigma_{pp}\sigma_{qq} - \frac{1}{3}\sigma^2_{\rm Y} \right]$$

where $\Theta[\cdot]$ is the Heaviside step function. The von Mises law has dislocation flow that is independent of the existing net dislocation density; it is appropriate on macroscopic scales where the geometrically unnecessary dislocations are thought to dominate plasticity.

5.3 Slip systems and crystal plasticity

A *slip system* is defined by the slip plane normal $\hat{\mathbf{n}}$ (mostly likely to be one of the close–packed planes), and the slip direction $\hat{\mathbf{b}}$ (usually parallel to directions of least interatomic spacing). These two vectors together with a third vector defined by $\hat{\mathbf{s}} \equiv \hat{\mathbf{b}} \times \hat{\mathbf{n}}$ forms a triad that spans a coordinate system. $\mathbf{s}$ denotes the direction of motion of screw dislocations on that particular slip system. Given a crystal structure, all the slip systems are defined. (There are 12 for FCC crystals, 24 or even possibly 48 for BCC crystals, etc.) A collection of the slip plane normals and

their corresponding slip directions defines the projection tensor or *Schmid tensor* $M_{ij}^{(n)}$:

$$M_{ij}^{(n)} \equiv \frac{1}{2b}\left(n_i^{(n)} b_j^{(n)} + n_j^{(n)} b_i^{(n)}\right) \tag{5.4}$$

The Schmid tensor $\boldsymbol{M}^{(n)}$ allows Zaiser *et al.* to formulate their theory using a scalar field. As an illustration for the use of $\boldsymbol{M}^{(n)}$, the true stress $\boldsymbol{\sigma}$ projected onto the n-th slip system gives the *resolved shear stress* $\tau^{(n)}$ according to

$$\tau^{(n)} = \sigma_{ij} M_{ij}^{(n)}. \tag{5.5}$$

To compare our dislocation model with the conventional engineering crystal plasticity theory, we have to relate the physicists' order parameters to the ones used by the engineers. Consider the dislocation loop α in the glide plane of the n-th slip system whose normal vector is $\mathbf{n}^{(n)}$.[3] Denote the velocity of the dislocation along the loop at $\xi(\mathbf{x})$ by $V_\alpha^{(n)}(\xi)$. The rate of change of the dislocated area $S_\alpha^{(n)}$ is therefore

$$\dot{S}_\alpha^{(n)} = \int_{l_\alpha^{(n)}} V_\alpha^{(n)}(\xi)\, d\xi\,. \tag{5.6}$$

The average rate of change of the distortion field due to such motion is $(1/V)[\mathbf{n}^{(n)} \otimes \mathbf{b}^{(n)}]\dot{S}_\alpha^{(n)} = (1/V)[\mathbf{n}^{(n)} \otimes \mathbf{b}^{(n)}] \int_{l_\alpha^{(n)}} V_\alpha^{(n)}(\xi)\, d\xi$. Summing the contribution over all mobile dislocations in the slip system yields the plastic distortion rate of the system:

$$\dot{\boldsymbol{\beta}}^{\mathrm{P}(n)} = \frac{1}{V}\sum_\alpha \left(\int_{l_\alpha^{(n)}} V_\alpha^{(n)}(\xi)\, d\xi\right)\left[\mathbf{n}^{(n)} \otimes \mathbf{b}^{(n)}\right] \tag{5.7}$$

Using the mean-value theorem, the integral in (5.7) can be written in terms of the average velocity of the dislocation $\bar{V}_\alpha^{(n)}$ as

$$\int_{l_\alpha^{(n)}} V_\alpha^{(n)}(\xi)\, d\xi = l_\alpha^{(n)} \bar{V}_\alpha^{(n)}. \tag{5.8}$$

[3]The derivation provided here follows closely that in Sia Nemat-Nasser [101].

And hence

$$\dot{\boldsymbol{\beta}}^{\mathrm{P}(n)} = \frac{1}{V}\sum_{\alpha} l_{\alpha}^{(n)} \bar{V}_{\alpha}^{(n)} \left[\mathbf{n}^{(n)} \otimes \mathbf{b}^{(n)}\right]. \tag{5.9}$$

The slip rate $\dot{\gamma}^{(n)}$ is normally defined in terms of the motion of the mobile dislocations in the corresponding slip system in the following way:

$$\dot{\gamma}^{(n)} \equiv \frac{1}{V}\sum_{\alpha} b\, l_{\alpha}^{(n)} \bar{V}_{\alpha}^{(n)} \simeq b\rho^{(n)} \bar{V}^{(n)} \tag{5.10}$$

This description of slip rate is called the *Orowan's relation* [102]. Since the average of the products is not the same as the product of the averages, $\bar{V}^{(n)}$ is regarded as the average dislocation velocity of the density of the mobile dislocations $\rho^{(n)}$ within the n-th slip system. Summing over all active slip systems in (5.9) with (5.10) gives the dislocation current $\boldsymbol{J}$:

$$\boldsymbol{J} = \sum_{n} \dot{\boldsymbol{\beta}}^{\mathrm{P}(n)} = \sum_{n} \dot{\gamma}^{(n)} \frac{1}{b} \left[\mathbf{n}^{(n)} \otimes \mathbf{b}^{(n)}\right] \tag{5.11}$$

It is straight forward to show that

$$\dot{\boldsymbol{\epsilon}}^{\mathrm{P}} = \sum_{n} \dot{\gamma}^{(n)} \boldsymbol{M}. \tag{5.12}$$

In the new notations, the rate of plastic work done on all crystals is

$$\int_{\mathrm{vol}} \sigma_{ij} \dot{\beta}_{ij}^{\mathrm{P}}\, d^3\mathbf{r} = \int_{\mathrm{vol}} \sum_{n} \tau^{(n)} \dot{\gamma}^{(n)}\, d^3\mathbf{r}. \tag{5.13}$$

The evolution of the system is determined by the slip-system's *constitutive relations* which could be dependent[4] or independent of the shear strain rate. To illustrate the use of notations, we construct a flow rule in the spirit of our evolution law. We are going to assume that $\bar{V}^{(n)}$ is overdamped;[5]

$$\bar{V}^{(n)}(\mathbf{x}) = D F_{\mathrm{PK}}^{(n)}(\mathbf{x}), \tag{5.14}$$

[4]As an example, see Mika, D.P. and Dawson [29].

[5]The mobility of dislocation normally also depends on, *e.g.*, precipitates, grain boundaries, dislocation pile-ups. Some of these obstacles are thermally activated, and hence the average dislocation velocity is sometimes modeled as an Arrhenius type equation $\bar{V} \propto \exp(-Q/k_{\mathrm{B}}T)$ for a process with the activation energy Q.

where D is the effective mobility coefficient. The Peach-Koehler force is given by $F^{(n)}_{\mathrm{PK}}(\mathbf{x}) = b\rho^{(n)}(\mathbf{x})\tau^{(n)}(\mathbf{x})$.[6] Under this assumption,

$$J_{ij} = \sum_n Db\,\rho^{(n)}\rho^{(n)}\tau^{(n)}n_i^{(n)}b_j^{(n)}\,. \tag{5.15}$$

When specified to one-slip system of parallel edge dislocations, the form of the current given above completely mimic our Peach–Koehler dislocation current $\boldsymbol{J}^{\mathrm{PK}}$ described in section 4.1.3 (equation 4.24) subject to the same slip configuration. The form of $\boldsymbol{J}$ as given here has in fact been used in the work of Zaiser *et al.* [34], aside from an extra order of ρ (see footnote 6 for more detail).

5.4 Frank's formula for a general grain boundary

Given a small-angle grain boundary, Frank provided a condition that the boundary has to satisfy in terms of a vector lying in the grain, the closure failure of the circuit, and the relative rotation between grains separated by the boundary. For simplicity, we shall restrict ourselves to a small angle of misfit θ. For the treatment of large-angle boundaries, see [103].

Let $\mathbf{V}$ be an arbitrary vector lying in the plane of a grain boundary, $\boldsymbol{\omega}$ be an axis defining the relative rotation between the two grains separated by the boundary whose magnitude gives the net rotation angle θ, and $\mathbf{b}$ be the sum of the Burgers vectors of the dislocations cut by $\mathbf{b}$, Frank's formula reads

$$\mathbf{b} = \mathbf{V} \times \boldsymbol{\omega}\,. \tag{5.16}$$

See [104] for the derivation,[7] and [105] for the formula with an arbitrarily large

[6] This is where we depart from Zaiser *et al.* [34]. Their form of Peach-Koehler force is not proportional to $\rho^{(n)}$. Instead, they defined $s_i = \pm 1$ which takes care of the sign of the i-th dislocation.

[7] There is a sign difference between the formula quoted here and that presented in [104]. This is due to the discrepancy in defining the Burgers vector.

angle θ.

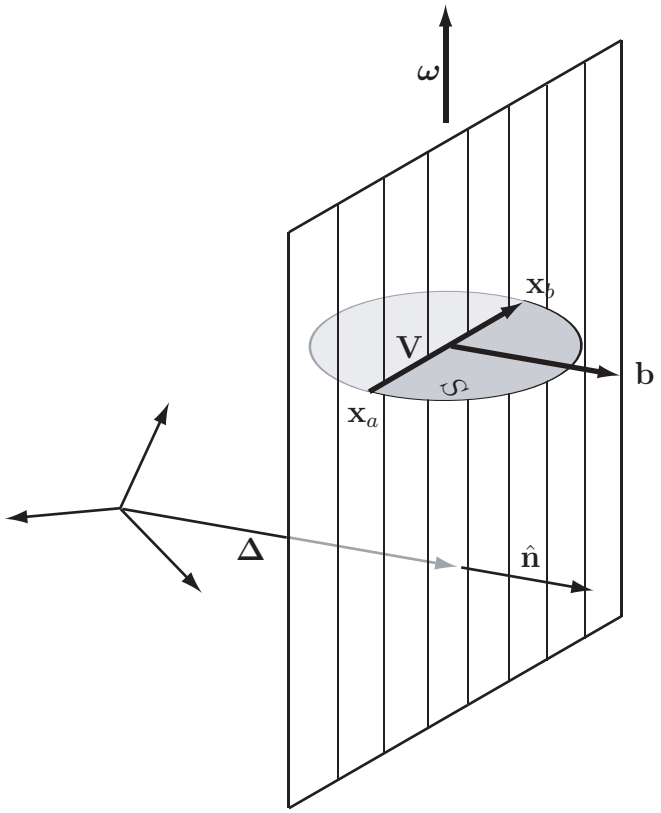

Figure 5.1: **The five-parameter general grain boundary.** The orientation of the plain defined by the vector normal $\hat{\mathbf{n}}$ requires two numbers. The other three go into the three components of the Rodriguez vector: the normal defining the axis of rotation and the angle of relative orientation.

Using the Nye tensor, we can rephrase (5.16), then compare it with our statement of stress-free boundaries. Let's start off by defining a Burgers circuit C enclosing a surface S that intersects a grain boundary at two points $\mathbf{x}_a$ and $\mathbf{x}_b$. The net Burgers vector encompassed by the surface is $\mathbf{b}$. Define $\mathbf{V}$ to be a vector lying in the boundary plane pointing from $\mathbf{x}_a$ to $\mathbf{x}_b$, $\mathbf{V} \equiv \mathbf{x}_b - \mathbf{x}_a$. We can represent this grain boundary by a constant matrix $\boldsymbol{\rho}^0$ multiplied by a plane defined by $\delta(\hat{\mathbf{n}} \cdot (\mathbf{x} - \boldsymbol{\Delta}))$, where $\hat{\mathbf{n}}$ is a unit vector normal to the plane, and $\boldsymbol{\Delta}$ is the

perpendicular vector pointing from the origin to the plane. (See figure 5.1.) From (2.9),

$$\begin{aligned} b_j &= \int_S \rho_{ij}\, dS_i \\ &= \int_S \rho^0_{ij}\, \delta(\hat{\mathbf{n}} \cdot (\mathbf{x} - \boldsymbol{\Delta}))[\hat{\mathbf{n}} \times \hat{\mathbf{V}}]_i\, dA\,. \end{aligned} \tag{5.17}$$

The δ-function serves to collapse the area integral into a line integral since the value is zero outside of the plane defined by $\mathbf{x} \cdot \hat{\mathbf{n}} = 0$:

$$\begin{aligned} b_j &= \int_{\mathbf{x_a}}^{\mathbf{x_b}} \rho^0_{ij}[\hat{\mathbf{n}} \times \hat{\mathbf{V}}]_i\, dl \\ &= \rho^0_{ij} \big|\mathbf{x_b} - \mathbf{x_a}\big| \varepsilon_{imn} \hat{n}_m \hat{V}_n \\ &= \rho^0_{ij}\, \varepsilon_{imn} \hat{n}_m V_n \end{aligned} \tag{5.18}$$

We can therefore relate the dislocation density to the rotation vector $\boldsymbol{\omega}$ using (5.16):

$$\begin{aligned} \varepsilon_{jpq}\, V_p\, \omega_q &= \rho^0_{ij}\, \varepsilon_{imn} \hat{n}_m V_n \\ 0 &= \rho^0_{ij}\, \varepsilon_{imn} \hat{n}_m V_n - \varepsilon_{jmn} V_m \omega_n \end{aligned} \tag{5.19}$$

With some relabeling, this becomes

$$0 = \left(\rho^0_{ij} \hat{n}_m + \delta_{ij} \omega_m\right) \varepsilon_{imn} V_n\,. \tag{5.20}$$

This is the Frank condition in the language of dislocation density tensor.

To take a step further, since $\mathbf{V}$ is a vector in the plane of the grain boundary, we can write $\mathbf{V}$ as $\mathbf{V} = \hat{\mathbf{n}} \times \mathbf{W}$ for any arbitrary vector $\mathbf{W}$ pointing anywhere except along $\hat{\mathbf{n}}$. We can substitute $\hat{\mathbf{n}} \times \mathbf{W}$ back into (5.20),

$$0 = \left(\rho^0_{ij} \hat{n}_m + \delta_{ij} \omega_m\right) \varepsilon_{imn} \varepsilon_{npq} \hat{n}_p W_q\,. \tag{5.21}$$

This condition holds regardless of $\mathbf{W}$. We can therefore safely ignore $\mathbf{W}$ in the

equation. The condition now becomes

$$\begin{aligned} 0 &= \left(\rho^0_{ij}\hat{n}_m + \delta_{ij}\omega_m\right)\varepsilon_{imn}\varepsilon_{npq}\hat{n}_p \\ &= \left(\rho^0_{ij}\hat{n}_m + \delta_{ij}\omega_m\right)(\delta_{ip}\delta_{mq} - \delta_{iq}\delta_{mp})\hat{n}_p \\ &= \hat{n}_i\rho^0_{ij}\hat{n}_q + \hat{n}_j\omega_q - \rho^0_{qj} - \delta_{qj}\omega_p\hat{n}_p\,. \end{aligned} \tag{5.22}$$

The first term goes to zero because the first index of ρ^0_{ij} designates the line component which always lies in the plane of the boundary. By definition, $\hat{\mathbf{n}}$ is perpendicular to the plane, therefore, $\hat{n}_i\rho^0_{ij} = 0$. The condition for $\boldsymbol{\rho}^0$ that makes a valid grain boundary is

$$\rho^0_{ij} = \omega_i\hat{n}_j - (\boldsymbol{\omega}\cdot\hat{\mathbf{n}})\delta_{ij}\,, \tag{5.23}$$

or:

$$\boxed{\boldsymbol{\rho}^{\mathrm{GB}} = \left[\boldsymbol{\omega}\otimes\hat{\mathbf{n}} - (\boldsymbol{\omega}\cdot\hat{\mathbf{n}})\,\mathbf{1}\right]\delta(\hat{\mathbf{n}}\cdot(\mathbf{x}-\boldsymbol{\Delta}))} \tag{5.24}$$

The well-known five degrees of freedom of a general grain boundary is apparent in this formulation. The relative rotation between two grains $\boldsymbol{\omega}$ has three degrees of freedom. The other two degrees of freedom are contained in $\hat{\mathbf{n}}$; since $\hat{\mathbf{n}}$ is a unit vector, only two angles are needed to define a plane.

To see the connection between our formalism in obtaining a general stress-free state in section 4.2.2, let us again rewrite the Fourier Transform of the general grain boundary $\widetilde{\boldsymbol{\rho}}^{\mathrm{GB}}$,

$$\widetilde{\rho}^{\mathrm{GB}}_{ij} = (2\pi)^2\,\frac{\delta(R^{-1}_{xp}k_p)\delta(R^{-1}_{yq}k_q)}{iR^{-1}_{zr}k_r}\,\omega_n E^n_{ij}\,\mathrm{e}^{-i\mathbf{k}\cdot\boldsymbol{\Delta}}\,, \tag{4.45'}$$

where all the variables are as defined previously. It is possible to perform the inverse transform of $\widetilde{\boldsymbol{\rho}}^{\mathrm{GB}}$ to arrive at its real space representation. The two δ-functions serve to define a plane in real space. The natural choice of coordinate is to make a rotational change of variables from (k_x, k_y, k_z) to (ξ_x, ξ_y, ξ_z) where

$\xi_i = R_{ij}^{-1} k_j$. In this coordinate, $\hat{\boldsymbol{\xi}}_z$ is perpendicular to the plane of the boundary. The other two basis vectors lie in the plane of the boundary.

The inverse transform can be written as

$$\begin{aligned}
\rho_{ij}^{\mathrm{GB}} &= \frac{1}{(2\pi)^3} \int \widetilde{\rho}_{ij}^{\mathrm{GB}} \mathrm{e}^{i\mathbf{k}\cdot\mathbf{x}} \, d^3\mathbf{k} \\
&= \frac{1}{2\pi} \int \frac{\delta(R_{xp}^{-1} k_p) \delta(R_{yq}^{-1} k_q)}{i R_{zr}^{-1} k_r} \, \omega_n E_{ij}^n \, \mathrm{e}^{i\mathbf{k}\cdot(\mathbf{x}-\boldsymbol{\Delta})} \, d^3\mathbf{k} \\
&= \frac{1}{2\pi} \int \frac{\delta(\xi_x)\delta(\xi_y)}{i\xi_z} \, \omega_n E_{ij}^n \, \mathrm{e}^{i\mathbf{k}\cdot(\mathbf{x}-\boldsymbol{\Delta})} \, d^3\boldsymbol{\xi} \, .
\end{aligned} \tag{5.25}$$

Note that since the new basis vectors are the rotation of the original set, its Jacobian is one. The next step is to express E_{ij}^n in terms of the new basis:

$$\begin{aligned}
E_{ij}^n &= ik_j \delta_{in} - ik_n \delta_{ij} \\
&= iR_{jm} R_{mp}^{-1} k_p \delta_{in} - iR_{nm} R_{mp}^{-1} k_p \delta_{ij} \\
&= iR_{jm} \xi_m \delta_{in} - iR_{nm} \xi_m \delta_{ij} \\
&= i\xi_m \left(R_{jm} \delta_{in} - R_{nm} \delta_{ij} \right)
\end{aligned} \tag{5.26}$$

Similarly,

$$\mathrm{e}^{i\mathbf{k}\cdot(\mathbf{x}-\boldsymbol{\Delta})} = \mathrm{e}^{iR_{ij} R_{jm}^{-1} k_m (x_i - \Delta_i))} = \mathrm{e}^{iR_{ij}\xi_j (x_i - \Delta_i)} \, . \tag{5.27}$$

Substituting these into (5.25) gives

$$\begin{aligned}
\rho_{ij}^{\mathrm{GB}} &= \frac{1}{2\pi} \int \frac{\delta(\xi_x)\delta(\xi_y)}{i\xi_z} \, \omega_n i\xi_m \left(R_{jm}\delta_{in} - R_{nm}\delta_{ij} \right) \mathrm{e}^{iR_{ij}\xi_j (x_i - \Delta_i)} \, d^3\boldsymbol{\xi} \\
&= \frac{1}{2\pi} \int_{-\infty}^{\infty} \frac{1}{i\xi_z} \omega_n i\xi_z \left(R_{jm}\delta_{in} - R_{nm}\delta_{ij} \right) \mathrm{e}^{iR_{iz}\xi_z (x_i - \Delta_i)} \, d\xi_z \\
&= \left(\omega_i R_{jz} - \omega_n R_{nz} \delta_{ij} \right) \underbrace{\frac{1}{2\pi} \int_{-\infty}^{\infty} \mathrm{e}^{iR_{iz}\xi_z (x_i - \Delta_i)} \, d\xi_z}_{\delta(R_{iz}(x_i - \Delta_i))} \, .
\end{aligned} \tag{5.28}$$

The rotation matrix $\boldsymbol{R}$ was so constructed that $\boldsymbol{R} \cdot \hat{\mathbf{z}} = \hat{\mathbf{n}}$, or $R_{iz} = \hat{n}_i$. Therefore,

$$\rho_{ij}^{\mathrm{GB}} = \left[\omega_i \hat{n}_j - (\boldsymbol{\omega} \cdot \hat{\mathbf{n}}) \delta_{ij} \right] \delta(\hat{\mathbf{n}} \cdot (\mathbf{x} - \boldsymbol{\Delta})) \, , \tag{5.29}$$

exactly the same as what we derived from the Frank's formula.

As a note in passing, from the form of the Peach–Koehler force $f_i = \varepsilon_{ijk}\sigma_{kl}\rho_{jl}$, we can write down the force on a grain boundary due to external stress $\boldsymbol{\sigma}^0$ as follows:

$$\mathbf{f} = \boldsymbol{\omega} \times (\boldsymbol{\sigma}^0 \cdot \hat{\mathbf{n}}) \tag{5.30}$$

CHAPTER 6

ANALYSIS OF THE EVOLUTION EQUATION IN ONE DIMENSION

Our evolution law, specialized to one dimension, shows dramatic simplification, *i.e.*, the equation of motion is local; the evolution of all state variables at one point depends only on quantities in the neighboring points. In section 6.1, we reformulate the evolution law (equation 2.19' together with the form of the dislocation current $\boldsymbol{J}$ in equation 4.24) in terms of the plastic distortion field $\boldsymbol{\beta}^{\mathrm{P}}$. The equation can be further simplified by mapping into the eigenbasis of the stress field (section 6.2). In the case where glide and climb are treated on an equal footing ($\lambda = 0$), we show in section 6.2.1 that the governing equation of the local Peach–Koehler force density, surprisingly, is Burgers equation—generally known to form wall singularities in finite time. The jump condition at the singularities is derived in section 6.3. Predictions and the mechanism of wall formation within our theory are discussed in section 6.4.

6.1 Implementation

Our preliminary numerical work suggested that the stationary state of the dislocation density tensor $\boldsymbol{\rho}$ form walls, or δ-function singularities in finite time. Instead of evolving $\boldsymbol{\rho}$ itself, we can, to the same effect, evolve the corresponding plastic distortion tensor $\boldsymbol{\beta}^{\mathrm{P}}$; the singularities in $\boldsymbol{\beta}^{\mathrm{P}}$ are milder (step functions), and the $\boldsymbol{\beta}^{\mathrm{P}}$ field is not subject to the gradient constraint imposed upon $\boldsymbol{\rho}$ ($\partial_i \rho_{ij} = 0$). Using equation (2.10), we can then get back $\boldsymbol{\rho}$ at any given time. Using $\boldsymbol{\beta}^{\mathrm{P}}$ rather than $\boldsymbol{\rho}$ is like solving electromagnetism problems using the vector potential $\mathbf{A}$

rather than the magnetic field $\mathbf{B} = \boldsymbol{\nabla} \times \mathbf{A}$; the awkward constraint $\boldsymbol{\nabla} \cdot \mathbf{B} = 0$ is avoided.

The evolution equation for $\boldsymbol{\beta}^{\mathrm{P}}$ is given by (2.20), together with the form of $\boldsymbol{D}^{\mathrm{PK}}$ in (4.19):

$$\frac{\partial \beta_{ij}^{\mathrm{P}}}{\partial t} = \frac{C(\boldsymbol{\rho})D}{2}\Big[\left(\sigma_{ic}\rho_{ac} - \sigma_{ac}\rho_{ic}\right)\rho_{aj} - \frac{\lambda}{3}\,\delta_{ij}\left(\sigma_{kc}\rho_{ac} - \sigma_{ac}\rho_{kc}\right)\rho_{ak}\Big] \tag{6.1}$$

The relative mobility rate between glide and climb motions is controlled by the parameter λ. In general equation (6.1) reaches a stationary state when the cross product between the Peach–Koehler force on the dislocation density and the dislocation there becomes zero. We shall see later that, in one dimension, the above condition implies that the Peach–Koehler force density of the system is zero everywhere. This condition holds regardless of whether or not the evolution is conservative. The form of the solutions in one dimension at large times (asymptotic solutions near the stationary states) will also be discussed.

Let us analyze our evolution equation in the case where the distribution of the dislocation (or the distortion field in this case) varies in one direction in space and is constant along the plane perpendicular to this direction. The equation in this case becomes local and, more importantly, hyperbolic. The method of characteristics is customarily employed to analyse this type of equation. We shall see the method allows us to show that our equation develops jumps in the plastic distortion field which translates to wall singularities in the dislocation field.

Equation (6.1) intrinsically involves $\boldsymbol{\beta}^{\mathrm{P}}$. The first step in trying to numerically evolve this tensor is to recast (6.1) into the form that explicitly involves $\boldsymbol{\beta}^{\mathrm{P}}$. Suppose $\boldsymbol{\rho}$ is constant in the x-y plane and the only variation of $\boldsymbol{\rho}$ is along the $\hat{\mathbf{z}}$ direction, the only non-zero derivative in this case is $\partial/\partial z$. The expression given

by (2.10) reduces to

$$\rho_{ij} = -\varepsilon_{izm}\partial_z \beta^{\mathrm{P}}_{mj}\,, \tag{6.2}$$

which is non-zero only when $i = x$ or $i = y$. From this, we end up with

$$\rho_{xj} = \partial_z \beta^{\mathrm{P}}_{yj}\,, \qquad \rho_{yj} = -\partial_z \beta^{\mathrm{P}}_{xj}\,, \qquad \rho_{zj} = 0\,. \tag{6.3}$$

Similarly, the expression for the stress field due to dislocations is immensely simpler. The expression of the dislocation density tensor with variations along the z-direction in Fourier space is $\widetilde{\boldsymbol{\rho}}(\mathbf{k}) = \widetilde{\boldsymbol{\rho}}(k_z)\delta(k_x)\delta(k_y)$. If one substitutes this form of $\widetilde{\boldsymbol{\rho}}$ into the expression for the stress field in Fourier space (equation 3.3'), one obtains

$$\widetilde{\boldsymbol{\sigma}}(\mathbf{k}) = \frac{(2\pi)^2 i\mu}{k_z}\,\delta(k_x)\delta(k_y) \begin{pmatrix} \frac{2}{1-\nu}(\nu\widetilde{\rho}_{xy} - \widetilde{\rho}_{yx}) & \widetilde{\rho}_{xx} - \widetilde{\rho}_{yy} & 0 \\ \widetilde{\rho}_{xx} - \widetilde{\rho}_{yy} & \frac{2}{1-\nu}(\widetilde{\rho}_{xy} - \nu\widetilde{\rho}_{yx}) & 0 \\ 0 & 0 & 0 \end{pmatrix}. \tag{6.4}$$

Direct substitution of (6.3) into (6.4) yields

$$\widetilde{\boldsymbol{\sigma}}(\mathbf{k}) = -(2\pi)^2\mu\,\delta(k_x)\delta(k_y) \begin{pmatrix} \frac{2}{1-\nu}(\widetilde{\beta}^{\mathrm{P}}_{xx} + \nu\widetilde{\beta}^{\mathrm{P}}_{yy}) & \widetilde{\beta}^{\mathrm{P}}_{xy} + \widetilde{\beta}^{\mathrm{P}}_{yx} & 0 \\ \widetilde{\beta}^{\mathrm{P}}_{xy} + \widetilde{\beta}^{\mathrm{P}}_{yx} & \frac{2}{1-\nu}(\nu\widetilde{\beta}^{\mathrm{P}}_{xx} + \widetilde{\beta}^{\mathrm{P}}_{yy}) & 0 \\ 0 & 0 & 0 \end{pmatrix}. \tag{6.5}$$

Unlike the expression of $\boldsymbol{\sigma}$ involving $\widetilde{\boldsymbol{\rho}}$, the stress in terms of $\widetilde{\boldsymbol{\beta}}^{\mathrm{P}}$ is not multiplied by a function of $\mathbf{k}$ and thus is easily transformed back to real space. One has to be careful when dealing with the zeroth mode when performing the inverse transform. Since a plastic distortion tensor is defined up to a constant tensor, two plastic distortion fields which differ by a constant should give the same stress field. Since the σ_{iz} and σ_{zi} components of the stress are always zero, it is enough to

express the field as a 2×2 matrix:[1]

$$\boldsymbol{\sigma}(z) = -\mu \begin{pmatrix} \frac{2}{1-\nu}(\bar{\beta}^{\mathrm{P}}_{xx} + \nu\bar{\beta}^{\mathrm{P}}_{yy}) & \bar{\beta}^{\mathrm{P}}_{xy} + \bar{\beta}^{\mathrm{P}}_{yx} \\ \bar{\beta}^{\mathrm{P}}_{xy} + \bar{\beta}^{\mathrm{P}}_{yx} & \frac{2}{1-\nu}(\nu\bar{\beta}^{\mathrm{P}}_{xx} + \bar{\beta}^{\mathrm{P}}_{yy}) \end{pmatrix} \tag{6.6}$$

Here $\bar{\beta}^{\mathrm{P}}_{ij}(z) = \beta^{\mathrm{P}}_{ij}(z) - \frac{1}{L}\int_0^L \beta^{\mathrm{P}}_{ij}(z')\,dz'$, removing the zero mode. Hence $\sigma(z)$ in one dimension is not an integral over space or a convolution, but a local formula in terms of the plastic distortion $\boldsymbol{\beta}^{\mathrm{P}}$.

From the relationship involving the dislocation density $\boldsymbol{\rho}$ and the plastic distortion tensor $\boldsymbol{\beta}^{\mathrm{P}}$ (equation 2.10), and the stress field expressed in terms of the plastic distortion tensor (equation 6.6), equation 6.1 gives a formula for the one-dimensional evolution equation for $\boldsymbol{\beta}^{\mathrm{P}}$. While the β^{P}_{zj} components do not evolve, the other components all evolve according to

$$\partial_t \beta^{\mathrm{P}}_{ij} = -\frac{CD}{2}\mathcal{F}\,\partial_z\!\left(\beta^{\mathrm{P}}_{ij} - \frac{\lambda}{3}\,\beta^{\mathrm{P}}_{kk}\delta_{ij}\right), \tag{6.7}$$

where i and j can be either x or y, while the β^{P}_{zl} components do not evolve. Again, the parameter λ varies the amount of climb; at low temperature $\lambda = 1$ removes the trace[2] of $\partial_t\boldsymbol{\beta}^{\mathrm{P}}$, enforces volume conservation, and hence forbids climb, while $\lambda = 0$ allows equal mobility for both glide and climb motion. The Peach–Koehler force density $\mathcal{F}(\boldsymbol{\beta}^{\mathrm{P}})$ in one dimension becomes

$$\mathcal{F}(\boldsymbol{\beta}^{\mathrm{P}}) = -\sigma_{ij}\frac{\partial\beta^{\mathrm{P}}_{ij}}{\partial z} = \frac{\partial\mathcal{E}(\boldsymbol{\beta}^{\mathrm{P}})}{\partial z}\,, \tag{6.8}$$

[1]The more invariant way of writing this is $\sigma_{ij} = -\bar{C}_{ijkm}\bar{\beta}^{\mathrm{P}}_{km}$, where $\bar{C}_{ijkm} = \mu\left[\delta_{ik}\delta_{jm} + \delta_{im}\delta_{jk} + \frac{2\nu}{1-\nu}\,\delta_{ij}\delta_{km}\right]$—in close analogy with Hooke's law, except that $\bar{C}$ is different from the elastic tensor $C_{ijkm} = \mu\left[\delta_{ik}\delta_{jm} + \delta_{im}\delta_{jk} + \frac{\nu}{1-2\nu}\,\delta_{ij}\delta_{km}\right]$.

[2]Because three components of the plastic distortion field, namely β^{P}_{zj}'s are inactive and do not contribute to the dislocation density $\boldsymbol{\rho}$ in one dimension, there are useful ways which one can take a trace without respecting the spherical symmetry. Appendix F discusses one such case.

where the elastic energy density

$$\begin{aligned}\mathcal{E}(\boldsymbol{\beta}^{\mathrm{P}}) &= \frac{\mu}{1-\nu}\left[\frac{1-\nu}{2}\left(\beta^{\mathrm{P}}_{xy}+\beta^{\mathrm{P}}_{yx}\right)^2+{\beta^{\mathrm{P}}_{xx}}^2+{\beta^{\mathrm{P}}_{yy}}^2+2\nu\beta^{\mathrm{P}}_{xx}\beta^{\mathrm{P}}_{yy}\right]\\ &= \mu\left[\frac{1}{2}\left(\beta^{\mathrm{P}}_{xy}+\beta^{\mathrm{P}}_{yx}\right)^2+\left({\beta^{\mathrm{P}}_{xx}}^2+{\beta^{\mathrm{P}}_{yy}}^2\right)+\frac{\nu}{1-\nu}\left(\beta^{\mathrm{P}}_{xx}+\beta^{\mathrm{P}}_{yy}\right)^2\right] \qquad (6.9)\\ &\geq 0,\end{aligned}$$

only involves the local plastic distortion tensor. Notice that the individual components of β^{P} in (6.7) are slaves to the evolution of the Peach–Koehler force density $\mathcal{F}$.

6.2 Eigenstress basis; pathway to Burgers equation

Near a wall singularity the dynamics are one-dimensional. The variations of the stress, plastic strain, and dislocation densities parallel to the wall asymptotically become unimportant compared to the gradients perpendicular to the wall as one approaches the singularity. We expect, therefore, to be able to study wall formation in three dimensions under the condition in which the fields vary only along the z direction. To simplify the discussion, we shall rescale the time to set $CD = 1$. Again, one-dimensional evolution law reads

$$\partial_t \beta^{\mathrm{P}}_{ij} = -\frac{CD}{2}\left(\partial_z \mathcal{E}\right)\partial_z\left(\beta^{\mathrm{P}}_{ij}-\frac{\lambda}{3}\,\beta^{\mathrm{P}}_{kk}\delta_{ij}\right). \qquad (6.10)$$

Note the striking simplification for $\lambda = 0$—each component of $\boldsymbol{\beta}^{\mathrm{P}}$ evolves in a way that depends on the other components only through the overall energy density $\mathcal{E}$. This surprising result will be important in section 6.2.1.

The equations of motion are best analyzed in the eigenbasis of $\bar{\boldsymbol{C}}$. Out of the six active components of $\boldsymbol{\beta}^{\mathrm{P}}$, $\bar{\boldsymbol{C}}$ only mixes up the 2×2 upper left-hand corner of $\boldsymbol{\beta}^{\mathrm{P}}$. The evolutions of the other components β^{P}_{xz} and β^{P}_{yz} therefore depend on

these four. The eigenmatrices $\boldsymbol{\tau}^{(\alpha)}$, comprising the (rescaled) Pauli matrices and identity matrix, and the corresponding eigenvalues $e^{(\alpha)}$ of $\bar{\boldsymbol{C}}$ are given in Table 6.1. By expanding the plastic distortion field according to $\beta_{ij}^{\mathrm{P}} = \sum_{\alpha=1}^{4} b^{(\alpha)} \tau_{ij}^{(\alpha)}$,

Table 6.1: The eigenmatrices and eigenvalues of $\bar{\boldsymbol{C}}$; the four columns give $\alpha = 1$, 2, 3, and 4 respectively.

$\boldsymbol{\tau}^{(\alpha)}$	$\sqrt{\frac{1-\nu}{4\mu(1+\nu)}}\begin{pmatrix}1 & 0\\ 0 & 1\end{pmatrix}$	$\frac{1}{\sqrt{4\mu}}\begin{pmatrix}0 & 1\\ 1 & 0\end{pmatrix}$	$\frac{1}{\sqrt{4\mu}}\begin{pmatrix}0 & -i\\ i & 0\end{pmatrix}$	$\frac{1}{\sqrt{4\mu}}\begin{pmatrix}1 & 0\\ 0 & -1\end{pmatrix}$
$e^{(\alpha)}$	$2\mu\left(\frac{1+\nu}{1-\nu}\right)$	2μ	0	2μ

$$\mathcal{E} = \frac{1}{2}\,\bar{C}_{ijkm}\beta_{ij}^{\mathrm{P}}\beta_{km}^{\mathrm{P}} = \frac{1}{2}\sum_{\alpha,\beta} b^{(\alpha)}b^{(\beta)}\underbrace{e^{(\alpha)}\tau_{ij}^{(\alpha)}\tau_{ij}^{(\beta)}}_{\delta_{\alpha\beta}} = \frac{1}{2}\sum_{\alpha} b^{(\alpha)}b^{(\alpha)}. \tag{6.11}$$

The choice of basis naturally separates the components of $\boldsymbol{\beta}^{\mathrm{P}}$ into two collections—the degrees of freedom responsible for the system's stress $\mathbf{a} \equiv \{b^{(1)}, b^{(2)}, b^{(4)}\}$, and stress-free states $\bar{\mathbf{a}} \equiv \{\beta_{xz}^{\mathrm{P}}, \beta_{yz}^{\mathrm{P}}, b^{(3)}\}$ containing (possibly continuous) variations of two tilt and one twist boundaries.

The evolution law for both $\mathbf{a}$ and $\bar{\mathbf{a}}$ can be found by expanding (6.10) in the new basis:

$$\begin{aligned}\sum_{\alpha}\tau_{ij}^{(\alpha)}\,\partial_t a^{(\alpha)} &= -\frac{1}{4}\sum_{\beta}\partial_z\left(a^{(\beta)}a^{(\beta)}\right)\left[\sum_{\alpha}\tau_{ij}^{(\alpha)}\,\partial_z a^{(\alpha)} - \frac{\lambda}{3}\left(\sum_{\alpha}\tau_{kk}^{(\alpha)}\,\partial_z a^{(\alpha)}\right)\delta_{ij}\right]\\ &= -\frac{1}{4}\sum_{\beta}\partial_z\left(a^{(\beta)}a^{(\beta)}\right)\sum_{\alpha}(1-\frac{2\lambda}{3}\,\delta_{1,\alpha})\tau_{ij}^{(\alpha)}\partial_z a^{(\alpha)}\\ &\sum_{\alpha}\tau_{ij}^{(\alpha)}\left[\partial_t a^{(\alpha)} + \left(\frac{1}{2} - \frac{\lambda}{3}\,\delta_{1,\alpha}\right)\partial_z\mathcal{E}\,\partial_z a^{(\alpha)}\right] = 0\end{aligned} \tag{6.12}$$

where we use $\mathcal{E} = 1/2\sum_{\alpha} a^{(\alpha)}a^{(\alpha)}$. Since $\boldsymbol{\tau}^{(\alpha)}$ is linearly independent, the summation is zero only when each component of α is zero:

$$\partial_t a^{(\alpha)} + \left(\frac{1}{2} - \frac{\lambda}{3}\,\delta_{1,\alpha}\right)\partial_z\mathcal{E}\,\partial_z a^{(\alpha)} = 0 \tag{6.13}$$

The stress-free components evolve in exactly the same fashion:

$$\partial_t \bar{a}^{(\alpha)} + \frac{1}{2}\,\partial_z \mathcal{E}\,\partial_z \bar{a}^{(\alpha)} = 0 \tag{6.14}$$

Equations 6.13 and 6.14 are manifestly hyperbolic, hence it is natural to employ the method of characteristics and the upwind finite difference scheme (appendix G) to theoretically analyze and numerically evolve the equations. The evolution of the strain energy density follows from equation 6.13 by contracting with $a^{(\alpha)}$:

$$\partial_t \mathcal{E} = -\frac{1}{2}(\partial_z \mathcal{E})\,\partial_z \left[\mathcal{E} - \frac{2\lambda}{3}\,a^{(1)}a^{(1)}\right] \tag{6.15}$$

6.2.1 Mapping to Burgers equation; climb & glide

We now specialize to the case of $\lambda = 0$, where glide and climb are treated on an equal footing (applicable to grain boundary formation during polygonization at high temperatures, for example). According to (6.13) the equation of motion for the total stress energy density $\mathcal{E}$ turns out to depend only upon itself, not the individual components of $\boldsymbol{\beta}^{\mathrm{P}}$:

$$\partial_t \mathcal{E} + \frac{1}{2}(\partial_z \mathcal{E})^2 = 0 \tag{6.16}$$

Notice that the rate of change of the elastic energy can be written simply as

$$\frac{d\mathcal{E}_{\mathrm{total}}}{dt} = \frac{d}{dt}\int \mathcal{E}\,dz = -\int \mathcal{F}^2(\boldsymbol{\beta}^{\mathrm{P}})\,dz\,, \tag{6.17}$$

which is a negative semidefinite quantity as expected.

Equation 6.16 can be cast into the famous Burgers equation [106, 107, 79] by defining $\mathcal{F} = \partial_z \mathcal{E}$:

$$\partial_t \mathcal{F} + \mathcal{F}\,\partial_z \mathcal{F} = 0 \tag{6.18}$$

The scalar $\mathcal{F}(z)$ is the net Peach–Koehler force density on the local dislocation density $\rho(z)$. Burgers equation is the archetype of hyperbolic partial differential

equations showing shock formation;[3] under Burgers equation $\mathcal{F}$ will develop sharp jumps downward after a finite evolved time. This jump in force density has a nice physical interpretation: the dislocations in the vicinity of the wall are being dragged toward the wall.

6.3 Jump condition

Once a wall forms, the differential equation no longer determines a unique solution. One must appeal to the integral form of the conservation of Burgers vector to dictate the choice of the correct solution. Consider a rectangular contour C connecting (x_a, z_L), (x_a, z_R), (x_b, z_R), and (x_b, z_L) cutting through the dislocation wall whose plane normal is $\hat{\mathbf{n}}$ at $(x_a, s(t))$ and $(x_b, s(t))$, where $s(t)$ is the position of the moving wall (figure 6.1). The rate of change of the net Burgers vector through the surface S bounded by C with the plane normal $\hat{\mathbf{t}}$ depends on the dislocation current $\boldsymbol{J}$ in and out of the loop according to $db_j/dt = -\oint_C J_{ij}\, dx_i$. Define $\hat{\mathbf{p}}$ to be a unit vector pointing along the wall from $(x_a, s(t))$ to $(x_b, s(t))$, then $(\hat{\mathbf{n}}, \hat{\mathbf{p}}, \hat{\mathbf{t}})$

[3]There exists a nonlinear transformation of the form $\mathcal{F} = -2\nu(\partial_z\phi)/\phi$ called the *Cole–Hopf* transformation which takes the *viscous Burgers' equation*

$$\partial_t \mathcal{F} + \mathcal{F}\,\partial_z \mathcal{F} = \nu\,\partial_z^2 \mathcal{F} \tag{6.19}$$

to a regular heat equation

$$\partial_t \phi = \nu\,\partial_z^2 \phi\,. \tag{6.20}$$

The explicit form of the solution with the initial profile $\mathcal{F}_0(z)$ is

$$\mathcal{F}(z,t) = \frac{\int_{-\infty}^{\infty} \frac{z-\eta}{t}\, \mathrm{e}^{-G/2\nu} d\eta}{\int_{-\infty}^{\infty} \mathrm{e}^{-G/2\nu} d\eta}; \quad \text{where} \quad G(\eta; z, t) = \int_0^{\eta} \mathcal{F}_0(\eta')\, d\eta' + \frac{(z-\eta)^2}{2t}\,. \tag{6.21}$$

The *entropy solution* to the Burgers' equation is obtained by taking a proper limit where $\nu \to 0$. Chapter 4 of G.B. Whitham (1974) [106] is devoted to solutions to Burgers' equation. Numerical schemes for solving the equation, and other hyperbolic equations, are discussed in chapter 5 of J.A. Sethian (1999) [108].

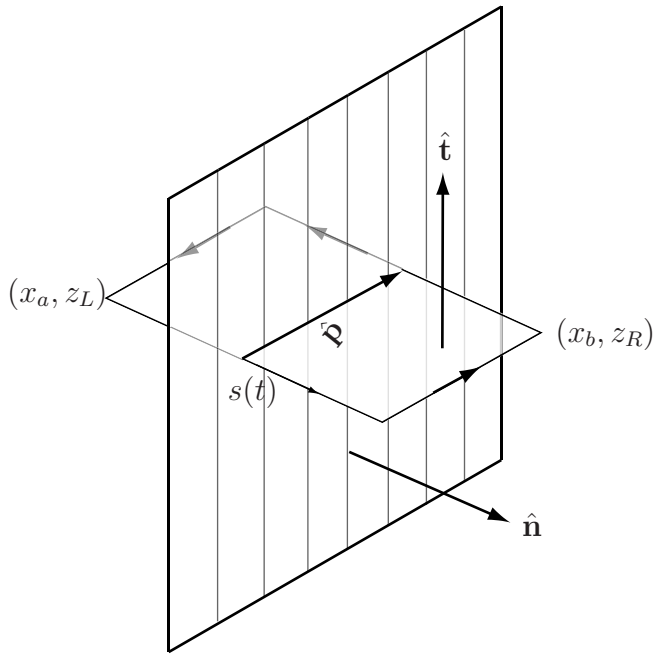

Figure 6.1: A rectangular contour joining (x_a, z_L), (x_a, z_R), (x_b, z_R), and (x_b, z_L) intersects a moving wall between $(x_a, s(t))$ and $(x_b, s(t))$.

form a triad. The net Burgers vector is expressible in terms of the Nye dislocation density $\boldsymbol{\rho}$ according to $b_j = \int_S \rho_{ij}\, dS_i$. Hence,

$$\frac{d}{dt}\int_S \rho_{ij}\, dS_i = -\oint_C J_{ij}\, dx_i\,. \tag{6.22}$$

In the limit of a thin contour where $x_a \to x_b$, the variation of $\boldsymbol{\rho}$ and $\boldsymbol{J}$ along $\hat{\mathbf{p}}$ is negligible. (In one dimension, this condition is automatically satisfied.) Moreover, the contributions of the contour integration of $\boldsymbol{J}$ along the two directions through the wall cancel. Thus equation 6.22 becomes

$$\frac{d}{dt}\left(\int_{z_L}^{z_R} \rho_{ij}\hat{t}_i\, dn\right)|x_b - x_a| = -|x_b - x_a|\hat{p}_i\left(J_{ij}(z_R) - J_{ij}(z_L)\right) \tag{6.23}$$

where the area integration of $\boldsymbol{\rho}$ reduces to a line integration along the direction

perpendicular to the wall. Upon differentiation, the left-hand side becomes

$$\begin{aligned}\frac{d}{dt}\int_{z_L}^{z_R}\rho_{ij}\hat{t}_i\,dn &= \frac{d}{dt}\int_{z_L}^{s(t)}\rho_{ij}\hat{t}_i\,dn + \frac{d}{dt}\int_{s(t)}^{z_R}\rho_{ij}\hat{t}_i\,dn \\ &= \hat{t}_i\rho_{ij}(z_L)\dot{s} - \hat{t}_i\rho_{ij}(z_R)\dot{s} + \int_{z_L}^{s(t)}\hat{t}_i\partial_t\rho_{ij}\,dn + \int_{s(t)}^{z_R}\hat{t}_i\partial_t\rho_{ij}\,dn\,.\end{aligned} \tag{6.24}$$

The last two integrals vanish as $z_L \to s^-(t)$ and $z_R \to s^+(t)$, leaving only

$$\frac{d}{dt}\int_{z_L}^{z_R}\rho_{ij}\hat{t}_i\,dn = -\hat{t}_i[\![\rho_{ij}]\!]\dot{s} = -\dot{s}\,\hat{p}_i[\![\hat{n}_k\partial_k\beta^{\mathrm{P}}_{ij}]\!], \tag{6.25}$$

where $[\![\cdot]\!]$ denotes the jump in the argument across the wall. The speed of the wall $\dot{s}(t)$ is along the direction normal to the wall. In general $\hat{\mathbf{p}}$ can point in any direction parallel to the wall, equation 6.23 holds regardless of the direction of $\hat{\mathbf{p}}$, and thus:

$$\dot{s}[\![\hat{n}_k\partial_k\beta^{\mathrm{P}}_{ij}]\!] = [\![J_{ij}]\!] \tag{6.26}$$

The jump condition (6.26) derived from the conservation of the density of dislocations is automatically satisfied by our transition from evolving $\boldsymbol{\rho}$ to evolving $\boldsymbol{\beta}^{\mathrm{P}}$, where we identify $\dot{\boldsymbol{\beta}}^{\mathrm{P}}$ with $\boldsymbol{J}$ (giving rise to our evolution equations). Consider a term in equation 6.26 corresponding to the wall velocity times the variation of $\boldsymbol{\beta}^{\mathrm{P}}$ on the right-hand side of the wall: $\dot{s}\,\hat{n}_k\partial_k\beta^{\mathrm{P}}_{ij}(z_R) = (d/dn)\beta^{\mathrm{P}}_{ij}(z_R)$. Viewing in the co-moving frame of the wall, this expression becomes

$$\dot{s}\,\frac{d\beta^{\mathrm{P}}_{ij}(z_R)}{dn} = \frac{ds}{dt}\cdot\lim_{n\to s^+(t)}\frac{d\beta^{\mathrm{P}}_{ij}(n)}{dn} = \lim_{n\to s^+(t)}\frac{dn}{dt}\frac{d\beta^{\mathrm{P}}_{ij}(n)}{dn} = \dot{\beta}^{\mathrm{P}}_{ij}(z_R) = J_{ij}(z_R), \tag{6.27}$$

and the jump condition follows immediately. Any numerical schemes we choose to solve the equations therefore automatically respect the conservation law stated above.

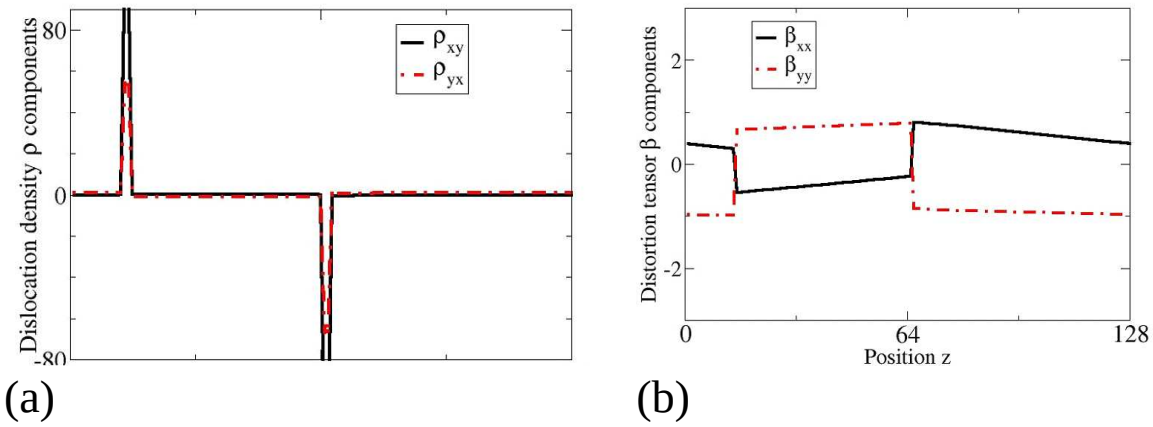

Figure 6.2: (a) **Dislocation density** tensor $\boldsymbol{\rho}$, one-dimensional simulation. (b) **Plastic distortion** tensor $\boldsymbol{\beta}^{\mathrm{P}}$ corresponding to (a). Notice that the asymptotic form for $\boldsymbol{\beta}^{\mathrm{P}}$ has not only jumps at the walls, but a linear slope between walls that scales at late times as $1/\sqrt{t-t_0}$.

6.4 Predictions & the asymptotics of wall formation

The mapping to $a^{(\alpha)}$ and $\bar{a}^{(\alpha)}$ allows us to predict three collective features in the time evolution of walls, the last two of which we observed in our simulations previous to this analysis (e.g., figure 6.2(b)).

(a) Burgers equation forms jump singularities in $\mathcal{F}$ at finite time, corresponding to cusps in the energy density $\mathcal{E}$. But the individual components $a^{(\alpha)}$ and $\bar{a}^{(\alpha)}$ contributing to $\mathcal{E}$ (equation 6.9) all show jumps at the singularity. To see this, note that according to the method of characteristics, each component of $a^{(\alpha)}$ and $\bar{a}^{(\alpha)}$ is constant along the characteristics family of $\mathcal{F}$. Since $\mathcal{F}$ possesses a jump, their characteristics must cross each other. Except in very rare initial profiles, each component of $a^{(\alpha)}$ and $\bar{a}^{(\alpha)}$ will therefore develop jump singularities. These jumps, however, must conspire to make $\mathcal{E}$ equal

on the two sides of the wall. In physical terms, our mechanism for wall formation involves a residual stress jump across the wall; this condition tells us that the net energy density (equation 6.9) due to the residual stress at a newly formed polygonized grain boundary will be the same on the two sides of the boundary.

(b) The velocity of the singularity in Burgers equation vanishes only if the jump is symmetric around zero. This implies that a stationary wall in our theory will have force density on the residual dislocations to the right and left equal and opposite: $\mathcal{F}_R = -\mathcal{F}_L$.

(c) At large time ($t \to \infty$), the solutions to Burgers equation between the singularities have the form $\mathcal{F} \sim (z - z_0)/(t - t_0)$. From $\mathcal{F} = \partial_z \mathcal{E}$, one finds

$$\mathcal{E} \sim \frac{1}{2} \frac{(z - z_0)^2}{t - t_0} + \mathcal{E}_0. \tag{6.28}$$

The asymptotic solution of $a^{(\alpha)}$ takes on the following form:

$$a^{(\alpha)} \sim \alpha^{(\alpha)} \frac{z - z_0}{\sqrt{t - t_0}} + \gamma^{(\alpha)} \tag{6.29}$$

Using $\mathcal{E} = \sum_\alpha a^{(\alpha)} a^{(\alpha)}$, one obtains the conditions among $\alpha^{(\alpha)}$ and $\gamma^{(\alpha)}$, consistent with the asymptotic form of $\mathcal{E}$:

$$\sum_\alpha \alpha^{(\alpha)} \alpha^{(\alpha)} = 1\,, \qquad \sum_\alpha \alpha^{(\alpha)} \gamma^{(\alpha)} = 0\,, \qquad \sum_\alpha \gamma^{(\alpha)} \gamma^{(\alpha)} = 2\mathcal{E}_0 \tag{6.30}$$

Figure 6.2(b) illustrates the components of $\boldsymbol{\beta}^{\mathrm{P}}$ at late times starting from random configurations and finally forming a pair of twist boundaries.

At low temperatures when the mobility rates between glide and climb are not the same ($\lambda \neq 0$), the evolution of the system becomes much more complicated. The method of characteristics reveals that the speed at which $a^{(1)}(z)$

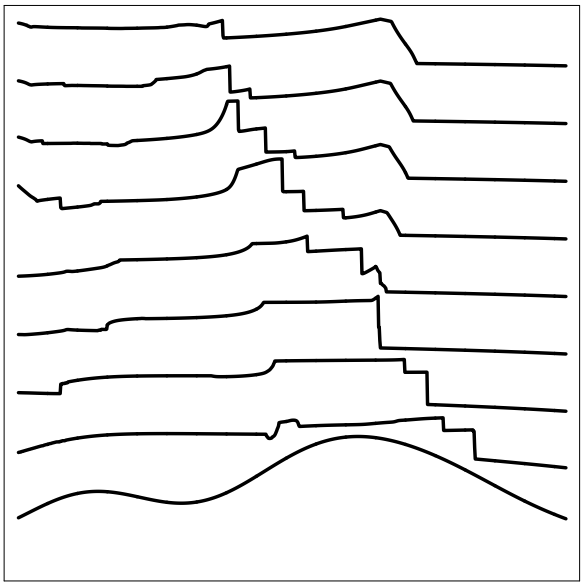

Figure 6.3: **Cell wall splitting** in a glide-only simulation; later times are displaced upward.

moves depends upon the relative mobility of glide and climb, and is different from the others. This mode is responsible for the local compression and expansion of the system along z. According to equation 6.13, the characteristic speed of $a^{(\alpha)}$ is $v^{(\alpha)} = (1/2 - (2\lambda/3)\delta_{1,\alpha})\mathcal{F}$. Effectively after each component forms a jump (corresponding to a wall), the jump tends to split due to the difference in velocities—showing behavior reminiscent of cell refinement seen experimentally. Figure 6.3 shows the numerical observation of wall splitting during evolution, while figure 6.4(b), (c), and (d) show mesh-size dependence of the splitting on 256, 512, and 1024 grid points respectively, starting with a pair of walls (figure 6.4(a)). Wall–splitting occurs regardless of the number of grid points.

Our prediction of jumps in residual stress during the high-temperature grain boundary formation and low-temperature cellular structure generation is timely. A number of high-profile experimental techniques using advanced X-ray and neutron

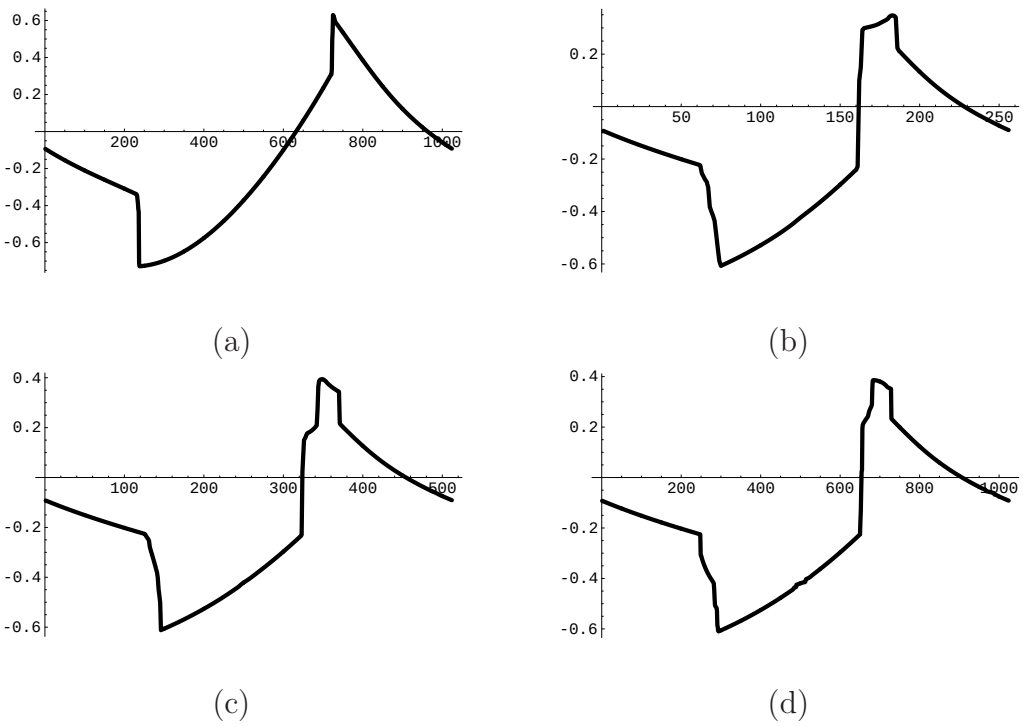

Figure 6.4: **Cell wall splitting (a)** Initially, a pair of sharp walls form from a smooth data set. The right wall splits into smaller walls. The simulations are run with **(b)** 256, **(c)** 512, and **(d)** 1024 grid points to check the mesh-size dependence.

scattering sources have been developed to give three-dimensional information on polycrystals, studying grain rotation [109, 110, 111, 112, 113, 114], cell splitting and rotation [115], residual stress [116, 117], texture and strain [118, 119, 27] (including in-situ deformation), strain [120, 121, 122], deformation microstructure [123], and 3D grain orientations sizes and strains [124]. Gene Ice (Oak Ridge National Labs, private communication) tells us even now that measurements at grain boundaries during polygonization should be straightforward at strains of 10^{-4}, and possible at strains of 10^{-5}.

CHAPTER 7

FINITE DIFFERENCE SIMULATIONS AND PREDICTIONS FOR DIFFERENT SLIP SUBSYSTEMS

Except in a few very simple cases, our evolution equation cannot be solved analytically. In this chapter, we address the implementations of our finite difference simulations and some of the results in one and two dimensions. We discuss, in section 7.1, both the upwind and the two Fourier regularization schemes for our numerics. Results in one dimension for a system with glide & climb and a system without climb, and the final state of a two-dimensional simulation forbidden climb are also presented.[1] In section 7.2, we propose to specialize our theory to systems with only one or a few active slip systems. We argue that our theory restricted to a single slip in two dimensions predicts not walls in the dislocation density but jumps in $\boldsymbol{\rho}$ corresponding to cusps in the distortion tensor.

7.1 Finite difference simulation

We simulate systems of spatial extent L in one or two dimensions, with periodic boundary conditions and no external stress. The initial plastic distortion field $\boldsymbol{\beta}^{\mathrm{P}}$ is a Gaussian random field with mean square amplitude β_0^{P} and root-mean-square decay length approximately $L/16$. In one dimension, we use the upwind scheme [125] as implemented by Press *et al.* [126] In two dimensions, except for a special case of one-slip system where the upwind scheme is applicable, we calculate $\boldsymbol{\sigma}$ using Fourier methods and regularize our equations by adding a fourth-order numerical viscosity[2] $-\epsilon^{(4)}\nabla^4\beta_{ij}^{\mathrm{P}}$ to equation 6.1. (A second-order viscosity $\nabla^2\beta_{ij}^{\mathrm{P}}$

[1] The result in this section was published by the author in [2].

[2] In two dimensions, we do not find numerical instabilities associated with solving the fourth order viscous term, traditionally known as *Burnett equation*, gener-

was not as successful in suppressing the instabilities.) In one dimension, we have checked that the upwind scheme produces the same solution as the viscosity regularization up to the point of shock formation (appendix G). We speculate that the wall dynamics regularization may be non-trivial and stochastic, emerging out of avalanches and critical depinning phenomena on sub-cell length scales—observed both experimentally [130] and theoretically [131] in systems with only one active slip system.

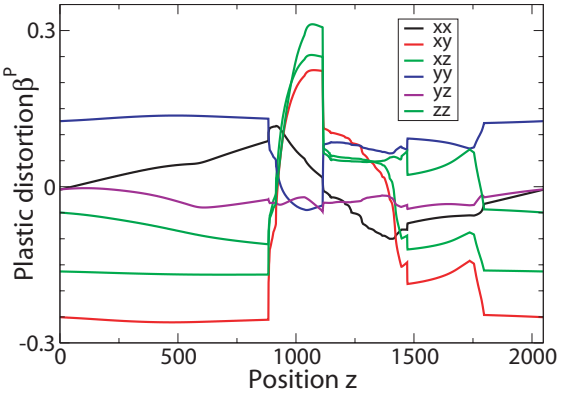

Figure 7.1: Plastic distortion tensor component β^{P}_{ij} in one dimension allowing only glide motion, after time $t = 20L^2/D\mu$, with 2048 mesh points. The shocks or jumps in the values correspond to the cell walls. Walls perpendicular to z that are stress free (satisfying Frank's condition) have no jump in β^{P}_{xx}, β^{P}_{yy} or $\beta^{\mathrm{P}}_{xy} + \beta^{\mathrm{P}}_{yx}$.

Figure 7.1 shows the final state of the plastic distortion $\boldsymbol{\beta}^{\mathrm{P}}$ in a one-dimensional system evolving under dislocation glide only (corresponding to plastic deformation, which experimentally leads to cell structure formation). Jump singularities in $\boldsymbol{\beta}^{\mathrm{P}}$ form after a short time, representing a wall of dislocations and an abrupt change in lattice orientation. The cell walls in our model are not grain boundaries, because they do not correspond to pure, simple rotations (they do not satisfy the Frank

ally seen in hypersonic flows models [127, 128], or the Boltzman equation for gas flow [129].

conditions [104]). There is a jump in the stress across each cell wall: the glide component of the forces from the two neighboring cells on $\boldsymbol{\rho}$ in a wall is equal, opposite, and compressive. Our model therefore predicts that the initial formation of cell walls during low-temperature plastic deformation is driven by a stress jump due to non-cancellation of the stress field of the constituent dislocations. As our system evolves, new cell walls form (intriguingly similar to the cell refinement seen experimentally [3, 16]) and the existing cell walls evolve to reduce their stress jumps.

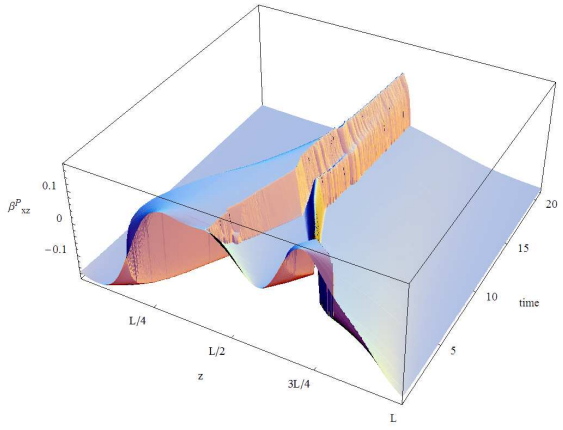

Figure 7.2: The xz-component of the plastic distortion tensor in one dimension up to time $t = 22L^2/D\mu$, with 2048 mesh points. The evolution allows both glide and climb motions. The walls move and coalesce until only a single wall survives.

Figure 7.2 shows the evolution of the plastic distortion in a system allowing both glide and climb, corresponding to high-temperature annealing of a plastically deformed structure. Here the initial singularities again are not grain boundaries, but walls of dislocations with net stress jumps. These walls then move and coalesce in response to the net force due to other dislocations, coarsening the resulting grain boundary structure.

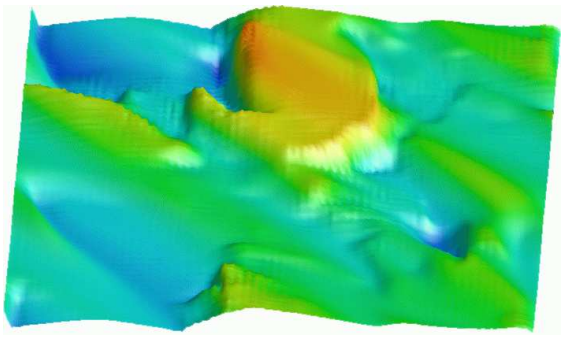

Figure 7.3: The yz-component of the plastic distortion tensor allowing only glide, in two dimensions after time $t = 9.15L^2/D\mu$.

Figure 7.3 shows the final state of $\boldsymbol{\beta}^{\mathrm{P}}$ in a two-dimensional plasticity simulation[3] (with glide and not climb). Notice the formation of sharp walls (mathematically demonstrated above only in one dimension). These walls separate relatively unstrained regions which we identify with the cells formed during plastic deformation. As in the one-dimensional simulations, the cell walls formed at short times have stress jumps.

7.2 Predictions for different slip systems in two dimensions

There is no broad, analytical understanding of the several distinct stages of hardening. Stage I hardening, for example, is characterized by a single active slip system and rather random dislocation patterns; stage III and IV hardening are characterized by multiple slip systems and cellular dislocation structures. Our continuum dislocation theory appears to provide an analytical explanation for the connection between slip systems and morphology.

The wall formation in our theory is striking and unmistakable—without need-

[3]Appendix H describes an alternative way of visualizing the result of a system with several active components efficiently.

ing dislocation nucleation, annihilation, or entanglement. Due to computational complexity, three dimensional simulations of line dislocations are still quite premature, and only recently have shown hints of wall formation [132]. There has been extensive work on discrete point dislocation simulations in two dimensions, where the numerics is much more controllable. Glide-only simulations with only one slip system [32, 4] do not form obvious walls. Single-slip system simulations that include climb [5] convincingly form walls, but through a different mechanism (a coarsening procedure involving the coalescing of small angle boundaries). 2D point-dislocation simulations with two active slip systems have also developed walls [94, 95, 93, 97, 96, 91, 92, 90]. No simple analytical understanding of this difference is gleaned from these microscopic simulations.

We can mimic these discrete dislocation simulations by starting our simulations with random initial conditions containing only edge dislocations, and by modifying our volume preserving term λ to enforce zero trace restricted to the non-zero components. Typical 2D simulations often incorporate point edge dislocations with tangents perpendicular to the simulation plane and Burgers vectors in the simulation plane. In agreement with experiment and the discrete dislocation simulations, we observe no cell wall structures in single slip. However, our model predicts a more subtle network of cusp singularities in the distortion field, corresponding to jumps in the dislocation density. There are two different ways in which we can map this into our one-dimensional simulation. If we start with only one non-zero component of $\boldsymbol{\rho}$, namely either ρ_{xz} or ρ_{yz} (edge dislocations with Burgers vector along the one-dimensionally varying axis $\hat{\mathbf{z}}$), the dislocations obey the zero-stress Frank condition and nothing evolves. If we start with only ρ_{zx} or ρ_{zy} non-zero (edge dislocations with Burgers vectors along one of the uniform directions) then

our evolution law produces only cusps, not jumps (figure 7.4(a)). We can motivate this using our mapping to Burgers equation. The net energy density $\mathcal{E}$ only forms cusps (conclusion (a) in section 6.2.1), and not walls. Jumps in $\boldsymbol{\beta}^{\mathrm{P}}$ are possible only if their contributions lead to continuation in $\mathcal{E}$. With only one non-zero component of $\boldsymbol{\beta}^{\mathrm{P}}$ (in this case β^{P}_{yx}, corresponding to ρ_{zx}), only cusp singularities can form.

A 2D single-slip, discrete-dislocation simulation with both glide and climb [5] showed the rapid disappearance of variations along the direction normal to the glide plane, leading to a state described by a continuum of low-angle grain boundary. This was followed by a slow coarsening process driven by the $\theta \log \theta$ term in the energy of these boundaries.[4] Our simulation allowing climb (with a smaller correlation length in the Gaussian random initial conditions) nicely reproduces the network of parallel walls (figure 7.4(b)) reproducing the result of the discrete simulation.

Finally, our climb-free simulations allowing two slip systems of parallel edge dislocations (figure 7.4(c)) do form the same kinds of sharp-walled cellular structures that we observe for general initial conditions, in agreement with the 2D discrete dislocation simulations. These simulations not only validate our closure approximation (reproducing the microscopic simulation) but also illustrate the fact that the formation of walls is not a generic result of energy minimization, but emerges from the nonlinear dynamics of the equations of motion.

[4]See section 4.2 for a discussion on the vanishing of a general grain boundary in the continuum limit.

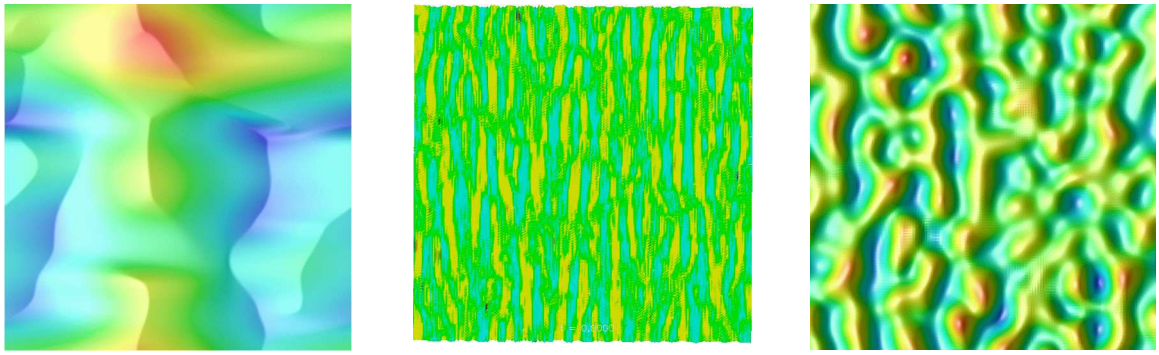

Figure 7.4: (a) **Cusps formed with one slip system.** Plastic distortion tensor β^{P}_{yx} formed by climb-free evolution of a Gaussian random initial state of edge dislocations pointing along $\hat{\mathbf{z}}$ with Burgers vector along $\pm\hat{\mathbf{x}}$. Notice that walls do not form with one slip system, only cusps in the distortion tensor; compare to [4]. (b) **Continuum of walls**. The dislocation density tensor ρ_{zx} evolved allowing both glide and climb from a random initial state of edge dislocations along $\mathbf{t} \parallel \hat{\mathbf{z}}$ with $\mathbf{b} \parallel \hat{\mathbf{x}}$. Notice that the dislocations arrange themselves into small-angle tilt boundaries at the lattice scale, but do not coarsen; compare to [5]. (c) **Cell walls** in a climb-free simulation with two active slip systems ρ_{zx} and ρ_{zy}, edge dislocations perpendicular to the simulation. Notice the walls separating cells. Here the smaller length scale reflects the smaller Gaussian correlation length we used for the initial conditions. Also, we only show ρ_{zx}, so the cell walls appear incomplete; the ρ_{zy} components fill in the gaps leading to a clear cellular pattern.

APPENDIX A

EUCLIDEAN TENSORS

A.1 Subscript notations

In this work, we denote a vector $\mathbf{a}$ of the Euclidean space $\mathbb{E}$ only by its element a_i. This is a shorthand notation for

$$\mathbf{a} \equiv a_i \hat{\mathbf{e}}_i \,, \tag{A.1}$$

where we employ the use of Einstein's convention of summing over repeated indices. $\hat{\mathbf{e}}_i$ is an element of $(\hat{\mathbf{e}}_1, \hat{\mathbf{e}}_2, \hat{\mathbf{e}}_3)$, a positive oriented orthonormal basis of $\mathbb{E}$ with dimension 3. Similarly a second-rank Euclidean tensor $\boldsymbol{A}$, represented by

$$\boldsymbol{A} \equiv A_{ij}(\hat{\mathbf{e}}_i \otimes \hat{\mathbf{e}}_j) \,, \tag{A.2}$$

is written simply as A_{ij}, and so on.

The contraction between any two tensors of arbitrary ranks are defined according to the dot product of the basis tensors,

$$\hat{\mathbf{e}}_i \cdot \hat{\mathbf{e}}_j = \delta_{ij} \tag{A.3}$$

where

$$\delta_{ij} = \begin{cases} 1, & i = j \\ 0, & i \neq j \end{cases} \tag{A.4}$$

is called *Kronecker delta*. For example, the dot product between two vectors $\mathbf{a}$ and $\mathbf{b}$ is

$$\mathbf{a} \cdot \mathbf{b} = a_i b_j (\hat{\mathbf{e}}_i \cdot \hat{\mathbf{e}}_j) = a_i b_j \, \delta_{ij} = a_i b_i \,, \tag{A.5}$$

or between two tensors $\boldsymbol{A}$ and $\boldsymbol{B}$,

$$\begin{aligned}\boldsymbol{A} : \boldsymbol{B} &= A_{ij}B_{km}(\hat{\mathbf{e}}_i \otimes \hat{\mathbf{e}}_j) : (\hat{\mathbf{e}}_k \otimes \hat{\mathbf{e}}_m) \\ &= A_{ij}B_{km}(\hat{\mathbf{e}}_i \cdot \hat{\mathbf{e}}_k) \otimes (\hat{\mathbf{e}}_j \cdot \hat{\mathbf{e}}_m) \\ &= A_{ij}B_{km}\,\delta_{ik}\delta_{jm} = A_{ij}B_{ij}\,.\end{aligned} \tag{A.6}$$

The third-rank *Levi–Civita* tensor is defined as

$$\boldsymbol{\varepsilon} = \mathrm{Det}(\hat{\mathbf{e}}_i, \hat{\mathbf{e}}_j, \hat{\mathbf{e}}_k)\hat{\mathbf{e}}_i \otimes \hat{\mathbf{e}}_j \otimes \hat{\mathbf{e}}_k\,. \tag{A.7}$$

It will be denoted by ε_{ijk}. From the property of the determinant,

$$\varepsilon_{ijk} = \begin{cases} 1, & \mathrm{Perm}[\{x, y, z\}] \\ -1, & \mathrm{Perm}[\{x, z, y\}] \\ 0, & \text{otherwise} \end{cases} \tag{A.8}$$

where Perm$[\cdot]$ gives all the cyclic permutations of its argument. We can use ε_{ijk} to formally define a cross product between two vectors:

$$\mathbf{a} \times \mathbf{b} = \boldsymbol{\varepsilon} : (\mathbf{a} \otimes \mathbf{b}) = \varepsilon_{ijk}a_jb_k\hat{\mathbf{e}}_i \Longrightarrow \varepsilon_{ijk}a_jb_k \tag{A.9}$$

The cross product between two tensors of arbitrary ranks can be defined in the same fashion.

A.2 Rotation

Given the group $SO(3) = \{\boldsymbol{A}|$ a 3×3 real matrix, $\det \boldsymbol{A} = 1, \boldsymbol{A}\boldsymbol{A}^t = \mathbf{1}\}$, the condition $\boldsymbol{A}\boldsymbol{A}^t = \mathbf{1}$ is equivalent to requiring that the three columns of $\boldsymbol{A} = [\mathbf{a}_1, \mathbf{a}_2, \mathbf{a}_3]$ be mutually perpendicular unit vectors. And that $\det \boldsymbol{A} = \mathbf{a}_1 \cdot (\mathbf{a}_2 \times \mathbf{a}_3) = 1$ means that the triplet is right handed. The three columns of $\boldsymbol{A}$ are also the images of the three unit vectors pointing along the positive $\hat{\mathbf{x}}$, $\hat{\mathbf{y}}$, and $\hat{\mathbf{z}}$ axes, respectively.

So $SO(3)$ can be thought of as the set of rotation in $\mathbb{R}^3$ or as the set of possible orientations of a rigid body.

Given two Cartesian coordinate systems with a common origin, the relative orientation can be described by three quantities. The most commonly known representation is the Euler angles of rotation, where three angles are needed to describe the relative orientation. The less commonly known system is ascribed to the French mathematician O. Rodrigues (1794-1851) [133], hence the name *Rodrigues rotation formula*. We are going to present the formula for Euler-angle rotation and provide a physically motivated derivation of the Rodrigues formula.[1]

A.2.1 Euler-angle rotation

The rotation matrices about $\hat{\mathbf{z}}$ and $\hat{\mathbf{x}}$ axes by an angle θ are given by

$$\boldsymbol{R}_z(\theta) = \begin{pmatrix} \cos(\theta) & -\sin(\theta) & 0 \\ \sin(\theta) & \cos(\theta) & 0 \\ 0 & 0 & 1 \end{pmatrix}, \quad \boldsymbol{R}_x(\theta) = \begin{pmatrix} 1 & 0 & 0 \\ 0 & \cos(\theta) & -\sin(\theta) \\ 0 & \sin(\theta) & \cos(\theta) \end{pmatrix}. \tag{A.10}$$

Any rotation $\boldsymbol{\gamma} \in SO(3)$ has a unique representation of the form

$$\boldsymbol{\gamma} = \boldsymbol{R}_z(\phi)\boldsymbol{R}_x(\theta)\boldsymbol{R}_z(\psi) \tag{A.11}$$

with $0 \leq \theta \leq \pi, 0 \leq \phi, \psi \leq 2\pi$ [135]. These angles are called the Euler angles. The map $(\psi, \theta, \phi) \mapsto \boldsymbol{\gamma}(\psi, \theta, \phi) = \boldsymbol{R}_z(\phi)\boldsymbol{R}_x(\theta)\boldsymbol{R}_z(\psi)$ provides a local coordinate system on a neighborhood of each point in $SO(3)$.

Note that the conventions of the axes of rotation and their order are by no means unique. There are a few conventions out there that are used equally as

[1] Goldstein (*Classical Mechanics* 1980) particularly provides a thorough derivation of the Rodrigues rotation formula [134].

often. For example, some author defines a series of rotations about $\hat{\mathbf{x}}$, $\hat{\mathbf{y}}$, and $\hat{\mathbf{z}}$ respectively. Another rotates first about $\hat{\mathbf{z}}$ then $\hat{\mathbf{y}}$, and finally about $\hat{\mathbf{z}}$ again. The general principle remains true; it is sufficient to define any relative orientation by three angle parameters.

A.2.2 Rodrigues rotation

An alternative, perhaps more natural, method of defining a rotation is done by specifying an angle ψ about a fixed axis of rotation given by a unit vector $\hat{\mathbf{n}}$. The rotation matrix, in this case, can be computed easily by appealing to a physical argument. Let $\mathbf{x}$ be any vector to be rotated about $\hat{\mathbf{n}}$ in the counter-clockwise direction by an angle ψ. If we regard ψ as a time variable, then the velocity of a particle at $\mathbf{x}$ in a circular orbit around $\hat{\mathbf{n}}$ with the unit angular speed is given by

$$\frac{d\mathbf{x}}{d\psi} = \hat{\mathbf{n}} \times \mathbf{x}. \tag{A.12}$$

The solution to the ODE is

$$\mathbf{x} = \mathrm{e}^{\psi \boldsymbol{A}} \mathbf{x}_0, \tag{A.13}$$

where $A_{ij} \equiv \varepsilon_{ijk} n_k$, and $\mathbf{x}_0$ denotes the initial position of the particle. Notice that since $\boldsymbol{A}$ is a skew-symmetric matrix, $\left(\mathrm{e}^{\psi \boldsymbol{A}}\right)^\dagger = \mathrm{e}^{\psi \boldsymbol{A}^\dagger} = \mathrm{e}^{-\psi \boldsymbol{A}} = \left(\mathrm{e}^{\psi \boldsymbol{A}}\right)^{-1}$, and $\det \mathrm{e}^{\psi \boldsymbol{A}} = \mathrm{e}^{\mathrm{tr}\, \psi \boldsymbol{A}} = \mathrm{e}^0 = 1$, therefore $\mathrm{e}^{\psi \boldsymbol{A}}$ is a valid rotation matrix.

The *Rodrigues vector* $\boldsymbol{\psi} \equiv \psi \hat{\mathbf{n}}$ defines the rotation matrix $\boldsymbol{R}(\boldsymbol{\psi}) \in \mathrm{SO}(3)$ associated with a rotation by an angle $|\boldsymbol{\psi}|$ about $\boldsymbol{\psi}$ according to

$$R_{ij}(\boldsymbol{\psi}) = \mathrm{e}^{\varepsilon_{ijk} \psi_k}. \tag{A.14}$$

By Taylor expanding the exponential, one obtains

$$\boldsymbol{R}(\boldsymbol{\psi}) = \boldsymbol{I} + \sin\psi \boldsymbol{A} + (1 - \cos\psi)\boldsymbol{A}^2, \tag{A.15}$$

where $\boldsymbol{I}$ is the identity matrix and $\boldsymbol{A}$ is as defined previously.

A.3 Cartesian isotropic tensors

An isotropic tensor of rank n has 3^n real components.[2] Let's denote a component of this tensor by $T_{ijk\ldots}$. Let R_{ij} be a component of a rotation matrix where $\boldsymbol{R} \in \mathrm{SO}(3)$. Then $\boldsymbol{T}$ has to satisfy the following transformation law,

$$T_{ijk\ldots} = R_{im}R_{jn}R_{kp}\ldots T_{mnp\ldots} \tag{A.16}$$

which means an isotropic tensor is invariant under an arbitrary rotation. A complete listing of isotropic Cartesian tensors of ranks up to eight were categorized by Kearsley and Fong in 1975 [59].

Table A.1: Linearly independent isotropic tensors of ranks up to six

Rank	Isotropic tensors
2	δ_{ij}
3	ε_{ijk}
4	$\delta_{ij}\delta_{km}$ $\quad$ $\delta_{ik}\delta_{jm}$ $\quad$ $\delta_{im}\delta_{jk}$
5	$\varepsilon_{ijk}\delta_{mp}$ $\quad$ $\varepsilon_{ijm}\delta_{kp}$ $\quad$ $\varepsilon_{ijp}\delta_{km}$ $\quad$ $\varepsilon_{ikm}\delta_{jp}$ $\quad$ $\varepsilon_{ikp}\delta_{mj}$ $\quad$ $\varepsilon_{imp}\delta_{jk}$
6	$\delta_{ij}\delta_{km}\delta_{pq}$ $\quad$ $\delta_{ij}\delta_{kp}\delta_{mq}$ $\quad$ $\delta_{ij}\delta_{kq}\delta_{mp}$ $\quad$ $\delta_{ik}\delta_{jm}\delta_{pq}$ $\quad$ $\delta_{ik}\delta_{jp}\delta_{mq}$ $\delta_{ik}\delta_{jq}\delta_{mp}$ $\quad$ $\delta_{im}\delta_{jk}\delta_{pq}$ $\quad$ $\delta_{im}\delta_{jp}\delta_{kq}$ $\quad$ $\delta_{im}\delta_{jq}\delta_{kp}$ $\quad$ $\delta_{ip}\delta_{jk}\delta_{mq}$ $\delta_{ip}\delta_{jm}\delta_{kq}$ $\quad$ $\delta_{ip}\delta_{jq}\delta_{km}$ $\quad$ $\delta_{iq}\delta_{jk}\delta_{mp}$ $\quad$ $\delta_{iq}\delta_{jm}\delta_{kp}$ $\quad$ $\delta_{iq}\delta_{jp}\delta_{km}$

All of isotropic tensors of rank greater than three can be constructed from the product of the isotropic tensor of rank two and three [137]. These are the Kronecker delta δ_{ij} and the Levi–Civita tensor ε_{ijk}.[3] To give some examples, Table A.1 shows distinct isotropic tensors of ranks 2, 3, 4, 5 and 6.

[2]For general accounts on tensors, consult, *e.g.* [136].

[3]Other common names for ε_{ijk} are a totally antisymmetric tensor or an alternating tensor.

An isotropic tensor of rank seven can be built up from the products of a totally antisymmetric tensor and two Kronecker deltas. From a combinatoric argument, there are 105 of these. However only 36 of them are linearly independent; the rest can be written down as various linear combinations of these 36 tensors. In this work, the evolution equation involves isotropic tensors up to rank eight. There are fundamentally 105 of these which can be constructed by tensor products of four Kronecker deltas. 91 of these are linearly independent, and hence, form a complete set of bases.[4] For an interested reader, the number of linearly independent fundamental isotropic tensors of rank n is

$$M(n) = \sum_{k=0}^{(n+1)/2} \left[\binom{n}{2k} - \frac{1}{2} \binom{n}{2k-1} \right] \binom{2k}{k}. \tag{A.17}$$

This formula can easily be obtained by a straight-forward group theoretic calculation.

A.4 Some useful properties involving δ_{ij} and ε_{ijk}

The following contractions are important in deriving many formulæ throughout this work:

$$\delta_{ii} = 3 \tag{A.18}$$

$$\delta_{ij}\delta_{jk} = \delta_{ik} \tag{A.19}$$

$$\varepsilon_{ijk}\delta_{jk} = 0 \tag{A.20}$$

$$\varepsilon_{ijk}\varepsilon_{ijk} = 6 \tag{A.21}$$

$$\varepsilon_{ijk}\varepsilon_{ijl} = 2\delta_{kl} \tag{A.22}$$

$$\varepsilon_{ijm}\varepsilon_{klm} = \delta_{ik}\delta_{jl} - \delta_{il}\delta_{jk} \tag{A.23}$$

[4] See appendix B.2 for how we arrived at this number.

APPENDIX B

SYMMETRIES AND INDEPENDENT TERMS IN D

B.1 Some facts about symmetry group

In this chapter, we shall only outline important definitions and quote some necessary results from group theory and the representation theory. There are plenty of classic textbooks on the subject for those interested [137, 138, 139, 140].

Definition 1 *A* group *is a set G together with an associative binary operation $G \times G \to G$ called* multiplication *having the following properties:*

- *There exists a unique element $E \in G$ called the* identity *such that $E \cdot g = g \cdot E = g$.*
- *For every element $g \in G$, there exists an element g^{-1}, called the* inverse *of g, such that $g \cdot g^{-1} = g^{-1} \cdot g = E$.*

In this work, we mainly focus on a rotational group $SO(3)$ which was briefly described in appendix A.2. This is an example of a *continuous group* which contains an infinite number of elements. It is, however, easier to work with a finite group, then generalize the results to a continuous group. Let's start off with a couple more definitions.

Definition 2 *Consider two finite groups G and G' with element $\{E, a, b, \ldots\}$ and $\{E', a', b', \ldots\}$. Suppose there is a mapping ϕ between the elements of G and G' which preserves their composition rules,* i.e., *if $a' = \phi(a)$ and $b' = \phi(b)$, then*

$$\phi(ab) = \phi(a)\phi(b) = a'b' \,. \tag{B.1}$$

A representation *of dimension n of an abstract group G is such mapping ϕ between the elements of G and the group of nonsingular $n \times n$ matrices with complex entries and ordinary matrix multiplication.*

According to this definition, if elements a and b of G are assigned matrices $\boldsymbol{D}(a)$ and $\boldsymbol{D}(b)$, then $\boldsymbol{D}(a) \cdot \boldsymbol{D}(b) = \boldsymbol{D}(ab)$. The nonsingular nature of the matrices is required because the inverses must be contained in the set.

Definition 3 *The representation $\boldsymbol{D}(g)$ and $\boldsymbol{D}'(g)$ are said to be* equivalent *if there exists a non-singular matrix $\boldsymbol{S}$ such that*

$$\boldsymbol{D}'(g) = \boldsymbol{S}^{-1}\boldsymbol{D}(g)\boldsymbol{S}. \tag{B.2}$$

And here comes the great orthogonality theorem.

Theorem 3 *Let a group G contain h elements with an element $g \in G$ and $\boldsymbol{D}^{(\alpha)}(g)$ and $\boldsymbol{D}^{(\beta)}(g)$ be two irreducible unitary representations with dimension n_α and n_β respectively. Then*

$$\sum_g \left[D_{ij}^{(\alpha)}(g)\right]^* D_{km}^{(\beta)}(g) = \frac{h}{n_\alpha}\delta_{\alpha\beta}\delta_{ik}\delta_{jm}, \tag{B.3}$$

where the sum is taken over all element $g \in G$.

Since all matrix representations related by a similarity transformation are equivalent representations of a group, it turns out that a property that is invariant to a similarity transformation can also provide a representation of the group. One such property is the *trace* or the *character* of the matrix which is often noted as $\chi^{(\alpha)}(g) \equiv \mathrm{Tr}[\boldsymbol{D}^{(\alpha)}(g)]$.

We can now make use of Theorem 3 to obtain a similar orthogonality relation for the trace. By contracting over the indices i, j and k, m in (B.3), we have

$$\sum_g \left[\chi^{(\alpha)}(g)\right]^* \chi^{(\beta)}(g) = h\,\delta_{\alpha\beta}\,. \tag{B.4}$$

Equation B.4 enables us to decompose any *reducible* representation into the sum of *irreducible* ones if the characters of both are known.

Definition 4 *A representation* $\boldsymbol{D}$ *is said to be* reducible *if after a suitable similarity transformation,* $\boldsymbol{D}$ *looks like,*

$$\boldsymbol{D}(g) = \begin{pmatrix} \begin{pmatrix} & & \\ & \boldsymbol{D}^{(\alpha)}(g) & \\ & & \end{pmatrix} & \mathbf{0} & \cdots & \mathbf{0} \\ \mathbf{0} & \begin{pmatrix} & & \\ & \boldsymbol{D}^{(\beta)}(g) & \\ & & \end{pmatrix} & \cdots & \mathbf{0} \\ \vdots & & \ddots & \end{pmatrix} \tag{B.5}$$

where $\boldsymbol{D}^{(\alpha)}(g), \boldsymbol{D}^{(\beta)}(g), \ldots$ *are called* irreducible *representations; they cannot be further decompose into the sum of subspaces by any coordinate transformation.*

One often writes (B.5) as

$$\boldsymbol{D}(g) = \boldsymbol{D}^{(\alpha)}(g) \oplus \boldsymbol{D}^{(\beta)}(g) \oplus \ldots \tag{B.6}$$

Suppose $a^{(\beta)}$ indicates the number of times the irreducible representation $\boldsymbol{D}^{(\beta)}$ is contained in $\boldsymbol{D}$, it immediately follows that

$$\chi(g) = \sum_{\beta} a^{(\beta)} \chi^{(\beta)}(g)\,. \tag{B.7}$$

Multiplying both sides of (B.7) by $\left[\chi^{(\alpha)}(g)\right]^*$ then sum over all g. Using (B.4), we have

$$a^{(\alpha)} = \frac{1}{h} \sum_{g} \chi(g) \left[\chi^{(\alpha)}(g)\right]^*, \tag{B.8}$$

which is the result that we're after.

There are several ways to construct a new representation given two other representations. The most common way is to perform a *direct product* or a *tensor product*. Consider $T : G \to GL(\mathbb{V})$ and $S : G \to GL(\mathbb{W})$, two representations of a group G. Let $\mathbb{V} \times \mathbb{W}$ be the Cartesian product of the two carrier spaces. This becomes a vector space upon defining the vector space operations:

$$a(v_1, w_1) + b(v_2, w_2) \equiv (av_1 + bv_2, aw_1 + bw_2), \tag{B.9}$$

where $a, b \in \mathbb{C}$. We then define an action of the group G on $\mathbb{V} \otimes \mathbb{W}$ through the representation $T \otimes S : G \to GL(\mathbb{V} \otimes \mathbb{W})$ by

$$T \otimes S(g)(v, w) = (T(g)v, S(g)w). \tag{B.10}$$

Matrix elements of the representation are given by

$$(T \otimes S)_{ia,jb}(g) \equiv T_{ij}(g)S_{ab}(g). \tag{B.11}$$

The character of the tensor product representation is

$$\chi^{T\otimes S}(g) = (T \otimes S)_{ia,ia}(g) = T_{ii}(g)S_{aa}(g) = \chi^T(g)\chi^S(g). \tag{B.12}$$

The character of the tensor product is just the product of the characters.

An important special case arises when one tries to perform the tensor product of a representation with itself. It turns out that the product, in this case, can be decomposed into two subspaces that are separately invariant under the action of the group. Note that

$$v_i w_j = \frac{1}{2}\left(v_i w_j + v_j w_i\right) + \frac{1}{2}\left(v_i w_j - v_j w_i\right). \tag{B.13}$$

In other words, every product can be written as the sum of a symmetric and an antisymmetric vectors—with the exception of the zero vector which is both

symmetric and antisymmetric. Therefore,

$$\mathbb{V} \otimes \mathbb{V} = (\mathbb{V} \circledS \mathbb{V}) \oplus (\mathbb{V} \circledA \mathbb{V}). \tag{B.14}$$

Let's now consider the action of the group on each subspace,

$$T \otimes T(g) v_i w_j = (T_{ki}(g) v_k, T_{lj}(g) w_l) = T_{ki}(g) T_{lj}(g) (v_k, w_l) = (T \otimes T)_{kl,ij}(g) v_k w_l. \tag{B.15}$$

From this, we obtain

$$\begin{aligned} T \otimes T(g)(v_i w_j \pm v_j w_i) &= \left[(T \otimes T)_{kl,ij}(g) \pm (T \otimes T)_{kl,ji}(g) \right] v_k w_l \\ &= \frac{1}{2} \left[(T \otimes T)_{kl,ij}(g) \pm (T \otimes T)_{kl,ji}(g) \right] \left[v_k w_l \pm v_l w_k \right] \\ &= \frac{1}{2} \left[T_{ki} T_{lj} \pm T_{kj} T_{li} \right] \left[v_k w_l \pm v_l w_k \right], \end{aligned} \tag{B.16}$$

where + and − represent that symmetric and antisymmetric operations respectively. We can easily figure out the character for each subspace, using $T_{ii}(g) = \chi^T(g)$ and $T_{ik}(g) T_{ki}(g) = \chi^T(g \cdot g)$,

$$\chi^{T \circledS T}(g) = \frac{1}{2} \left(\left(\chi^T(g) \right)^2 + \chi^T(g \cdot g) \right), \tag{B.17}$$

$$\chi^{T \circledA T}(g) = \frac{1}{2} \left(\left(\chi^T(g) \right)^2 - \chi^T(g \cdot g) \right). \tag{B.18}$$

The properties presented above for finite groups can be quite naturally generalized to continuous groups. Each irreducible representation now contains an infinite sequence of matrices, however the dimension of the representation remains finite. The great orthogonality theorem and the corresponding character formula become

$$\int d\boldsymbol{\mu}(g) \, \left[D^{(\alpha)}_{ij}(g) \right]^* D^{(\beta)}_{km}(g) = \frac{1}{n_\alpha} \delta_{\alpha\beta} \delta_{ik} \delta_{jm} \int d\boldsymbol{\mu}(g) \,, \tag{B.19}$$

and

$$\int d\boldsymbol{\mu}(g) \left[\chi^{(\alpha)}(g) \right]^* \chi^{(\beta)}(g) = \delta_{\alpha\beta} \,. \tag{B.20}$$

The number of irreducible representations of type $\boldsymbol{D}^{(\alpha)}(g)$ contained in $\boldsymbol{D}(g)$ is

$$a^{(\alpha)} = \int d\boldsymbol{\mu}(g)\, \chi(g)\, \left[\chi^{(\alpha)}(g)\right]^*, \tag{B.21}$$

where $\chi(g) = D_{ii}(g)$, and $[\chi^{(\alpha)}(g)]^* = [D^{(\alpha)}_{ii}(g)]^*$.

Instead of summing over all elements in the group as in the case of a finite group, one needs to define an invariant integration for a continuous group. This invariant volume element (nonvanishing n-form) is called *Haar measure*. We shall give an explicit expression of the Haar measure in terms of coordinates of a general Lie group [141]. Let $\mathbf{y} = (y^1, \ldots, y^r)$ be the coordinates of the translation of $\mathbf{x} = (x^1, \ldots, y^r)$ by $g \in G$. Then $\mathbf{y} = \mathbf{m}(g, \mathbf{x})$ such that $dy^j = (\partial y^j/\partial x^i)dx^i = (\partial m^j/\partial x^i)dx^i$. Therefore,

$$dy^1 \wedge \ldots \wedge dy^r = \det\left[\frac{\partial m^j(g,\mathbf{x})}{\partial x^i}\right] dx^1 \wedge \ldots \wedge dx^r. \tag{B.22}$$

If $\mathbf{x} = 0$, the coordinate of the identity, then y is the coordinates of g. So the volume element at g, denoted by $d^r\mathbf{y}$ is given by

$$d^r\mathbf{y} = \det\left[\frac{\partial m^j(g,\mathbf{x})}{\partial x^i}\right]_{\mathbf{x}=0} d^r\mathbf{x}\,. \tag{B.23}$$

Since this measure is invariant by definition, its value must be the same for any $g \in G$. It is easiest to pick the identity element E:

$$d\boldsymbol{\mu}(g) = d\boldsymbol{\mu}(E) \equiv d^r\mathbf{x} = \left(\det\left[\frac{\partial m^j(g,\mathbf{x})}{\partial x^i}\right]_{\mathbf{x}=0}\right)^{-1} dV\,, \tag{B.24}$$

where $dV = d^r\mathbf{y}$ is the ordinary Euclidean volume element of $\mathbb{R}^r$.

Two representations of $SO(3)$ namely the Euler-angle rotation, and the Rodrigues rotation were introduced earlier in appendix A.2. The Haar measure for these representations are

$$d\boldsymbol{\mu}^{\text{Euler}} = \frac{1}{8\pi^2}\sin(\theta)\, d\theta d\psi d\phi\,, \tag{B.25}$$

$$d\boldsymbol{\mu}^{\text{Rodrigues}} = \frac{1}{4\pi^2}\sin^2\left(\frac{\psi}{2}\right)\sin(\theta)\, d\theta d\phi d\psi\,. \tag{B.26}$$

The three parameters θ, ψ, ϕ are the three Euler angles defined in appendix A.2, while θ and ϕ in the second line are the zenith and the azimuth angles indicating the direction that $\hat{\mathbf{n}}$ points.

B.2 Number of basis tensors in D

We are interested in finding the number of isotropic basis tensors with a set of symmetries. Armed with tools from the previous section, it is just a matter of a few integrations to get to the answer. Before we tackle the actual question, let's work out an easy example first. As we learn earlier in appendix A.3 that there are 91 linearly independent isotropic tensors of rank eight. To see how this number was derived, notice that a general eighth rank tensor is constructed by taking tensor products of eight rank-1 tensors (or vectors). We seek to count the number of times the isotropic representations of the rotation group occurs within the products. In other words, we want to obtain $a^{(0)}$ in the decomposition,

$$\otimes^8 \underline{\mathbf{1}} = a^{(0)}\underline{\mathbf{0}} \oplus a^{(1)}\underline{\mathbf{1}} \oplus \ldots \oplus a^{(8)}\underline{\mathbf{8}}\,, \tag{B.27}$$

where $\underline{\mathbf{0}}$ is a "scalar" representation, something that's invariant under the action of the group, $\underline{\mathbf{1}}$ is a "vector" representation, $\underline{\mathbf{2}}$ is a second rank, symmetric, traceless tensor, and so on. This is a common notation among physics community where representations are labeled by their dimensions.

As we learned from the previous section that characters of the direct products are equal to products of the characters, we can immediately write down the character of the L.H.S. of (B.27),

$$\chi^{\otimes^8 \underline{\mathbf{1}}}(\boldsymbol{R}) = (\chi^{(1)}(\boldsymbol{R}))^8. \tag{B.28}$$

It turns out that the Rodrigues representation is the most natural representation to use here. $\boldsymbol{R}$ therefore signifies the Rodrigues rotation matrix.

It is easy to tabulate $\chi^{(n)}(\boldsymbol{R})$ in the Rodrigues representation given $\chi^{(0)}(\boldsymbol{R})$ and $\chi^{(1)}(\boldsymbol{R})$. Since

$$\underline{\boldsymbol{n}} \otimes \underline{\mathbf{1}} = \underline{\boldsymbol{n-1}} \oplus \underline{\boldsymbol{n}} \oplus \underline{\boldsymbol{n+1}}, \tag{B.29}$$

taking the trace of both sides, we then get the recurrence relation,

$$\chi^{(n+1)}(\boldsymbol{R}) = \chi^{(n)}(\boldsymbol{R})\chi^{(1)}(\boldsymbol{R}) - \chi^{(n-1)}(\boldsymbol{R}) - \chi^{(n)}(\boldsymbol{R}). \tag{B.30}$$

The values of $\chi^{(0)}(\boldsymbol{R})$ is just 1. We can read off the value of $\chi^{(1)}(\boldsymbol{R})$ directly from (A.15) which turns out to be $1 + 2\cos(\psi)$, therefore,

$$\chi^{(n)}(\boldsymbol{R}) = 1 + 2\sum_{m=1}^{n} \cos(m\psi). \tag{B.31}$$

We are now ready to calculate $a^{(0)}$ in this case. From (B.21),

$$\begin{aligned} a^{(0)} &= \int d\boldsymbol{\mu}(g)\, \chi^{\otimes^8 \underline{\mathbf{1}}}(\boldsymbol{R}) \left[\chi^{(0)}(\boldsymbol{R})\right]^* \\ &= \frac{1}{4\pi^2} \int_0^{\pi} d\theta \int_0^{2\pi} d\phi \int_0^{2\pi} d\psi\, \sin^2\left(\frac{\psi}{2}\right) \sin(\theta)\, \left(1 + 2\cos(\psi)\right)^8 \cdot 1 \\ &= 91. \end{aligned} \tag{B.32}$$

■

The problem of finding out the number of $\underline{\mathbf{0}}$ representations within $D_{ijkmpqrs}$ can be solved in exactly the same way. Let's examine the symmetries of $D_{ijkmpqrs}$ closely again. From (4.28) and (4.30), we have

$$D_{ijkmpqrs} = D_{ijkmqprs} = D_{ijrspqkm} = D_{jikmpqrs} = D_{pqkmijrs}. \tag{B.33}$$

We can treat $D_{ijkmpqrs}$ as a direct product of two fouth-rank tensors,

$$D_{ijkmpqrs} = B^1_{ijpq} B^2_{krms}\,. \tag{B.34}$$

From the symmetries, one can see that B^1_{ijpq} is symmetric under interchanging $i \leftrightarrow j$ and $p \leftrightarrow q$, and the group $(i,j) \leftrightarrow (p,q)$. Symbolically one can represent B^1_{ijpq} as

$$B^1_{ijpq} \Rightarrow (\underline{\mathbf{1}} \circledS \underline{\mathbf{1}}) \circledS (\underline{\mathbf{1}} \circledS \underline{\mathbf{1}}). \tag{B.35}$$

Similarly,

$$B^2_{krms} \Rightarrow (\underline{\mathbf{1}} \otimes \underline{\mathbf{1}}) \circledS (\underline{\mathbf{1}} \otimes \underline{\mathbf{1}}). \tag{B.36}$$

Using (B.17), the character of $D_{ijkmpqrs}$ is

$$\begin{aligned}
\chi^{\boldsymbol{D}}(\boldsymbol{R}) &= \chi^{(\underline{\mathbf{1}} \circledS \underline{\mathbf{1}}) \circledS (\underline{\mathbf{1}} \circledS \underline{\mathbf{1}})}(\boldsymbol{R}) \chi^{(\underline{\mathbf{1}} \otimes \underline{\mathbf{1}}) \circledS (\underline{\mathbf{1}} \otimes \underline{\mathbf{1}})}(\boldsymbol{R}) \\
&= \frac{1}{2}\left(\left(\chi^{\underline{\mathbf{1}} \circledS \underline{\mathbf{1}}}(\boldsymbol{R})\right)^2 + \chi^{\underline{\mathbf{1}} \circledS \underline{\mathbf{1}}}(\boldsymbol{R} \cdot \boldsymbol{R}) \right) \cdot \frac{1}{2}\left(\left(\chi^{\underline{\mathbf{1}} \otimes \underline{\mathbf{1}}}(\boldsymbol{R})\right)^2 + \chi^{\underline{\mathbf{1}} \otimes \underline{\mathbf{1}}}(\boldsymbol{R} \cdot \boldsymbol{R}) \right) \\
&= \frac{1}{2}\Bigg[\frac{1}{4}\left(\left(\chi^{(1)}(\boldsymbol{R})\right)^2 + \chi^{(1)}(\boldsymbol{R} \cdot \boldsymbol{R}) \right)^2 \\
&\qquad + \frac{1}{2}\left(\left(\chi^{(1)}(\boldsymbol{R} \cdot \boldsymbol{R})\right)^2 + \chi^{(1)}(\boldsymbol{R} \cdot \boldsymbol{R} \cdot \boldsymbol{R} \cdot \boldsymbol{R}) \right) \Bigg] \\
&\qquad \cdot \frac{1}{2}\left[\left(\chi^{(1)}(\boldsymbol{R})\right)^4 + \left(\chi^{(1)}(\boldsymbol{R} \cdot \boldsymbol{R})\right)^2 \right] \\
&= (1 + 2\cos(\psi))^3 (3 + 2\cos(2\psi))(1 + 4\cos(\psi) + 2\cos(3\psi)).
\end{aligned} \tag{B.37}$$

A similar integration as performed in (B.32) gives 15.

■

We would like to note in passing that since the tensor product of two representations is reducible, it is possible to decompose them into the sum of the irreducible ones. Let's consider as an example, the product of two vectors $\mathbf{v}$ and $\mathbf{u}$, then

$$v_i u_j = \underbrace{\frac{1}{3} v_k u_k \delta_{ij}}_{\underline{\mathbf{0}}} + \underbrace{\frac{1}{2}\left(v_i u_j - v_j u_i\right)}_{\underline{\mathbf{1}}} + \underbrace{\left(\frac{1}{2}\left(v_i u_j + v_j u_i\right) - \frac{1}{3} v_k u_k \delta_{ij} \right)}_{\underline{\mathbf{2}}}. \tag{B.38}$$

The general description involving the use of Clebsch–Gordan coefficients was discussed at great length in Gordon Baym's *Lectures on Quantum Mechanics* [142].

APPENDIX C

FOURIER TRANSFORMS

C.1 Definitions

In this work, the convention of the Fourier transform that we adopt is the following:

$$\widetilde{f}(\mathbf{k}) = \int f(\mathbf{r}) \mathrm{e}^{-i\mathbf{k}\cdot\mathbf{r}} d^3\mathbf{r}\,, \tag{C.1}$$

where the integration is taken over all space. Similarly, the inverse transform is defined as

$$f(\mathbf{r}) = \frac{1}{(2\pi)^3} \int \widetilde{f}(\mathbf{k}) \mathrm{e}^{i\mathbf{k}\cdot\mathbf{r}} d^3\mathbf{k}\,. \tag{C.2}$$

As an illustration, let us compute one term that appears in the stress equation (3.1). Define

$$f_{\alpha\beta\gamma}(\mathbf{r}) \equiv \frac{\partial^3 |\mathbf{r}-\mathbf{r}'|}{\partial x'_\alpha \partial x'_\beta \partial x'_\gamma}\,. \tag{C.3}$$

It is not hard to show that

$$f_{\alpha\beta\gamma} = \frac{1}{R^3}\left(\delta_{\alpha\beta}R_\gamma + \delta_{\beta\gamma}R_\alpha + \delta_{\alpha\gamma}R_\beta\right) - \frac{3}{R^5} R_\alpha R_\beta R_\gamma\,, \tag{C.4}$$

where $R_\alpha = (r_\alpha - r'_\alpha)$. To solve this, we employ the symmetry of $f_{\alpha\beta\gamma}$. The most general form of $\widetilde{f}_{\alpha\beta\gamma}$ that can be made up of one vector $\mathbf{k}$ and two isotropic tensors of second rank and third rank is

$$\widetilde{f}_{\alpha\beta\gamma}(\mathbf{k}) = a(k^2)k_\alpha k_\beta k_\gamma + b(k^2)\delta_{\alpha\beta}k_\gamma + c(k^2)\delta_{\alpha\gamma}k_\beta + d(k^2)\delta_{\beta\gamma}k_\alpha + e(k^2)\varepsilon_{\alpha\beta\gamma}\,. \tag{C.5}$$

Since $f_{\alpha\beta\gamma}$ is symmetric over interchanging any two of the three indices, we can immediately get rid of the last term. Since the material is isotropic, there is no distinction between α-, β-, and γ-direction. We can then deduce that $a = b = c$.

From dimensional analysis, we can redefine a, b and explicitly write out the k^2 dependence,

$$\widetilde{f}_{\alpha\beta\gamma}(\mathbf{k}) = \frac{a}{k^4} k_\alpha k_\beta k_\gamma + \frac{b}{k^2} \left(\delta_{\alpha\beta} k_\gamma + \delta_{\alpha\gamma} k_\beta + \delta_{\beta\gamma} k_\alpha\right). \tag{C.6}$$

We can now determine a and b. This can be done by performing inner products between $\boldsymbol{f}$ and three $\mathbf{k}$'s.

$$\begin{aligned}
\widetilde{f}_{\alpha\beta\gamma} k_\alpha k_\beta k_\gamma &= ak^2 + b(3k^2) \\
&= \int d^3\mathbf{R}\, \mathrm{e}^{-i\mathbf{k}\cdot\mathbf{R}} \left[\frac{3}{R^5}(\mathbf{k}\cdot\mathbf{R})^3 - \frac{3}{R^3} k^2 (\mathbf{k}\cdot\mathbf{R})\right] \\
&= \int d^3\mathbf{R}\, \mathrm{e}^{-ikR\cos(\theta)} \frac{3k^3}{R^2} \left[\cos^3(\theta) - \cos(\theta)\right] \\
&= 8\pi i k^2 .
\end{aligned}$$

Or

$$a + 3b = 8\pi i . \tag{C.7}$$

Note that on the second line, we Fourier transform the inner product using (C.4). We now need a similar relation in order to determine the coefficient a and b. An obvious candidate would be

$$\begin{aligned}
\widetilde{f}_{\alpha\beta\gamma} \delta_{\alpha\beta} k_\gamma &= \frac{a}{k^4} k^4 + \frac{b}{k^2}(3k^2 + k^2 + k^2) \\
&= a + 5b \\
&= \int d^3\mathbf{R}\, \mathrm{e}^{-i\mathbf{k}\cdot\mathbf{R}} \left[\frac{3}{R^3}(\mathbf{k}\cdot\mathbf{R}) - \frac{1}{R^3} k^2 (5\mathbf{k}\cdot\mathbf{R})\right] \\
&= -2k \int d^3\mathbf{R}\, \mathrm{e}^{-ikR\cos(\theta)} \frac{\cos(\theta)}{R^2} \\
a + 5b &= 8\pi i .
\end{aligned} \tag{C.8}$$

It is clear from (C.7) and (C.8) that $a = 8\pi i$ and $b = 0$. Finally we have,

$$\widetilde{f}_{\alpha\beta\gamma}(\mathbf{k}) = \frac{8\pi i}{k^4} k_\alpha k_\beta k_\gamma . \tag{C.9}$$

C.2 Convolution theorem

Convolution theorem states that the Fourier transform of the convolution between two functions is simply the product of the two functions transformed, and vice versa. The convolution is defined by

$$(f * g)(\mathbf{r}) \equiv \int f(\mathbf{r}-\mathbf{r}')g(\mathbf{r}')\, d^3\mathbf{r}' \,. \tag{C.10}$$

The proof of the theorem is simply a matter of substitution of the definitions. Let's start off by substituting the definition of the inverse transform into (C.10),

$$\begin{aligned}
(f * g)(\mathbf{r}) &\equiv \int f(\mathbf{r}-\mathbf{r}')g(\mathbf{r}')\, d^3\mathbf{r}' \\
&= \iiint d^3\mathbf{r}' \frac{d^3\mathbf{k}}{(2\pi)^3}\frac{d^3\mathbf{k}'}{(2\pi)^3}\, \widetilde{f}(\mathbf{k})\mathrm{e}^{i\mathbf{k}\cdot(\mathbf{r}-\mathbf{r}')}\, \widetilde{g}(\mathbf{k}')\mathrm{e}^{i\mathbf{k}'\cdot\mathbf{r}'} \\
&= \iint \frac{d^3\mathbf{k}}{(2\pi)^3}\frac{d^3\mathbf{k}'}{(2\pi)^3}\, \widetilde{f}(\mathbf{k})\widetilde{g}(\mathbf{k}')\mathrm{e}^{i\mathbf{k}\cdot\mathbf{r}} \underbrace{\left(\int d^3\mathbf{r}'\mathrm{e}^{i(\mathbf{k}'-\mathbf{k})\cdot\mathbf{r}'}\right)}_{(2\pi)^3\delta(\mathbf{k}'-\mathbf{k})} \\
\int \frac{d^3\mathbf{k}}{(2\pi)^3}\, \widetilde{(f*g)}(\mathbf{k})\mathrm{e}^{i\mathbf{k}\cdot\mathbf{r}} &= \int \frac{d^3\mathbf{k}}{(2\pi)^3}\, \widetilde{f}(\mathbf{k})\widetilde{g}(\mathbf{k})\mathrm{e}^{i\mathbf{k}\cdot\mathbf{r}} \,.
\end{aligned} \tag{C.11}$$

Therefore we can identify the integrands on both sides,

$$\boxed{\widetilde{(f*g)}(\mathbf{k}) = \widetilde{f}(\mathbf{k})\widetilde{g}(\mathbf{k})} \tag{C.12}$$

As an example, let's calculate the Fourier transform of the first term of the stress field due to dislocation density in (3.1),

$$\sigma^{(1)}_{\alpha\beta} = -\frac{\mu}{8\pi}\int d^3\mathbf{r}'\, \varepsilon_{im\alpha}\rho_{\beta m} f_{ijj}(\mathbf{r}')(\mathbf{r}-\mathbf{r}') \,. \tag{C.13}$$

Apply the rule (C.12) to $\sigma^{(1)}_{\alpha\beta}$, we immediately arrive at

$$\widetilde{\sigma}^{(1)}_{\alpha\beta}(\mathbf{k}) = -\frac{\mu}{8\pi}\varepsilon_{im\alpha}\widetilde{f}_{ijj}(\mathbf{k})\widetilde{\rho}_{\beta m}(\mathbf{k}) \,. \tag{C.14}$$

Using (C.9) for $\widetilde{f}_{ijj}(\mathbf{k})$, we then have

$$\widetilde{\sigma}^{(1)}_{\alpha\beta}(\mathbf{k}) = -\frac{i\mu}{k^2}\,\varepsilon_{im\alpha}k_i\widetilde{\rho}_{\beta m}(\mathbf{k})\,. \tag{C.15}$$

Two other terms can be calculated in exactly the same way.

APPENDIX D

FUNDAMENTAL EQUATIONS OF ELASTICITY THEORY

In the classical elasticity theory, the problems consist of finding relationships between state variables such as displacement field u_i, strain field ϵ_{ij}, and stress field σ_{ij} at an arbitrary point subject to various constraints such as a distribution of dislocations, boundary effects, an external body force, etc. There are many standard textbooks on elasticity theory that provide details about the subject [143, 144]. Here we shall only give a brief discussion and provide simple relations that connect various quantities together.

For deformations considered in our work, the total strain $\boldsymbol{\epsilon}^{\mathrm{T}}$ can be decomposed into two pieces: the elastic strain $\boldsymbol{\epsilon}^{\mathrm{E}}$ and the plastic strain $\boldsymbol{\epsilon}^{\mathrm{P}}$,

$$\epsilon_{ij}^{\mathrm{T}} = \epsilon_{ij}^{\mathrm{E}} + \epsilon_{ij}^{\mathrm{P}} \,. \tag{D.1}$$

If one is given a distortion field $\boldsymbol{\beta}$, one can find the corresponding strain field by symmetrizing over the two indices,

$$\epsilon_{ij} = \frac{1}{2} \left(\beta_{ij} + \beta_{ji} \right) . \tag{D.2}$$

The equation is valid on the three types of strain fields.

The total strain must be compatible; there must exist a total displacement field $\mathbf{u}$ such that

$$\epsilon_{ij}^{\mathrm{T}} = \frac{1}{2} \left(\frac{\partial u_i}{\partial x_j} + \frac{\partial u_j}{\partial x_i} \right) , \tag{D.3}$$

or equivalently,

$$\varepsilon_{pki} \varepsilon_{qmj} \frac{\partial^2 \epsilon_{ij}^{\mathrm{T}}}{\partial x_k \partial x_m} = 0 \,. \tag{D.4}$$

The equation (D.4) is called the *compatibility conditions*.

The elastic strain tensor $\boldsymbol{\epsilon}^{\mathrm{E}}$ is related to the stress field $\boldsymbol{\sigma}$ through *Hooke's law*:

$$\sigma_{ij} = C_{ijkm}\,\epsilon^{\mathrm{E}}_{km} \tag{D.5}$$

The tensor relating the two quantities C_{ijkm} is commonly known as the *elastic moduli tensor* or the *stiffness tensor*. Since the stress and strain tensors are both symmetric, $C_{ijkm} = C_{jikm} = C_{ijmk} = C_{jimk}$. Out of all possible 36 components, an isotropic material only contains two independent constants,[1]

$$C_{ijkm} = \lambda\,\delta_{ij}\delta_{km} + \mu\,(\delta_{ik}\delta_{jm} + \delta_{im}\delta_{jk})\,, \tag{D.6}$$

where we choose to express C_{ijkm} in terms of the two Lamé constants. One can express the two Lamé coefficients λ and μ in terms of two of the following three quantities, Bulk modulus K, Poisson's ratio ν, and Young's modulus E_c:

$$\begin{aligned}
\lambda = \quad & \frac{3K\nu}{1+\nu} && = \frac{3K(3K-E_c)}{9K-E_c} && = -\frac{\nu E_c}{(1+\nu)(-1+2\nu)}\,, \\
\mu = -\frac{3K(-1+2\nu)}{2(1+\nu)} \quad & && = \frac{3KE_c}{9K-E_c} && = \frac{E_c}{2(1+\nu)}
\end{aligned}$$

It is also possible to invert (D.5) and express the strain components in terms of the stress components. The tensor S_{ijkm} that relates the two quantities is called the *compliance tensor*,

$$\epsilon^{\mathrm{E}}_{ij} = S_{ijkm}\,\sigma_{km}\,. \tag{D.7}$$

For an isotropic material,

$$S_{ijkm} = \frac{1}{2\mu}\left(\delta_{ik}\delta_{jm} + \delta_{im}\delta_{jk} - \frac{\nu}{1+\nu}\,\delta_{ij}\delta_{km}\right). \tag{D.8}$$

[1] See, *e.g.* [143] for a nice discussion on how to use symmetries in getting rid of the other 34 constants.

APPENDIX E

PROOF OF STRESS-FREE DECOMPOSITION THEOREM

E.1 The proof

Let $\widetilde{\rho}^{\mathrm{SF}}$ represent a stress-free dislocation density which can be decomposed in the following way,

$$\widetilde{\rho}_{ij}^{\mathrm{SF}}(\mathbf{k}) = \widetilde{\Lambda}^{l}(\mathbf{k}) E_{ij}^{l} = \int_{-\infty}^{\infty} d\Delta \int d\Omega \int d^{3}\boldsymbol{\omega} \, \left(a[\mathbf{k}, \boldsymbol{\omega}, \Omega, \Delta] \cdot \widetilde{\rho}_{ij}^{\mathrm{GB}}[\mathbf{k}, \boldsymbol{\omega}, \Omega, \boldsymbol{\Delta}] \right), \tag{4.47'}$$

where $a[\mathbf{k}, \boldsymbol{\omega}, \Omega, \Delta]$ is defined by (4.48). It is to be shown that one retains the original form of $\widetilde{\rho}_{ij}^{\mathrm{SF}}(\mathbf{k})$ upon the substitution of the expression for a into (4.47').

$$\begin{aligned}
\widetilde{\rho}_{ij}^{\mathrm{SF}}(\mathbf{k}) &= \int_{-\infty}^{\infty} d\Delta \int d\Omega \int d^{3}\boldsymbol{\omega} \, \frac{i}{(2\pi)^{3}\pi^{3/2}} \omega_{l} \, \mathrm{e}^{-|\boldsymbol{\omega}|^{2}} \\
&\qquad \times \int_{-\infty}^{\infty} dk' \, k'^{3} \widetilde{\Lambda}^{l} \left[\{ k' \sin(\theta)\cos(\phi), k' \sin(\theta)\sin(\phi), k'\cos(\theta) \} \right] \mathrm{e}^{ik'\Delta} \\
&\qquad\qquad \times (2\pi)^{2} \, \frac{\delta(R_{xp}^{-1}k_p)\delta(R_{yq}^{-1}k_q)}{iR_{zr}^{-1}k_r} \, \omega_n E_{ij}^{n} \, \mathrm{e}^{-i\mathbf{k}\cdot\boldsymbol{\Delta}} \\
&= \frac{1}{4\pi} \int_{-\infty}^{\infty} d\Delta \int d\Omega \underbrace{\left(\frac{2}{\pi^{3/2}} \int d^{3}\boldsymbol{\omega} \, \omega_l \omega_n \, \mathrm{e}^{-|\boldsymbol{\omega}|^{2}} \right)}_{\delta_{ln}} E_{ij}^{n} \\
&\qquad \times \frac{\delta(R_{xp}^{-1}k_p)\delta(R_{yq}^{-1}k_q)}{R_{zr}^{-1}k_r} \, \mathrm{e}^{-i\mathbf{k}\cdot\boldsymbol{\Delta}} \int_{-\infty}^{\infty} dk' \, k'^{3} \widetilde{\Lambda}^{l} \left[\ldots \right] \mathrm{e}^{ik'\Delta} \\
&= \frac{E_{ij}^{l}}{4\pi} \int_{-\infty}^{\infty} d\Delta \int_{0}^{2\pi} d\phi \int_{-\pi/2}^{\pi/2} d\theta \, \sin(\theta) \\
&\qquad \times \frac{\delta(R_{xp}^{-1}k_p)\delta(R_{yq}^{-1}k_q)}{R_{zr}^{-1}k_r} \, \mathrm{e}^{-i\mathbf{k}\cdot\boldsymbol{\Delta}} \int_{-\infty}^{\infty} dk' k'^{3} \widetilde{\Lambda}^{l} \left[\ldots \right] \mathrm{e}^{ik'\Delta}
\end{aligned} \tag{E.1}$$

According to the two δ-functions and the form of the rotation matrix $\boldsymbol{R}$ as defined in (4.46), we can rewrite the δ-functions such that the arguments only

involve the two angles of rotation. Using $\delta(g(x)) = \sum_a \delta(x-a)/|g'(a)|$, where the sum is taken over all a's with $g(a) = 0$ and $g'(a) \neq 0$ [145],

$$\delta(R_{yq}^{-1}k_q)\delta(R_{xp}^{-1}k_p) = \delta(k_x\sin(\phi) - k_y\cos(\phi)) \\ \times \delta\left(k_x\cos(\theta)\cos(\phi) + k_y\cos(\theta)\sin(\phi) - k_z\sin(\theta)\right) \quad \text{(E.2)}$$

The first δ-function, $\delta(R_{yq}^{-1}k_q)$, gives

$$\delta(k_x\sin(\phi) - k_y\cos(\phi)) = \frac{1}{\sqrt{k_x^2+k_y^2}}\left[\delta\left(\phi-\phi_{01}\right) + \delta\left(\phi-\phi_{02}\right)\right], \quad \text{(E.3)}$$

where $\phi_{01} = \sin^{-1}\left(\frac{k_y}{\sqrt{k_x^2+k_y^2}}\right)$ and $\phi_{02} = \sin^{-1}\left(\frac{-k_y}{\sqrt{k_x^2+k_y^2}}\right)$. What this does is to replace

$$\sin(\phi) \to \pm\frac{k_y}{\sqrt{k_x^2+k_y^2}}, \qquad \cos(\phi) \to \pm\frac{k_x}{\sqrt{k_x^2+k_y^2}},$$

where $+$ and $-$ signs correspond to ϕ_{01} and ϕ_{02} respectively. With the above replacement rules, the second δ-function becomes

$$\delta\left(k_x\cos(\theta)\cos(\phi) + k_y\cos(\theta)\sin(\phi) - k_z\sin(\theta)\right) = \frac{1}{k}\,\delta(\theta - \pm\theta_0), \quad \text{(E.4)}$$

where $\theta_0 = \cos^{-1}\left(\frac{k_z}{k}\right)$ with the $\pm$ convention used above, and $k = |\mathbf{k}|$. In effect, this makes

$$\sin(\theta) \to \frac{\sqrt{k_x^2+k_y^2}}{|\mathbf{k}|}, \qquad \cos(\theta) \to \frac{k_z}{|\mathbf{k}|}, \qquad \mathrm{e}^{-i\mathbf{k}\cdot\boldsymbol{\Delta}} \to \mathrm{e}^{-ik\Delta}.$$

Equation (E.1) becomes

$$\widetilde{\rho}_{ij}^{\mathrm{SF}} = \frac{E_{ij}^l}{4\pi}\int_{-\infty}^{\infty} d\Delta \int_0^{2\pi} d\phi \int_{-\pi/2}^{\pi/2} d\theta\, \sin(\theta)\frac{1}{R_{zr}^{-1}k_r}\int_{-\infty}^{\infty} k'^3\widetilde{\Lambda}^l \mathrm{e}^{ik'\Delta}\, dk' \\ \frac{1}{\sqrt{k_x^2+k_y^2}}\frac{1}{k}\left[\delta(\phi-\phi_{01})\delta(\theta-\theta_0) + \delta(\phi-\phi_{02})\delta(\theta+\theta_0)\right]. \quad \text{(E.5)}$$

We then get rid of the two δ-functions by integrating over the angles. After the integrations,

$$R_{zr}^{-1}k_r = k_x\sin(\theta)\cos(\phi) + k_y\sin(\theta)\sin(\phi) + k_z\cos(\theta) \to \pm k,$$

and $\mathrm{e}^{-i\mathbf{k}\cdot\boldsymbol{\Delta}} = \mathrm{e}^{-iR_{zr}^{-1}k_r\Delta} \to \mathrm{e}^{\mp ik\Delta}$. Since the δ-function of θ is split into two terms, (E.5) becomes, after integrating out the angles,

$$\begin{aligned}\widetilde{\rho}_{ij}^{\mathrm{SF}} = \quad & \frac{E_{ij}^l}{4\pi}\int_{-\infty}^{\infty} dk' \left(\frac{k'}{k}\right)^3 \widetilde{\Lambda}^l\left[\left\{\frac{k'}{k}k_x, \frac{k'}{k}k_y, \frac{k'}{k}k_z\right\}\right]\int_{-\infty}^{\infty}\mathrm{e}^{-i(k-k')\Delta}\,d\Delta \\ & +\frac{E_{ij}^l}{4\pi}\int_{-\infty}^{\infty} dk' \left(\frac{k'}{-k}\right)^3 \widetilde{\Lambda}^l\left[-\left\{\frac{k'}{k}k_x, \frac{k'}{k}k_y, \frac{k'}{k}k_z\right\}\right]\int_{-\infty}^{\infty}\mathrm{e}^{-i(k+k')\Delta}\,d\Delta\end{aligned} \tag{E.6}$$

The two integrations over Δ give $2\pi\delta(k-k')$ and $2\pi\delta(k+k')$ respectively. Let's have a look at the second term. We can make a change of variable where $k' \to -k'$:

$$\begin{aligned}\widetilde{\rho}_{ij}^{\mathrm{SF}(II)} &= -\frac{E_{ij}^l}{2}\int_{\infty}^{-\infty} d(-k') \left(\frac{k'}{-k}\right)^3 \widetilde{\Lambda}^l\left[-\left\{\frac{k'}{k}k_x, \frac{k'}{k}k_y, \frac{k'}{k}k_z\right\}\right]\delta(k+k') \\ &= \frac{E_{ij}^l}{2}\int_{-\infty}^{\infty} dk' \left(\frac{k'}{k}\right)^3 \widetilde{\Lambda}^l\left[\left\{\frac{k'}{k}k_x, \frac{k'}{k}k_y, \frac{k'}{k}k_z\right\}\right]\delta(k-k')\end{aligned} \tag{E.7}$$

The two terms combined give

$$\begin{aligned}\widetilde{\rho}_{ij}^{\mathrm{SF}} &= E_{ij}^l\int_{-\infty}^{\infty} dk' \left(\frac{k'}{k}\right)^3 \widetilde{\Lambda}^l\left[\left\{\frac{k'}{k}k_x, \frac{k'}{k}k_y, \frac{k'}{k}k_z\right\}\right]\delta(k-k') \\ &= \widetilde{\Lambda}^l[\mathbf{k}]E_{ij}^l\end{aligned} \tag{E.8}$$

■

E.2 Some examples

Let's take one of the simplest examples which is a twist boundary. According to (4.44) the boundary, in Fourier space, can be written as

$$\widetilde{\boldsymbol{\rho}}^{\mathrm{twist}} = -\frac{nb}{ik_z}\,\delta(k_x)\delta(k_y)\boldsymbol{E}^z. \tag{4.44'}$$

The form of $a[\mathbf{k}, \boldsymbol{\omega}, \Omega, \Delta]$, according to (4.48), in this case is

$$\begin{aligned}a^{\mathrm{twist}} &= \frac{i\omega_z}{(2\pi)^3\pi^{3/2}}\,\mathrm{e}^{-|\boldsymbol{\omega}|^2}\int_{-\infty}^{\infty} dk'\,k'^3\frac{(-nb)\,\delta(k'\sin\theta\cos\phi)\delta(k'\sin\theta\sin\phi)}{ik'\cos\theta}\,\mathrm{e}^{ik'\Delta} \\ &= -\frac{nb\,\omega_z\mathrm{e}^{-|\boldsymbol{\omega}|^2}}{(2\pi)^3\pi^{3/2}}\frac{\delta(\sin\theta\cos\phi)\delta(\sin\theta\sin\phi)}{\cos\theta}\int_{-\infty}^{\infty} dk'\mathrm{e}^{ik'\Delta} \\ &= -\frac{nb\,\omega_z\mathrm{e}^{-|\boldsymbol{\omega}|^2}}{(2\pi)^3\pi^{3/2}}\frac{\delta(\sin\theta\cos\phi)\delta(\sin\theta\sin\phi)}{\cos\theta}\,2\pi\delta(\Delta).\end{aligned} \tag{E.9}$$

The combination of δ-function implies that $\phi = 0$ or ϕ, thus

$$a^{\text{twist}} = -\frac{nb\,\omega_z \mathrm{e}^{-|\boldsymbol{\omega}|^2}}{(2\pi)^2\pi^{3/2}}\,\delta(\cos\phi)\delta(\sin\phi)\delta(\Delta), \tag{E.10}$$

implying that such a wall can be created by only one regular straight wall.

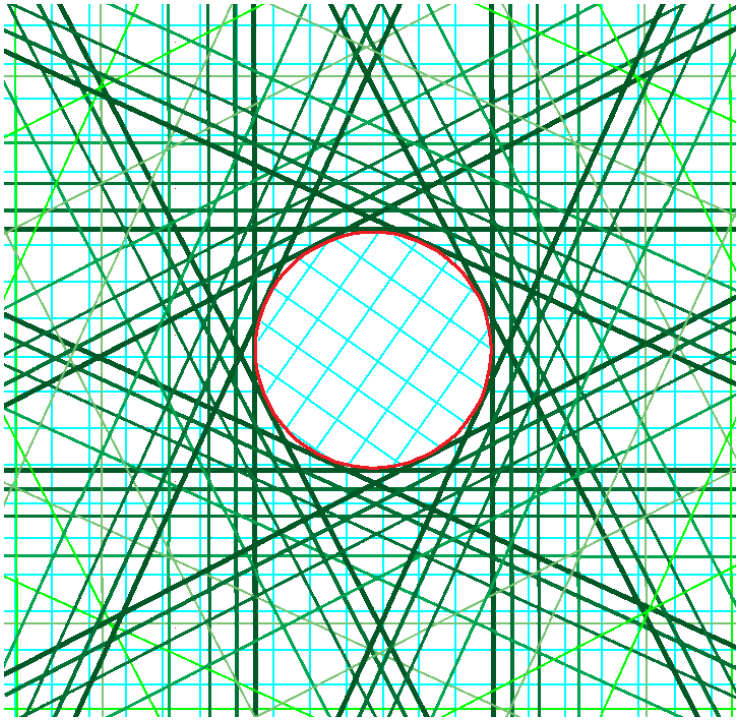

Figure E.1: **A circular grain boundary** can be decomposed into a series of flat walls whose density decays as $1/\Delta^3$ away from the center of the cylindrical cell.

A more complicated example is the case where one cuts out a cylindrical portion of radius R inside a crystal with the axis of symmetry pointing along $\hat{\mathbf{z}}$, rotates it, and pastes it back (figure E.1). The resulting boundary is a circular grain boundary which can be represented in Fourier space as follows:

$$\widetilde{\boldsymbol{\rho}}^{\text{circ}} = \mathcal{J}_1\left(\sqrt{k_x^2 + k_y^2}\,R\right)\frac{\delta(k_z)}{\sqrt{k_x^2 + k_y^2}}\boldsymbol{E}^z, \tag{E.11}$$

where $\mathcal{J}_1(\cdot)$ is the Bessel function of type 1. In this case,

$$\begin{aligned} a^{\text{circ}} &= \frac{i\omega_z}{(2\pi)^3\pi^{3/2}}\,\mathrm{e}^{-|\boldsymbol{\omega}|^2}\int_{-\infty}^{\infty}dk'\,k'^3\frac{\mathcal{J}_1\left(|k'\sin\theta|\,R\right)}{|k'\sin\theta|}\delta(k'\cos\theta)\,\mathrm{e}^{ik'\Delta} \\ &= \frac{i\omega_z}{(2\pi)^3\pi^{3/2}}\,\mathrm{e}^{-|\boldsymbol{\omega}|^2}\underbrace{\delta(\cos\theta)}_{\text{implies }\theta=\pi/2}\underbrace{\int_{-\infty}^{\infty}dk'\,|k'|\mathcal{J}_1(|k'|R)\,\mathrm{e}^{ik'\Delta}}_{\frac{-2iR}{(\Delta^2-R^2)^{3/2}}\Theta(\Delta-R)} \\ &= \frac{2R\,\omega_z\mathrm{e}^{-|\boldsymbol{\omega}|^2}}{(2\pi)^3\pi^{3/2}(\Delta^2-R^2)^{3/2}}\,\delta(\cos\theta)\Theta(\Delta-R). \end{aligned} \tag{E.12}$$

This example emphasizes the important point that we mentioned earlier that any stress-free dislocation configuration can be decomposed into the superposition of flat cell walls. In particular, here we represent a cylindrical wall as an infinite sum of flat walls with whose amplitudes go down as $1/\Delta^3$ with distance Δ away from the center of the cylindrical segment starting from the radius R from the center.

APPENDIX F

ONE DIMENSIONAL EVOLUTION LAW WITH THE MODIFIED TRACE

In one dimension, according to equation 6.3, three of nine components of the plastic distortion field β^{P}_{zj} do not correspond to any dislocation content. These three fields are, thus, irrelevant and never evolved—except for one component, *i.e.*, β^{P}_{zz} when glide and climb are not treated equally by adjusting the value of λ (so that $\lambda \neq 0$) multiplied with $\mathrm{tr}(\boldsymbol{\beta}^{\mathrm{P}})$ in (6.10). By violating spherical symmetry, there are ways of taking the trace without involving β^{P}_{zz}. The modified version of equation 6.10, treating xx and yy the same way, becomes

$$\partial_t \beta^{\mathrm{P}}_{ij} = -\frac{1}{2}\left(\partial_z \mathcal{E}\right)\partial_z\left(\beta^{\mathrm{P}}_{ij} - \frac{\lambda}{2}\,\beta^{\mathrm{P}}_{kk}\delta_{ij}\right), \tag{F.1}$$

where δ_{ij} represents the 2×2 identity matrix. We can perform the mapping to $a^{(\alpha)}$ variables as done in section 6.2.1. This gives

$$\partial_t a^{(\alpha)} + \left(\frac{1-\lambda\,\delta_{1,\alpha}}{2}\right)\partial_z \mathcal{E}\,\partial_z a^{(\alpha)} = 0 \tag{F.2}$$

The modified equation F.2 becomes identical to the original description (6.13) when the mobility of glide and climb is the same ($\lambda = 0$), and the conclusions stated in section 6.2.1 continue to hold. The form of the modified equation permits the analysis at the other extreme limit where the volume is conserved ($\lambda = 1$). Here, $a^{(1)}$ is time-independent, and thus $a^{(1)}(z,t) = a^{(1)}_0(z)$. At late stage, the system behaves in one of the following two ways:

(a) According to equation 6.15 specialized to $\lambda = 1$,

$$\partial_t \mathcal{E} = -\frac{1}{2}(\partial_z \mathcal{E})\,\partial_z\left[\mathcal{E} - \frac{1}{2}\,a^{(1)}_0 a^{(1)}_0\right] \tag{F.3}$$

which is satisfied when the system's elastic energy is (piecewise) constant; $\mathcal{E}$ = constant $\equiv \mathcal{E}_0$. Consequently $a^{(2)}(z)$ and $a^{(3)}(z)$ do not change with time, and their values combine to make the energy constant according to $\mathcal{E}_0 = (1/2)(a_0^{(1)}a_0^{(1)} + a^{(2)}a^{(2)} + a^{(3)}a^{(3)})$. Here, and generally when $\lambda \neq 0$, $a^{(2)}$ and $a^{(3)}$ are no longer piecewise linear; their asymptotic functional forms are determined by the initial state of $a^{(1)}$.

(b) The time-independence of $a_0^{(1)}(z)$ also gives rise to another possible late-time solution.[1] Because $\partial_t \mathcal{E} = \partial_t(\mathcal{E} - (1/2)a_0^{(1)}a_0^{(1)})$,

$$\partial_t \left[\mathcal{E} - \frac{1}{2}\, a_0^{(1)} a_0^{(1)} \right] = -\frac{1}{2} (\partial_z \mathcal{E})\, \partial_z \left[\mathcal{E} - \frac{1}{2} a_0^{(1)} a_0^{(1)} \right]. \tag{F.6}$$

In this case, $\mathcal{E}_0' \equiv \mathcal{E} - (1/2)a_0^{(1)}a_0^{(1)}$ is constant, and thus $\mathcal{F} = \partial_z \mathcal{E} = \partial_z((1/2)a_0^{(1)}a_0^{(1)})$. It follows from the constraint of the energy on $a^{(\alpha)}$ that

$$\partial_z \left(a^{(2)} a^{(2)} + a^{(3)} a^{(3)} \right) = 0. \tag{F.7}$$

The jump discontinuities of the Peach–Koehler force density $\mathcal{F}$ across cell boundaries result in the continuity of the strain energy density even when climb is forbidden.

[1] We have found a family of possible solutions that do not seem to show up in our simulations. For example,

$$\mathcal{E} = \int_{z_0}^{z} A \pm \frac{1}{2}\sqrt{A^2 + C}\, dz' - \frac{C}{8}(t - t_0) \tag{F.4}$$

is a solution to equation F.3 with an arbitrary constant C, and $A \equiv \partial_z((1/2)a_0^{(1)}a_0^{(1)})$. This leads to $\mathcal{F} = A \pm (1/2)\sqrt{A^2 + C}$ and

$$a^{(\alpha)} = f\left[t - 2 \int_{z_0}^{z} \mathcal{F}^{-1}(z')\, dz' \right] \qquad \text{for } \alpha \neq 1, \tag{F.5}$$

for an arbitrary function $f[\cdot]$, constrained to $\mathcal{E} = (1/2)a^{(\alpha)}a^{(\alpha)}$.

Figure F.1 shows the plot of $\mathcal{F}$ at large time (solid line) against $\partial_z[(1/2)a_0^{(1)}a_0^{(1)}]$ (dotted line). The separation of regions of $\mathcal{F}$ into conclusion (a) and (b) is clear. So far we are unable to predict when a transition from (a) to (b), and vice versa, would occur. Note that, unlike the case with $\lambda/3$, this theory does not have the wall–splitting feature.

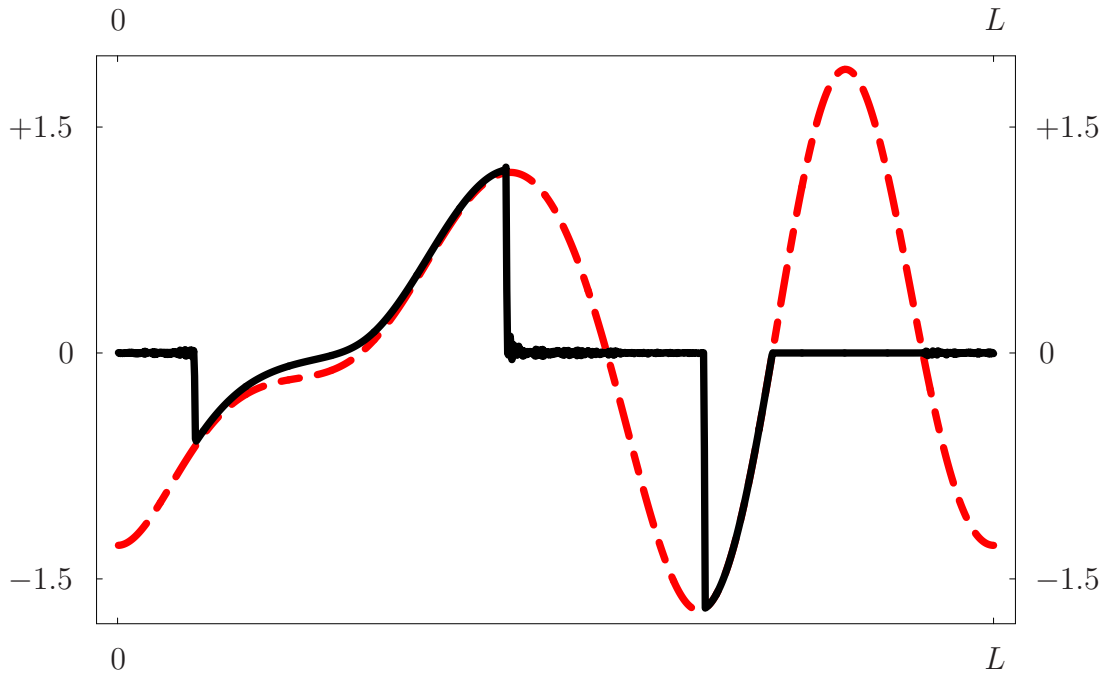

Figure F.1: The Peach–Koehler force density $\mathcal{F}$ in solid line is shown against $\partial_z[(1/2)a_0^{(1)}a_0^{(1)}]$ in dotted line. Regions with constant $\mathcal{E}$ appears as zero (conclusion (a)) while the rest traces the initial curve of $\partial_z[(1/2)a_0^{(1)}a_0^{(1)}]$ (conclusion (b)).

APPENDIX G

UPWIND VERSUS FOURIER REGULARIZATION SCHEMES

Consider a function $u(z,t)$ which satisfies the hyperbolic equation

$$\partial_t u + a(z,t)\partial_z u = 0, \tag{G.1}$$

in which the propagation speed depends on a known function $a(z,t)$. An appropriate numerical scheme should consider the direction of information transfer such that the data at a downstream location only includes the domain of dependence of an upstream location. In particular, information flows along the *characteristics*; consider a family of lines parametrized by s in the z-t space defined by $dz/dt = a(z,t)$, by the chain rule,

$$\frac{du(z(s),t(s))}{ds} = \partial_t u \frac{dt}{ds} + \partial_z u \frac{dz}{ds} = \frac{dt}{ds}\left[\partial_t u + \frac{dz}{dt}\partial_z u\right] = 0. \tag{G.2}$$

Thus, $u(z_0,t)$ is constant along the trajectory of $z_0(s)$ which is a solution to $dz/dt = a(z,t)$.

The simplest of such scheme is the single-sided differencing

$$\frac{u_i^{n+1} - u_i^n}{\Delta t} = -\left[\max(0,a_i)D^{-z}u_i^n + \min(0,a_i)D^{+z}u_i^n\right], \tag{G.3}$$

where the correct direction of the upwinding depends on the sign of a. The operators D^{+z} and D^{-z} in equation G.3 are defined by

$$D^{+z}u_i^n \equiv \frac{u_{i+1}^n - u_i^n}{\Delta z}, \qquad D^{-z}u_i^n \equiv \frac{u_i^n - u_{i-1}^n}{\Delta z}.$$

When the propagation speed a is positive, information flows from left to right, and backward differencing D^{-z} is chosen, and vice versa. Component-wise, our evolution law in one dimension (equation 6.13) is of the form given in equation G.1.

In this case, the differencing direction is given by the sign of $\mathcal{F}$, and the equations can be integrated out in the standard way as prescribed above.

The evolution law for our dislocation theory is, in general, not hyperbolic. We appeal to Fourier regularization methods to numerically solve the equations of motion. There exists, however, some simple cases where we can use the above upwind scheme to numerically integrate the equations. Consider, as an example, a single-slip system of parallel edge dislocations lying along the z-direction, with Burgers vectors pointing in the x-direction, forbidding climb. The only relevant component is β^{P}_{yx} giving rise to ρ_{zx} according to $\rho_{zx} = -\partial_x \beta^{\mathrm{P}}_{yx}$.[1] The equation of motion for β^{P}_{yx} obeys

$$\partial_t \beta^{\mathrm{P}}_{yx} = \left(\sigma_{yx} \partial_x \beta^{\mathrm{P}}_{yx}\right) \partial_x \beta^{\mathrm{P}}_{yx} \,, \tag{G.4}$$

where $\widetilde{\sigma}_{yx} = -\frac{2\mu}{1-\nu} \frac{k_x k_y^2}{k_x^2+k_y^2} \widetilde{\beta}^{\mathrm{P}}_{yx}$. The term in the parentheses, $\sigma_{yx} \partial_x \beta^{\mathrm{P}}_{yx}$, is the characteristic speed, and thus signifies the direction of the flow. The appropriate differencing operator $D^{\pm x}$ can be selected accordingly. In cases where more than one slip-system is active, the evolution equation for each component does not decouple. Without hyperbolicity, there is no natural basis where these equations nicely separate. The transformation to a system of decoupled equations, if existed, has to be done in a case-by-case basis.

In cases where suitable upwind scheme cannot be constructed, the most straightforward approach to prevent numerical instability is to add an artificial viscous term to the equation. The additional term adds a diffusive smoothing at sharp corners. The amount of needed artificial diffusion has to be carefully picked so that it can prevent the instability and not cause significant rounding at edges.

[1] In general $\rho_{zx} = \partial_y \beta^{\mathrm{P}}_{xx} - \partial_x \beta^{\mathrm{P}}_{yx}$, and β^{P}_{xx} also contributes to ρ_{zx}. Since we forbid the climb motion, the trace of $\boldsymbol{J}$, or equivalently, the trace of $\boldsymbol{\beta}^{\mathrm{P}}$ has to be zero. Thus, the evolution of β^{P}_{xx} is suppressed, and its value remains zero.

The evolution law with a diffusive term added becomes

$$\partial_t \beta_{ij}^{\mathrm{P}} = J_{ij}^{\mathrm{N.L.}} + J_{ij}^{\mathrm{Diff}}, \tag{G.5}$$

where $J_{ij}^{\mathrm{N.L.}}$ is the actual dislocation current given by the theory, while J_{ij}^{Diff} is the required viscosity term with an appropriate order. In this work, we invoke two forms of diffusive terms: $J_{ij}^{\mathrm{Diff}^{(2)}} = \epsilon^{(2)} \nabla^2 \beta_{ij}^{\mathrm{P}}$ and $J_{ij}^{\mathrm{Diff}^{(4)}} = -\epsilon^{(4)} \nabla^2 \beta_{ij}^{\mathrm{P}}$. The first form, appearing in the heat equation, has a long history and is used regularly in many types of problems. The second form is more effective in suppressing high-frequency fluctuations and is what we adopt for problems in two dimensions.

Equation G.5 is solved in a two-step process. (1) The solution is advanced forward in time by a half incremental step $\Delta t/2$ using the method of choice (here we use 3rd-order TVD Runge–Kutta as outlined in [146]) *without* the diffusive term. The spatial derivatives are calculated with regular central differencing. (2) We then solve the equation with the diffusive piece, omitting $J_{ij}^{\mathrm{N.L.}}$, explicitly in Fourier space according to

$$\widetilde{\beta}_{ij}^{\mathrm{P}}(k_x, k_y, t + \Delta t) = \begin{cases} \mathrm{e}^{-\epsilon^{(2)} k^2 (\Delta t/2)} \widetilde{\beta}_{ij}^{\mathrm{P}}(k_x, k_y, t + \Delta t/2) \\ \\ \mathrm{e}^{-\epsilon^{(4)} k^4 (\Delta t/2)} \widetilde{\beta}_{ij}^{\mathrm{P}}(k_x, k_y, t + \Delta t/2) \end{cases}, \tag{G.6}$$

where $k \equiv (k_x^2 + k_y^2)^{1/2}$. The real-space solution is obtained after an inverse transformation.

Figure G.1 shows the results of a one-component $\boldsymbol{\beta}^{\mathrm{P}}$ simulation in one dimension at, using $\Delta z = 1/1024$, $\Delta t = 4 \times 10^{-5}$, and $\epsilon^{(2)} = \epsilon^{(4)} = 4.55 \times 10^{-8}$, plotted at every 1000 time steps. The simulations using the upwind and both diffusion schemes are plot on top of one another. The results due to all three schemes agree very well at early times. While the upwind and the fourth-order diffusion schemes continue to match long after the formation of jump singularities, the second-order

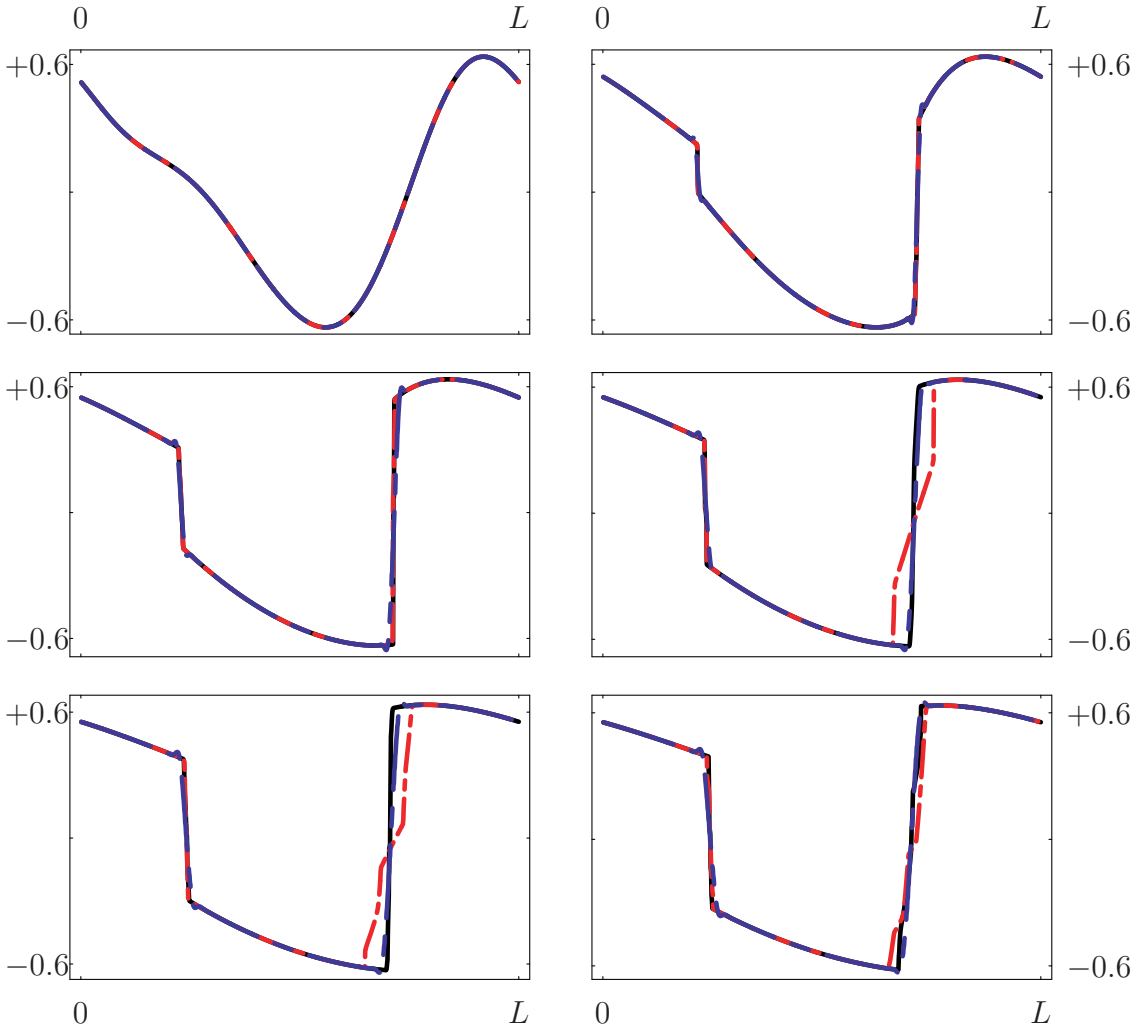

Figure G.1: **Comparison between three numerical schemes:** The results from numerical simulations using upwind, second-order diffusion, and fourth-order diffusion schemes are plotted on top of each other, with an interval of $1000\Delta t$ (time flows from left to right, then top to bottom). The second-order result (shown in red) differs from the other two during the intermediate times, and later converges at large times.

scheme differs from the other two in a substantial way. The wall tends to spread out but remains stable. The discrepancies gradually diminish at large times. Results in the regions away from the singularities appear to be identical at all times.

APPENDIX H

VISUALIZING DISLOCATION DENSITY IN TWO DIMENSIONS

In one dimension where a dislocation density is allowed to vary only along one direction, derivatives with respect to the varying dimension (taken to be along $\hat{\mathbf{z}}$) supplies a one-to-one relationship between each component of a plastic distortion field β^{P}_{ij} and a corresponding component of the dislocation field ρ_{ij}, namely,

$$\rho_{xj} = \partial_z \beta^{\mathrm{P}}_{yj} \,, \qquad \rho_{yj} = -\partial_z \beta^{\mathrm{P}}_{xj} \,, \qquad \rho_{zj} = 0 \,. \tag{6.3'}$$

It is therefore natural to plot the components of $\boldsymbol{\beta}^{\mathrm{P}}$ since they are the basis of choice, and their slopes directly provide information about $\boldsymbol{\rho}$. In two dimensions where dislocations vary along a plane perpendicular to $\hat{\mathbf{z}}$, the relationships between the components of $\boldsymbol{\beta}^{\mathrm{P}}$ and $\boldsymbol{\rho}$ are more involved:

$$\rho_{xj} = -\partial_y \beta^{\mathrm{P}}_{zj} \,, \qquad \rho_{yj} = \partial_x \beta^{\mathrm{P}}_{zj} \,, \quad \rho_{zj} = -\partial_x \beta^{\mathrm{P}}_{yj} + \partial_y \beta^{\mathrm{P}}_{xj} \,. \tag{H.1}$$

Plots of the components of β^{P}_{ij}, therefore, do not give direct, physical pictures of the system. We would like to come up with a representation that best describes the dislocation contents without undergoing laborious numerical operations.

The simplest and perhaps most intuitive of such schemes is the contour plot of β^{P}_{zj} together with the density plot of ρ_{zj}. Consider $f(x, y) = \beta^{\mathrm{P}}_{zj}$ for a given j. Along a contour $f(x, y) = f_0$, the directional derivative along the contour $\mathbf{v} \cdot \boldsymbol{\nabla} f(x, y)$ is zero by definition. This implies that the tangential vector $\mathbf{v}$ along the contour is perpendicular to $\boldsymbol{\nabla} f$.[1] We can construct $\mathbf{v}$ directly from $\boldsymbol{\nabla} f$ by requiring that their dot product vanishes:

$$\mathbf{v} = \begin{pmatrix} -\partial_y f(x, y) \\ \partial_x f(x, y) \end{pmatrix} \tag{H.2}$$

[1]The statement $\mathbf{v} \cdot \boldsymbol{\nabla} f = 0$ also implies that, since $\mathbf{v}$ points along a contour line, $\boldsymbol{\nabla} f$ is always perpendicular to the contour lines—a well-known fact in calculus.

Comparing (H.1) and (H.2), we can represent ρ_{xj} and ρ_{yj} realistically as families of contour lines of β^{P}_{zj} colored according to the value of j. In this respect, the condition $\partial_i \rho_{ij} = 0$ is automatically satisfied because each contour is closed (or periodically continued). Most graphic software programs (including OpenDX®) should already contain a routine that draws contour lines of a function.

Most of the work is concentrated on representing ρ_{zj}. The field ρ_{zj} is first computed according to (H.1), then rendered as density background with the amount of red, green, and blue determined by its value for each j. Regions with no dislocations are painted in gray. This method allows us to encapsulate the information of all nine components of $\boldsymbol{\rho}$ within one image. Figure H.1 shows a typical two-dimensional data using this scheme.

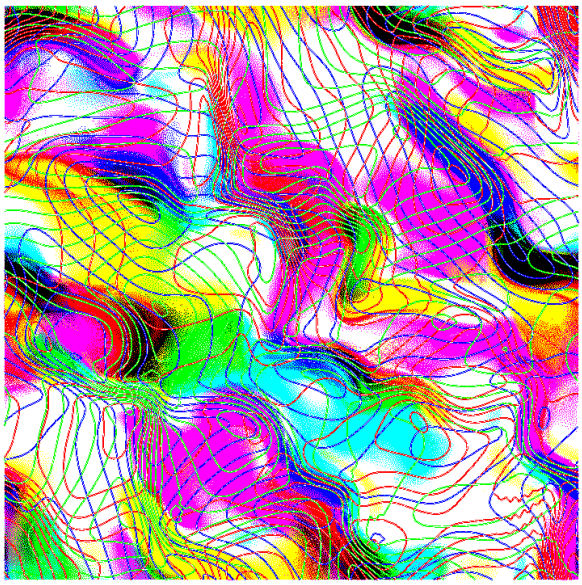

Figure H.1: **Two-dimensional simulation**, showing all evolving components of the tensor $\boldsymbol{\rho}$. The color map shows the dislocation density for dislocations with tangent vectors $\mathbf{t}$ pointing out of the plane, with RGB representing the three directions for the Burgers vectors $\mathbf{b}$ and gray representing no dislocations. The red, green, and blue lines are representative dislocations lying in the plane, again with the same three Burgers vectors.

BIBLIOGRAPHY

[1] A. Cho, Science **311**, 1361 (2006).

[2] S. Limkumnerd and J. P. Sethna, Phys. Rev. Letters **96**, 095503 (2006).

[3] D. A. Hughes, D. C. Chrzan, Q. Liu, and N. Hansen, Phys. Rev. Lett. **81**, 4664 (1998).

[4] M. C. Miguel, A. Vespignani, S. Zapperi, J. Weiss, and J.-R. Grasso, Nature **410**, 667 (2001).

[5] D. B. Barts and A. E. Carlsson, Philosophical Magazine A **75**, 541 (1997).

[6] D. Kuhlmann-Wilsdorf and N. Hansen, Scripta Metall. Mater. **24**, 1557 (1991).

[7] D. A. Hughes and N. Hansen, Metall. Trans. A **24**, 2021 (1993).

[8] D. A. Hughes and N. Hansen, Scripta Metall. Mater. **33**, 315 (1995).

[9] D. A. Hughes and N. Hansen, Phys. Rev. Lett. **87**, 135503 (2001).

[10] D. A. Hughes, Surface and Interface Analysis **31**, 560 (2001).

[11] J. Schiøtz, F. D. D. Tolla, and K. W. Jacobsen, Nature **391**, 561 (1998).

[12] H. V. Swygenhoven, Science **296**, 66 (2002).

[13] J. Schiøtz and K. W. Jacobsen, Science **301**, 1357 (2003).

[14] D. A. Hughes, Q. Liu, and D. C. Chrzan, Acta Mater. **45**, 105 (1997).

[15] A. Godfrey and D. A. Hughes, Acta Mater. **48**, 1897 (2000).

[16] J. P. Sethna, V. Coffman, and E. Demler, Phys. Rev. B **67**, 184107 (2003).

[17] J. D. Eshelby, Solid state physics 3, pages 79–144, Academic Press, San Diego, 1956.

[18] E. Kröner, *Kintinuumstheorie der Versetzungen und Eigenspannungen*, Springer Verlag, Berlin, 1958.

[19] E. Kröner, in *Physics of Defects—Les Houches Session XXXV, 1980*, edited by R. Balian, M. Kléman, and J.-P. Pourier, page 215, North Holland, Amsterdam, 1981.

[20] A. M. Kosevich, Sov. Phys. JETP **15**, 108 (1962).

[21] T. Mura, Phil. Mag. **8**, 843 (1963).

[22] T. Mura, *Micromechanics of Defects in Solids*, chapter 1.10, Martinus Nijhoff Publishers, The Hague, The Netherlands, 2nd edition, 1991.

[23] J. F. Nye, Act. Metall. **1**, 153 (1953).

[24] A. Arsenlis and D. M. Parks, Journal of the Mechanics and Physics of Solids **50**, 1979 (2002).

[25] A. Arsenlis, D. M. Parks, R. Becker, and V. V. Bulatov, Journal of the Mechanics and Physics of Solids **52**, 1213 (2004).

[26] N. R. Barton and P. R. Dawson, Modelling Simul. Mater. Sci. Eng. **9**, 433 (2001).

[27] P. Dawson, D. Boyce, S. MacEwen, and R. Rogge, Materials Science and Engineering A **313**, 123 (2001).

[28] A. Ma, F. Roters, and D. Raabe, Acta Materialia **54**, 2169 (2006).

[29] D. P. Mika and P. R. Dawson, Acta. Mater. **47**, 1355 (1999).

[30] D. Raabe and R. C. Becker, Modeling Simul. Mater. Sci. Eng. **8**, 445 (2000).

[31] G. I. Taylor, J. Inst. Metals **62**, 307 (1938).

[32] B. Bakó and I. Groma, Phys. Rev. B **60**, 122 (1999).

[33] I. Groma, Phys. Rev. B **56**, 5807 (1997).

[34] M. Zaiser, M. C. Miguel, and I. Groma, Phys. Rev. B **64**, 224102 (2001).

[35] A. Acharya and A. Roy, Journal of the Mechanics and Physics of Solids **54**, 1687 (2006).

[36] A. Acharya and A. Sawant, Journal of the Mechanics and Physics of Solids , In press (2006).

[37] A. El-Azab, Phys. Rev. B **61**, 11956 (2000).

[38] A. Roy and A. Acharya, Journal of the Mechanics and Physics of Solids **53**, 143 (2005).

[39] A. Roy and A. Acharya, Journal of the Mechanics and Physics of Solids **54**, 1711 (2006).

[40] D. Kuhlmann-Wilsdorf, Mater. Sci. Engr. A **113**, 1 (1989).

[41] D. Kuhlmann-Wilsdorf, Physica Status Solidi (a) **149**, 225 (1995).

[42] F. C. Frank, Phil. Mag. **42**, 809 (1951).

[43] W. Pantleon, Mater. Sci. Tech. **21**, 1392 (2005).

[44] W. Pantleon, Private communication.

[45] C. S. Barrett and L. H. Levenson, Trans. AIME **137**, 112 (1940).

[46] B. Bay, N. Hansen, D. A. Hughes, and D. Kuhlmann-Wilsdorf, Acta Metall. Mater. **40**, 205 (1992).

[47] F. C. Frank, Disc. Faraday Soc. **25**, 19 (1958).

[48] R. deWit, Linear theory of static disclinations, in *Fundamental Aspects of Dislocation Theory*, edited by J. A. Simmons, R. deWit, and R. Bullough, pages 651–80, National Bureau of Standards, 1969.

[49] R. deWit, J. Appl. Phys. **42**, 3304 (1971).

[50] B. K. D. Gairola, Nonlinear elastic problems, in *Dislocations in Solids*, edited by F. R. N. Nabarro, volume 1, pages 223–342, North-Holland Publishing Company, Amsterdam, the Netherlands, 1979.

[51] D. Walgraef and E. C. Aifantis, Int. J. Eng. Sci. **23**, 1351 (1985).

[52] J. Pontes, D. Walgraef, and E. C. Aifantis, (2005), Preprint submitted to Elsevier Science.

[53] S. I. Selitser and J. W. M. Jr, Acta Metall. Mater. **42**, 3985 (1994).

[54] D. A. Hughes, Private communication.

[55] M. Peach and J. S. Koehler, Phys. Rev. **80**, 436 (1950).

[56] J. P. Hirth and J. Lothe, *Theory of Dislocations*, chapter 4, page 105, Krieger Publishing Company, reprint edition edition, 1992.

[57] J. D. Jackson, *Classical Electrodynamics*, chapter 5, page 179, John Wiley & Sons, Inc., 3rd edition, 1999.

[58] J. M. Rickman and J. Viñals, Phil. Mag. A **75**, 1251 (1997).

[59] E. A. Kearsley and J. T. Fong, Jour. Res. Nat. Bur. Stand. **79B**, 49 (1975).

[60] M. Marcus and H. Minc, *A Survey of Matrix Theory and Matrix Inequalities*, chapter 4.12, page 69, Dover, New York, NY, 1992.

[61] C. R. Johnson, Amer. Math. Monthly **77**, 259 (1970).

[62] J. P. Sethna and M. Huang, Meissner effects and constraints, in *1991 Lectures in Complex Systems, SFI Studies in the Sciences of Complexity, Proc. Vol. XV*, edited by L. Nadel and D. Stein, pages 267–76, Addison Wesley, New York, 1992, cond-mat/9204010.

[63] A. H. Cottrell, *Dislocations and Plastic Flow in Crystals*, page 38, Oxford University Press, Oxford, UK, 1953.

[64] D. McLean, *Grain Boundaries in Metals*, Oxford University Press, 1957.

[65] A. P. Boresi and R. J. Schmidt, *Advanced Mechanics of Materials*, chapter 4, John Wiley & Sons, Inc., New York, NY, 6th edition, 2003.

[66] D. L. Holt, J. Appl. Phys. **41**, 3197 (1970).

[67] J. Lepinoux and L. P. Kubin, Scripta Metall. **21**, 833 (1987).

[68] A. Gullouglu, D. Srolovitz, R. LeSar, and P. Lomdahl, Scripta Metall. **23**, 1347 (1989).

[69] N. M. Ghoniem, J. R. Matthews, and R. J. Amodeo, Res Mech. **29**, 197 (1990).

[70] V. A. Lubarda, J. A. Blume, and A. Needleman, Acta Metall. Mater. **41**, 625 (1993).

[71] N. A. Fleck and J. W. Hutchinson, J. Mech. Phys. Solids **41**, 1825 (1993).

[72] E. C. Aifantis, Trans. ASME J. Eng. Mat. Tech. **106**, 326 (1984).

[73] E. C. Aifantis, Towards a continuum approach to dislocation patterning, in *Dislocations in Solids—Recent Advances, AMD-63, ASME*, pages 23–33, 1984.

[74] J. Kratochvil, Scr. Metall. Mater. **24**, 891 (1990).

[75] J. Kratochvil, Scr. Metall. Mater. **24**, 1225 (1990).

[76] Y. Bréchet and F. Louchet, Solid State Phenom. **3 & 4**, 347 (1988).

[77] M. Saxlová, J. Kratochvil, and J. Zatloukal, Mater. Sci. Eng. A **234–36**, 205 (1997).

[78] P. Hähner, Appl. Phys. A **62**, 473 (1996).

[79] J. P. Sethna, M. Rauscher, and J.-P. Bouchaud, Europhysics Letters **65**, 665 (2004).

[80] M. L. Falk and J. S. Langer, Phys. Rev. E **57**, 7192 (1998).

[81] J. S. Langer, Phys. Rev. E **64**, 011504 (1998).

[82] N. P. Bailey, J. Schiøtz, A. Lemaître, and K. W. Jacobsen, (submitted) (2006).

[83] M. Ortiz and E. A. Repetto, J. Mech. Phys. Solids **47**, 397 (1999).

[84] P. R. Dawson, D. P. Mika, and N. R. Barton, Scripta Materialia **47**, 713 (2002).

[85] T. Rasmussen et al., Phys. Rev. Lett. **79**, 3676 (1997).

[86] T. Vegge, T. Rasmussen, T. Leffers, O. B. Pedersen, and i K. W. Jacobsen, Phys. Rev. Lett. **85**, 3866 (2000).

[87] M. C. Miguel and S. Zapperi, Science **312**, 1151 (2006).

[88] M. Zaiser, Advances in Physics **55**, 185 (2006).

[89] J. P. Sethna, K. A. Dahmen, and C. R. Myers, Nature **410**, 242 (2001).

[90] A. N. Gullouglu and C. S. Hartly, Model. Simul. Mater. Sci. Eng. **1**, 383 (1993).

[91] I. Groma and G. S. Pawley, Philos. Mag. A **67**, 1459 (1993).

[92] I. Groma and G. S. Pawley, Mater. Sci. Eng. A **164**, 306 (1993).

[93] R. Fournet and J. M. Salazar, Physical Review B **53**, 6283 (1996).

[94] A. A. Benzerga, Y. Bréchet, A. Needleman, and E. Van der Giessen, Modeling and Simulation in Materials Science **12**, 159 (2004).

[95] A. A. Benzerga, Y. Bréchet, A. Needleman, and E. Van der Giessen, Acta Materialia **53**, 4765 (2005).

[96] I. Groma and B. Bakó, Phys. Rev. Lett. **84**, 1487 (2000).

[97] D. Gómez-García, B. Devincre, and L. Kubin, Physical Review Letters **96**, 125503 (2006).

[98] S. N. Varadhan, A. J. Beaudoin, A. Acharya, and C. Fressengeas, Modelling Simulation Mater. Sci. Eng (submitted) (2006).

[99] L. Prandtl, In Proceedings of the 1st International Congress on Applied Mechanics, Delft , 43 (1924).

[100] E. Reuss, Zeits. angew. Math. Mech. (ZAMM) **10**, 266 (1930).

[101] S. Nemat-Nasser, *Plasticity: A Treatise on Finite Deformation of Heterogeneous Inelastic Materials*, Cambridge University Press, Cambridge, UK, 2004.

[102] E. Orowan, Philos. Trans. R. Soc. London A **52**, 8 (1940).

[103] W. T. Read and W. Shockley, Phys. Rev. **78**, 275 (1950).

[104] W. T. Read, *Dislocations in Crystals*, pages 182–3, McGraw-Hill Book Company, Inc., New York, NY, 1953.

[105] F. C. Frank, *Carnegie Institute of Technology Symposium on the Plastic Deformation of Crystalline Solids (Pittsburgh Report)*, pages 150–1, Office of Naval Research (NAVEXOS-P-834), 1950.

[106] G. B. Whitham, *Linear and Nonlinear Waves*, Wiley-Interscience, New York, 1974.

[107] U. Frisch and J. Bec, Burgulence, in *Les Houches 2000: New Trends in Turbulence*, edited by M. Lesieur, A.Yaglom, and F. David, pages 341–83, Springer EDP-Sciences, Berlin, 2001.

[108] J. A. Sethian, *Level Set Methods and Fast Marching Methods*, Cambridge University Press, Cambridge, UK, 2nd edition, 1999.

[109] L. Margulies, G. Winther, and H. F. Poulsen, Science **291**, 2392 (2001).

[110] F. Heidelbach, Science **291**, 2330 (2001).

[111] Z. Shan et al., Science **305**, 654 (2004).

[112] E. Ma, Science **305**, 623 (2004).

[113] M. Chen and X. Yan, Science **308**, 356c (2005).

[114] Z. Shan et al., Science **308**, 356d (2005).

[115] B. Jakobsen et al., Science **312**, 889 (2006).

[116] N. Tamura et al., Strain and texture in al-interconnect wires measured by x-ray microbeam diffraction, in *Materials Reliability in Microelectronics IX, MRS Spring 1999 meeting*, edited by C. Volkert, A. Verbruggen, and D. Brown, volume 563, pages 175–80, MRS Proceedings, 1999.

[117] S. P. Baker, A. Kretschmann, and E. Arzt, Acta Materialia **49**, 2145 (2001).

[118] J. Chung et al., X-ray microbeam measurement of local texture and strain in metals, in *Materials Reliability in Microelectronics IX, MRS Spring 1999 meeting*, edited by C. Volkert, A. Verbruggen, and D. Brown, volume 563, pages 169–74, MRS Proceedings, 1999.

[119] J. V. Bernier and M. P. Miller, J. Appl. Cryst. **39**, 358 (2006).

[120] U. Lienert et al., Acta Materialia **52**, 4461 (2004).

[121] L. Margulies, T. Lorentzen, H. F. Poulsen, and T. L. Leffers, Acta Materialia **50**, 1771 (2002).

[122] M. P. Miller, J. V. Bernier, J.-S. Park, and A. Kazimirov, Review of Scientific Instruments **76**, 113903 (2005).

[123] B. Larson et al., 3-d measurements of deformation microstructure in al(0.2submicron resolution white x-ray microbeams, volume 590, pages 247–52, MRS Proceedings, Materials Research Society, 2000.

[124] B. C. Larson, W. Yang, G. E. Ice, J. D. Budai, and G. Z. Tischler, Nature **415**, 887 (2002).

[125] C. W. Shu and S. Osher, Jour. Comp. Phys. **83**, 32 (1989).

[126] W. Press, S. A. Teukolsky, W. T. Vetterling, and B. P. Flannery, *Numerical Recipes in C++*, Cambridge University Press, Cambridge, 2nd edition, 2002.

[127] P. Rosenau, Phys. Rev. A **40**, 7193 (1989).

[128] R. K. Agarwal, K. Yun, and R. Balakrishnan, Physics of Fluids **13**, 3061 (2001).

[129] C. D. Levermore and W. J. Morokoff, SIAM J. Appl. Math. **59**, 72 (1998).

[130] T. Richeton, J. Weiss, and F. Louchet, Nature Materials **4**, 465 (2005).

[131] M. C. Miguel, A. Vespignani, M. Zaiser, and S. Zapperi, Phys. Rev. Letters **89**, 165501 (2002).

[132] R. Madec, B. Devincre, and L. Kubin, Scripta Metallurgica **47**, 689 (2002).

[133] G. Hamel, *Theoretische Mechanik, Eine Einhertliche Einführung in die Gesamte Mechanik*, chapter 4, Springer-Verlag, Berlin, Germany, 1949.

[134] H. Goldstein, *Classical Mechanics*, chapter 4–7, page 164, Addison-Wesley Publishing Company, Inc., Reading, MA, 2nd edition, 1980.

[135] M. A. Naimark, *Linear Representation of the Lorentz Group*, Pergamon Press, London, 1964.

[136] H. Jeffreys and B. S. Jeffreys, *Methods of Mathematical Physics*, chapter 3, Cambridge University Press, Cambridge, UK, 1946.

[137] H. Weyl, *The Classical Groups*, Princeton University Press, Princeton, NJ, 1939.

[138] M. Hamermesh, *Group Theory and its Application to Physical Problems*, Dover, New York, NY, 1989, The classical textbook written especially for physicists.

[139] J. Rotman, *An Introduction to the Theory of Groups*, Allyn and Bacon, New York, NY, 3rd edition, 1984.

[140] E. Wigner, *Group Theory and its Application to the Quantum Mechanics of Atomic Spectra*, Academic Press, New York, NY, 1959, A superb textbook written by the master of group theory himself.

[141] S. Hassini, *Mathematical Physics: A Modern Introduction to Its Foundations*, chapter 27.1.4, pages 832–3, Springer-Verlag, New York, NY, 1998.

[142] G. Baym, *Lectures on Quantum Mechanics*, chapter 17, Addison-Wesley Publishing Company, Redwood city, CA, 1993.

[143] R. P. Feynman, R. B. Leighton, and M. Sands, *The Feynman Lectures on Physics*, volume 2, chapter 39, Addison-Wesley Publishing Company, 1964.

[144] J. M. Gere, *Mechanics of Materials*, Brooks/Cole Thomson Learning, 5th edition, 2001, This book is geered toward engineering applications. Specialized topics include thermal effects, dynamic loading, non-prismatic members, and various examples on combined loadings, and stress concentrations.

[145] G. B. Arfken and H. J. Weber, *Mathematical Methods for Physicists*, chapter 1, page 84, Academic Press, New York, NY, 4th edition, 1995.

[146] S. Osher and C. W. Shu, SIAM J. Numer. Anal. **28**, 907 (1991).